REPORT DOCUMENTATION PAGE

OMB No. 0704-0188

...nk)	2. REPORT DATE	3. REPORT TYPE AND DATES COVERED
	Feb. 20, 1993	Final Report 1/1/88 to 7/31/92

4. TITLE AND SUBTITLE

Physical Chemical Studies on Molecular Composite Compositions

5. FUNDING NUMBERS

61102F 2303 A3

6. AUTHOR(S)

Guy C. Berry

7. PERFORMING ORGANIZATION NAME(S) AND ADDRESS(ES)

Carnegie-Mellon University
5000 Forbes Avenue
Pittsburgh, PA 15213-3890

8. PERFORMING ORGANIZATION REPORT NUMBER

AFOSR-TR- 93 0206

9. SPONSORING/MONITORING AGENCY NAME(S) AND ADDRESS(ES)

AFOSR/NC
Building 410, Bolling AFB DC
20332-6448

10. SPONSORING/MONITORING AGENCY REPORT NUMBER

AFOSR-89-0125

11. SUPPLEMENTARY NOTES

12a. DISTRIBUTION/AVAILABILITY STATEMENT

APPROVED FOR PUBLIC RELEASE; DISTRIBUTION IS UNLIMITED.

12b. DISTRIBUTION CODE

13. ABSTRACT (Maximum 200 words)

Research in three areas is described: nonlinear optical (NLO) properties of nematic solutions of PBT; the refractive indices of nematic solutions of PBT; and the rheological properties of blends of PBT and nylon-66, or PBO and PabBO, where PBT is *trans*-poly(1,4-phenylene-2,6-benzobisthiazole), PBO is *cis*-poly(1,4-phenylene-2,6-benzobisoxazole), PabBO is poly(2,5–benzoxazole), and nylon-66 is poly(hexamethylene adipamide). Fully aligned monodomains of nematic solutions of PBT were used in the first two parts. An unexpected NLO behavior was observed in which the maximum NLO third-harmonic generation did not occur with light polarized along the molecular axis of the rodlike PBT, even though the refractive index is maximum for that case—possible reasons for this behavior are discussed. The rheology of miscible blends of the rodlike chains with flexible or semiflexible chains is discussed using a model accounting for constraints on the rodlike dynamics imposed by the flexible or semiflexible components. It is shown that information from phase equilibria is essential to such an analysis, as the dynamic constraints are correlated with the factors that cause the formation of the nematic phase in such blends.

14. SUBJECT TERMS	15. NUMBER OF PAGES
Rodlike Polymer, Liquid Crystal, Nonlinear Optics, Rheology, Molecular Composite	92
	16. PRICE CODE

17. SECURITY CLASSIFICATION OF REPORT	18. SECURITY CLASSIFICATION OF THIS PAGE	19. SECURITY CLASSIFICATION OF ABSTRACT	20. LIMITATION OF ABSTRACT
UNCLASSIFIED	UNCLASSIFIED	UNCLASSIFIED	

TABLE OF CONTENTS

FIGURE CAPTIONS

A-1

TABLE CAPTIONS

PHYSICAL-CHEMICAL STUDIES ON RODLIKE POLYMER COMPOSITIONS

The following is a final report for work of AFOSR–89–0125, covering the period January 1988 through July 1992. The work is structured into three parts: Part 1 on nonlinear optical properties of nematic solutions of PBT, Part 2 on the refractive indices of nematic solutions of PBT, and Part 3 on the rheological properties of blends of PBT and nylon-66, or PBO and PabBO, where PBT is *trans*-poly(1,4-phenylene-2,6-benzobisthiazole), PBO is *cis*-poly(1,4-phenylene-2,6-benzobisoxazole), PabBO is poly(2,5–benzoxazole), and nylon-66 is poly(hexamethylene adipamide). An appendix is provided with summaries of the personnel and the publications from the work described.

PART 1: NONLINEAR OPTICAL PROPERTIES OF PBT IN NEMATIC SOLUTIONS .

H. Mattoussi, G. C. Berry, and G. D. Patterson

ABSTRACT

Third-order nonlinear optical properties of lyotropic liquid crystal poly(1,4-phenylene-2,6-benzobisthiazole), PBT, solutions are studied by third harmonic generation measurements. Besides the enhancement observed for this coefficient with respect to the pure PBT, coupling is observed between the mean field nematic director **n** and the incident fundamental polarization E_o. Different geometries, with respect to the relative orientation of E_o and **n**, provided different harmonic Maker Fringe Patterns. These data are compared using refractive index measurements, independently achieved on these materials, and necessary for Maker Fringe analysis.

INTRODUCTION

Nonlinear optical properties of organic materials have been of intense interest for the past decade and more, e.g., see references [1-6]. Applications are understood for materials exhibiting both second and third order nonlinear optical susceptibilities $\chi^{(2)}$ and $\chi^{(3)}$, respectively . In the dipole approximation, these functions appear in an expansion of the macroscopic polarization $\mathbf{P}(\omega)$ of a material under the influence of light propagating with frequency ω with applied field **E** (e.g., see the references cited above):

$$\mathbf{P}(\omega) = \varepsilon_o \sum_{n=1} \chi^{(n)}(-\omega; \omega_1,\omega_2,...,\omega_n)\, \mathbf{E}(\omega_1)\mathbf{E}(\omega_2)...\mathbf{E}(\omega_n) \qquad (1a)$$

$$P_i(\omega) = \varepsilon_o[\chi^{(1)}_{ij} E_j + \chi^{(2)}_{ijk} E_jE_k + \chi^{(3)}_{ijkl} E_jE_kE_l + ...] \qquad (1b)$$

where the sum of the frequencies in the brackets vanishes (e.g., for n=3, $\omega = \omega_1 + \omega_2 + \omega_3$, etc.), e.g., see reference [7,8]; the component notation in Eqn. (1b), in which the dependence on frequency is suppressed for convenience, will be discussed below. The sign attached to a frequency is positive or negative as the photon is absorbed or emitted, respectively. The dipole approximation is valid when the polarization at a site is not strongly coupled to the electromagnetic fields acting at distant sites. The approximation may have to be with materials exhibiting delocalized charges, in which case a more complex representation involving the wave vectors **k** of each interacting electromagnetic wave, but is assumed valid

here unless otherwise noted. The susceptibilities $\chi^{(n)}(-\omega; \omega_1,\omega_2,...,\omega_n)$ are macroscopic properties. Their relation to molecular characteristics is discussed below. Since realization of a nonzero $\chi^{(2)}(-\omega; \omega_1,\omega_2)$ requires a noncentrosymmetric structure, it will not be considered here as the materials proposed for study inherently exhibit centrosymmetry. It should be realized that the susceptibility $\chi^{(n)}(-\omega; \omega_1,\omega_2,...,\omega_n)$ depends not only on the frequencies appearing in its argument, but also on all intermediate linear combinations of those frequencies that appear in a sum to ω, e.g., $\omega_1 + \omega_2$, $\omega_1 + \omega_n$,, etc. Thus, the optical characteristics of the material at each of these intermediate frequencies is important. Given an orthonormal basis e_i, the components of $\chi^{(3)}$ may be expressed in the form

$$\chi_{ijkl}^{(3)} = e_i.\chi^{(3)}e_je_ke_l \tag{2}$$

For reasons of symmetry, the tensor for $\chi^{(3)}(-3\omega; \omega,\omega,\omega)$ is invariant with respect to permutation of its last three indices.

The macroscopic third-order susceptibility tensor $\chi^{(3)}(-\omega; \omega_1,\omega_2,\omega_3)$ may be related to the molecular cubic hyperpolarizability $\gamma(-\omega; \omega_1,\omega_2,\omega_3)$ by the expression

$$\chi^{(3)}(-\omega; \omega_1,\omega_2,\omega_3) = f(\omega)f(\omega_1)f(\omega_2)f(\omega_3)N\gamma(-\omega; \omega_1,\omega_2,\omega_3) \tag{3}$$

where the f( ) are local field factors and N is the number of molecules per unit volume. An eventual goal is to be able to reliably estimate $\gamma(-\omega; \omega_1,\omega_2,\omega_3)$ from information on the molecular structure, and to be able to maximize the desired response by manipulation of the latter. Although formal expressions are available for $\gamma(-\omega; \omega_1,\omega_2,\omega_3)$, theoretical developments are far less developed than for the corresponding quadratic hyperpolarizability $\beta(-\omega; \omega_1,\omega_2)$ [7-9]

The third-order susceptibility may be studied by two principal methods, third harmonic generation and degenerate four wave mixing. These provide the susceptibility tensors $\chi^{(3)}(-3\omega; \omega,\omega,\omega)$ and $\chi^{(3)}(-\omega; \omega,-\omega,\omega)$, respectively. The quantity $\chi^{(3)}(-\omega; \omega,-\omega,\omega)$ has been studied for films of PBT (no solvent) [10], and $\chi^{(3)}(-3\omega; \omega,\omega,\omega)$ has been studied for a aligned nematic solutions of PBT in methane sulfonic acid [11], and isotropic films of PBT in a polymeric matrix [12]. Since only the function $\chi^{(3)}(-\omega; \omega,-\omega,\omega)$ is studied here, the notation will be simplified in the following to denote $\chi^{(3)}(-3\omega; \omega,\omega,\omega)$ simply as $\chi^{(3)}$. The

bold-face notation indicates a tensor. For an isotropic material, the spatial average gives the corresponding psuedo-scalar $\chi^{(3)}_{ISO}$.

The molecular structures of poly[1,4-phenylene-2,6-benzobisthiazole], PBT, and poly[1,4-phenylene-2,6-benzobisoxazole], PBO, have suggested that they might exhibit substantial nonlinear optical behavior related to a third-order nonlinear susceptibility [**10-13**]. Further, the ability to form fully aligned nematic solutions of PBT, PBO, and related materials [**14**] (see below) affords the possibility that careful study of these might provide insight to the molecular characteristics related to enhanced γ. Studies on well aligned nematic solutions will allow elucidation of the components of the third-order susceptibility tensor $\chi^{(3)}$, for comparison with molecular structure.

EXPERIMENTAL

As noted above, the nonlinear optical (NLO) properties of PBT, have been studied in the solid state (thin films) [**10,12,15**]. This rodlike polymer forms a nematic phase when dissolved in suitable solvents and at appropriate concentrations [**11,14**]. Measurements of the third-order susceptibility have been carried out in our laboratory on PBT in nematic and isotropic solutions using a third harmonic generation (THG) technique [**11**]. The PBT (M_w = 34,000) was provided by SRI International. Solutions of the rodlike PBT, were prepared in methane sulfonic acid (MSA). Dissolution is accompanied by protonation of the solute macromolecules [**16**]. Nematic solutions are formed for volume fraction φ above a critical value φ^* [2], where $\varphi^* \approx 0.03$ for the PBT used. The alignment procedure is described elsewhere [**14,17**]. It consists of a surface alignment preparation using a suitable flow in a rectangular channel, followed by exposure to an external magnetic field (5 to 7 Tesla) to speed the bulk alignment. With suitable surface alignment, the bulk alignment is stabilized for an indefinite duration. Flat cells, provided by Hellma Cells Inc. with parallel walls (l/4 surface flatness) were used; 350 mm sample thickness.

The Maker Fringe Pattern (MFP) [**1,2,18,19**] generated with light at wavelength 514 nm on rotation of a plane sample in an incident beam with wavelength 1542 nm was used to evaluate the third-order susceptibility. The THG apparatus [**11**] utilized a Raman Cell filled with methane gas to provide a fundamental intensity at wavelength λ = 1542 nm when pumped at λ = 1064 nm by a pulsed Nd:YAG laser, generating a third harmonic signal $I_{3\omega}$ at λ = 514 nm. The incident beam is split into two beams, directed to the sample and the reference. A weakly focused beam generated a sufficiently intense signal for accurate

detection. The reference (Fused silica) accounts for fluctuations in the incident intensity. The reduced intensity is given by

$$R(\vartheta) = \frac{I_{3\omega}(\vartheta)_{SAMP}}{I_{3\omega}(0)_{REF}} \tag{4}$$

where SAMP and REF stand for the sample and reference, respectively, and ϑ is the incidence angle. Since the signal was nil for λ in the range 540 to 700 nm, any fluorescence contribution to $I_{3\omega}(\vartheta)$ was negligible. The Maker fringe pattern exhibits symmetry about the position with the angle ϑ between the normal to the plane and the incident beam equal to zero [**11,18**] A general expression for $R(\vartheta)$ for an isotropic material gives [**1,2,18,19**]:

$$R(\vartheta) = K_R\left(\frac{[Q(\vartheta)W(\vartheta)]_{SAMP}}{[Q(0)W(0)]_{REF}}\right)^2 \tag{5}$$

$$W(\vartheta) = \frac{|\chi^{(3)}_{EFF}|}{|n_{3\omega}^2 - n_\omega^2|}\sin\psi(\vartheta) \tag{6}$$

where $|\chi^{(3)}_{EFF}|$ is the modulus of the effective component of $\chi^{(3)}$, e.g., see Eqn. (2), $Q(\vartheta)$ is a weakly decreasing function of increasing angle, related in part to Fresnel factors ($Q(0)$ is unity), n is the refractive index at the indicated frequency, K_R is the ratio of the incident beam directed to the sample to that directed to the reference, and $2\psi(\vartheta)/\pi$ is equal to the ratio

$L/L_c(\vartheta)$ of the physical thickness L to the coherence length L_c, with [**1,2,18,19**]

$$L_c(\vartheta) = \lambda/6|n_{3\omega}\cos(\vartheta'_{3\omega}) - n_\omega\cos(\vartheta'_\omega)| \tag{7a}$$

$$L_c(0) = \lambda/6|n_{3\omega} - n_\omega| \tag{7b}$$

Here, the the propagation angles ϑ' of the rays in the sample are related to ϑ through Snell's law, using the appropriate refractive index, see below. The dependence on ϑ produces the Maker fringe pattern. In practice, the parameter K_R is evaluated by determination of $R_{STD}(0)$ for the response to a standard with known $|\chi^{(3)}_{EFF}|$, $n_{3\omega}$, n_ω, and thickness L. A BK7 plate was used as the standard in the cited study. It should be noted that R(0) may take on any value from ze.o to its value R_{MAX} for $\psi=0$, as $\psi(\vartheta)$ is not usually zero at $\vartheta=0$. However, $\sin\psi$ may be taken as unity for the successive maxima in the fri..ge pattern, providing on method to estimate of $|\chi^{(3)}_{EFF}|/|n_{3\omega}^2 - n_\omega^2|$ from data on $R(\vartheta)$.

For an anisotropic material, the parameter $|\chi^{(3)}_{EFF}|$ becomes the modulus of an appropriate component of the tensor $\chi^{(3)}$, depending on the polarization of the light and the orientation of the director, see below.

RESULTS

A typical Maker fringe pattern obtained with isotropic solutions of PBT is given in Fig 1, showing the fringe pattern for a 200 μm thick sample of an isotropic solution of PBT in methane sulfonic acid, with 0.02 weight fraction w polymer. The fringe pattern is symmetric, as expected, but does not appear to go to zero at the successive minima. The weak dependence of $Q(\vartheta)$ on ϑ is evident in the slow variation of the successive maxima with ϑ. The fringe pattern for a fused silica sample (1000 μm thick) is shown for comparison. The very much stronger signal exhibited by the PBT solution reveals a larger $|\chi^{(3)}_{EFF}|/w|n_{3\omega}^2 - n_\omega^2|$ for that material in comparison to the fused silica (w is 50-fold larger for the latter than for the PBT sample). The strong signal from the PBT solution permits neglect of contributions from the pyrex cell walls by comparison. It is not possible to determine $|\chi^{(3)}_{EFF}|$ from these data without estimates of $n_{3\omega}$ and n_ω. Measurements of the latter are discussed below.

As seen in the preceding, the refractive indices of the anisotropic nematic fluid, and their wavelength dispersions, are very important parameters in the study of THG. They are also important to the evaluation of the order parameter S of the nematic fluid. Aligned nematic solutions of PBT exhibit appreciable birefringence and dichroism [13,14,17]. Thus, the birefingence Δn may be evaluated as the difference n_e-n_o of the extraordinary and ordinary refractive indices n_e and n_o, respectively. In terms of the volume fraction φ of the polymer, and the order parameter $S(\varphi)$,

$$\Delta n = (\Delta n)_o \varphi S(\varphi) \qquad (8)$$

where $(\Delta n)_o$ is the value of Δn for φ and S both equal to unity; of course, $S(\varphi)$ is zero for $\varphi < \varphi_{NI}$, where φ_{NI} is the concentration required to form the nematic phase Two related methods to determine n_e and n_o were used in reference [17] to determine n_e and n_o over a range of $\varphi > \varphi_{NI}$ and wavelength λ. As these methods are discussed in detail in reference [17], they will not be elaborated here (but see Facilities). Suffice it to say that the apparatus and sample

cells used for the THG measurement may also be used to determine the refractive indices and their dependence on λ. Data have been obtained over the range of wavelengths from 514 to 1907 nm, and for concentrations from $1.1\varphi_{NI}$ to $2\varphi_{NI}$. When cast in the familiar form

$$\frac{(n^2 - 1)}{(n^2 + 2)} = K \frac{\lambda_m^{-2}}{\lambda_m^{-2} - \lambda^{-2}} \tag{9}$$

the data on the solution used in these studies gave λ_m equal to 250 and 200 nm for n_e and n_o, respectively, and K equal to 0.27 in both cases. Moreover, over the concentration range studied, the birefringence
$\Delta n = n_e - n_o$ at $\lambda = 633$ nm was fitted by [17]

$$\Delta n = 1.46(\varphi - 0.0020); \qquad \varphi > 1.1\varphi_{NI} \tag{10}$$

As discussed in reference [17], one major surprise was the observation that $S(\varphi)$ appears to be independent of φ, and about equal to 0.94 over the concentration range from $1.1\varphi_{NI}$ to $2.2\varphi_{NI}$. This is not the behavior expected, for example, in the theory due to Flory [20], or that due to Onsager [21]. The observed behavior of the nematic PBT solutions may be due to the alignment of these solutions in a strong magnetic field, and the constraints imposed by the surfaces.

The MFP's obtained with an isotropic PBT solution displayed the anticipated form, with symmetric oscillations with (essentially) zero intensity at the minima. In the concentration range of interest, the third harmonic (THG) signal from the PBT solute dominates that from the solvent and the cell. No depolarized signal could be measured for the isotropic solution. Making use of the refractive index data discussed in the preceding, the measured $R(\vartheta)$ gave $|\chi^{(3)}_{ISO}|/\varphi \approx 12 \quad 10^{-12}$ (e.s.u.). By comparison, values of $|\chi^{(3)}_{EFF}|$ have been reported for PBT of $1 \quad 10^{-12}$ (e.s.u.) from studies of $\chi^{(3)}(-\omega; \omega,-\omega,\omega)$ on a thin film [10] to $12 \quad 10^{-12}$ (e.s.u.) from studies of $\chi^{(3)}(-3\omega; \omega,\omega,\omega)$ on a thin films of PBT mixed with nylon [12].

With nematic solutions, the response $R(\vartheta)$ depends on the polarizations of the incident light an the detected THG signal, and the orientation of these relative to the sample director (the preferred optical axis). Several geometric arrangements are of interest, depending on the relative orientations of the polarizations of the incident and THG fields, E_o and $E_{3\omega}$, respectively, and the director n of the monodomain with respect to the axis of rotation; the latter was always vertical in the arrangements used. The large birefringence of the PBT

monodomain complicates the analysis is some cases, as a relevant refractive index varies with q for certain arrangements, see below. In the following, the notation gives the orientations of these fields in the order $E_{3\omega}$:n:E_o, e.g., V-H-H signifies an arrangement with $E_{3\omega}$ vertical (parallel to the rotation axis) and both E_o and n horizontal. As may be seen in the preceding, it is necessary to know $n_{3\omega}$ and n_ω to determine $|\chi^{(3)}_{EFF}|$ from $R(\vartheta)$.

The MFP for $R_{VHV}(\vartheta)$ and $R_{HVH}(\vartheta)$ were equivalent (except for small difference in amplitude due to the Fresnel factors), as expected since all rays propagate with refractive index n_o. The depolarized signals (e.g., $R_{HHV}(\vartheta)$ and $R_{VVH}(\vartheta)$) were both nil. The analysis using the measured refractive indices gave $|\chi^{(3)}_{VHV}|/\varphi = |\chi^{(3)}_{HVH}|/\varphi \approx 0.6$ 10-12 (e.s.u.), which is smaller than $|\chi^{(3)}_{ISO}|/\varphi$, as expected if the components to $\chi^{(3)}$ along the chain axis exceed those orthogonal to that axis. In component notation, $|\chi^{(3)}_{VHV}|$ and $|\chi^{(3)}_{HVH}|$ both correspond to $|\chi^{(3)}_{yyyy}|$, with the x and z cartesian coordinates along the director and orthogonal to the sample plane, respectively.

An example of the MFP's for $R_{VVV}(\vartheta)$ for an aligned nematic solution of PBT is shown in Fig. 2. The magnitude of the THG signal is noteworthy, as is the marked deviation of the minima from zero. The locus of the minima forms a smooth curve with a shallow maximum at ϑ=0. An analogous experiment to that for $R_{VVV}(\vartheta)$ was carried out with the interference filter usually used to isolate the line at 3ω (i.e., λ = 514 nm) replaced by an interference filter to isolate light at 546 nm wavelength. The absence of any signal at the latter wavelength shows that simple fluorescence does not contribute to $R_{VVV}(\vartheta)$ for the materials studied. Similar behavior was observed for $R_{HHH}(\vartheta)$, except that the number of fringes was different, reflecting the different refractive indices in $L_c(\vartheta)$. The signal $R_{VXV}(\vartheta)$ could be maximized by setting the analyzer at about 40° to the vertical (i.e., X neither V nor H), showing that the THG response exhibits a complex polarization of the THG behavior. The analysis proceeds using only n_e at 3ω and ω for $R_{VVV}(\vartheta)$, but is more complicated for $R_{HHH}(\vartheta)$, involving both n_e and n_o; the difference in the fringe periodicity reflects this difference. Analysis gives $|\chi^{(3)}_{VVV}|/\varphi \approx 40$ 10-12 (e.s.u.), appreciably larger than $|\chi^{(3)}_{ISO}|/\varphi$, as expected. In the cartesian coordinates specified above, $|\chi^{(3)}_{VVV}|$ and $|\chi^{(3)}_{HHH}|$ both correspond to $|\chi^{(3)}_{xxxx}|$.

As shown in Fig 3, for $R_{HVV}(\vartheta)$, the $(n_o)_{3\omega}$ and $(n_e)_\omega$ are very close, leading to fringes so widely spaced that only the central region is observed. For $R_{VHH}(\vartheta)$, n_ω varies from n_o for zero ϑ, to n_e for large ϑ, greatly complicating analysis of the MFP, and leading to enhanced $R_{VHH}(\vartheta)$ at large ϑ. As expected, R(0) is identical for the two cases. The results gave

$|\chi^{(3)}_{HVV}|/\varphi \approx 0.2$ 10-12 (e.s.u.), which is comparable to the small value found for $|\chi^{(3)}_{HVH}|/\varphi$. In the cartesian coordinates specified above, $|\chi^{(3)}_{HVV}|$ and $|\chi^{(3)}_{VHH}|$ both correspond to $|\chi^{(3)}_{yxxx}|$.

The MFP's for $R_{VVH}(\vartheta)$ and $R_{HHV}(\vartheta)$ were both found to have negligible intensity, showing that both $|\chi^{(3)}_{HVV}|$ and $|\chi^{(3)}_{HHV}|$ are very small in comparison with the susceptibilities given above. In the cartesian coordinates specified above, $|\chi\backslash S((3),HVV)|$ and $|\chi\backslash S((3),VHH)|$ both correspond to $|\chi^{(3)}_{xyyy}|$.

DISCUSSION

Summarizing the results, in component notation, $|\chi\backslash S((3),xxxx)| >> |\chi\backslash S((3),yyyy)| > |\chi^{(3)}_{yxxx}| > |\chi^{(3)}_{xyyy}|$, but $|\chi^{(3)}_{xxxx}|$ is not the largest component of $\chi^{(3)}$. Thus, the maximum component to γ appears to be slightly off the molecular axis, see below.

Owing to the depolarized character of the THG response, the numerical values reported may be suspect, e.g., the appropriate value of $n_{3\omega}$ may not be specified by the polarization of the detected beam, as was assumed in the preceding. In work in progress, a fully aligned, defect-free monodomain of the same solution has been prepared in a wedge -shaped cell. Future work using this cell will avoid the variation of the refractive indices with conditions (e.g., ϑ in the preceding) as the MFP is obtained. With the latter cell, the ratio analogous to $R(\vartheta)$ may expressed in the form

$$R(q) = K_R\left(\frac{[Q(q)W'(q)]_{SAMP}}{[Q(0)W(0)]_{REF}}\right)^2 \tag{11}$$

where the physical thickness L(q) is a function of the translational position q along an axis perpendicular to the incident light beam, and in the plane of incidence, and W'(q) is given by [22]

$$W'(q) = \frac{|\chi^{(3)}_{EFF}|}{|n_{3\omega}^2 - n_{\omega}^2|} C[\eta, \psi(q)] \tag{12}$$

with $C[\eta, \psi(q)]$ given by

$$C^2[\eta, \psi(q)] = \exp(-\eta^2)\left(\sin^2[\psi(q)] + \frac{\exp(\eta^2) - 1}{2}\right) \tag{13}$$

where $2\psi(q)/\pi$ is given by $L(q)/L_c(0)$, with $L_c(0)$ given by Eqn. (7), and the (variable) physical thickness L(q) given by

$$L(q) = L(q_{ref}) + (q - q_{ref})\tan\alpha \tag{14}$$

with α the wedge angle and q_{ref} an arbitrary reference position, and

$$\eta = \frac{\pi d_o \tan\alpha}{4L_c(0)} \tag{15}$$

with d_o the beam waist parameter. For $\eta<<1$, as would normally apply, $C[\eta, \psi(q)] \approx \sin[\psi(q)]$. Thus, in this experiment, R(q) oscillates with q to give fringes of equal amplitude, with a period independent of q (or η). The separation Δq between extrema is equal to $2L_c(0)/\tan\alpha$, providing an estimate of $L_c(0)$. The latter may be used to evaluate the important factor $|n_{3\omega}^2 - n_\omega^2|$ as $(n_{3\omega} + n_\omega)\lambda_\omega/6L_c(0)$, given reasonable estimates of $n_{3\omega}$ and n_ω.

The strongly depolarized THG response obtained with the aligned nematic solution of the rodlike PBT is surprising. It requires that an electronic transition involved in the NLO response of the solvated PBT is at an appreciable angle to the chain axis. This is distinctly different from the result of calculations on conjugated *cis* and *trans* polyenes, for which it is predicted that the principal component to γ will have all electromagnetic fields polarized along the molecular axis [23]. The structures of the PBX chains (i.e., PBT and PBO) may be represented as

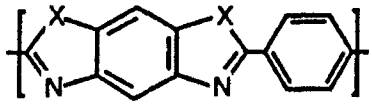

cis PBX

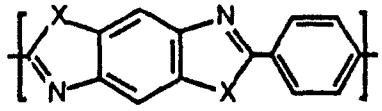

trans PBX

PBX Structures

where -X- is -S- (PBT) or -O- (PBO); the upper and lower structures correspond to the so-called *cis* and *trans* structures, respectively. The studies described above utilized *trans*-PBT. Thus, a possible candidate for a vector associated with an electronic transition off axis to the rodlike molecular axis is the vector along the sulfur-sulfur atoms in the repeating unit of the chain. This possibility opens the question of whether γ for *trans*-PBT is influenced by the polymeric rodlike character of the molecule, or whether γ would be essentially the same for a short oligomeric *trans*-PBT as for a long-chain molecule, perhaps even a model of the repeat unit (i.e., the repeat unit terminated by protons). More generally, the objective is to determine what molecular characteristics are related to γ. Contributions to γ have several origins.(electronic, vibrational and dipolar). As is well-known [8,24], for a conjugated chain, electron delocalization may be treated in perturbation to give a linear polarizability $\propto x^3$, and cubic hyperpolarizability $\gamma_{xxxx} \propto x^m$, where x is the conjugated chain length, and m is predicted to be in the range 5 to 7. The wavelength λ_{max} of the extinction associated with the conjugated length also depends on x, with $\lambda_{max} \propto x$. Thus, this model gives $\gamma_{xxxx} \propto \lambda_{max}^5$. An analysis of data on several conjugated chains gave $\gamma_{xxxx} \propto \lambda_{max}^m$, but m was found to be close to 9.4, far greater than the anticipated exponent [25]. In either case, it seems that γ_{xxxx} will be very sensitive to a conjugation length x, but that accurate prediction of x and of the dependence of γ_{xxxx} on x will be difficult.

In the preceding, it has implicitly been assumed that the absorption bands do not lie close to any of the frequencies ω, 2ω or 3ω. If that assumption is not valid, then $\chi^{(3)}$ becomes complex, with resultant resonance enhancement to the modulus. For example, in the simplest case of a three-level approximation for a material with resonances at ϖ_1, $\varpi_2 < \varpi_1$, and $\varpi_3 < \varpi_2$, the dominant terms in the real and imaginary components of $\gamma(-3\omega, \omega,\omega,\omega)$ as three-photon resonance is approached may be expressed as [8]

$$\text{Re } \gamma(-3\omega, \omega,\omega,\omega) \propto \frac{\varpi_1 - 3\omega}{[(\varpi_1 - 3\omega)^2 + \Omega^2][\varpi_1 - \omega][\varpi_2 - 2\omega]} \tag{16a}$$

$$\text{Im } \gamma(-3\omega, \omega,\omega,\omega) \propto \frac{\Omega}{[(\varpi_1 - 3\omega)^2 + \Omega^2][\varpi_1 - \omega][\varpi_2 - 2\omega]} \tag{16b}$$

where W is the absorption band line width. As may be seen, the modulus of $\gamma(-3\omega, \omega,\omega,\omega)$ will be enhanced if the material exhibits three-photon resonance with $\varpi_1=3\omega$,

or resonance with $\varpi_1=\omega$, etc. This effect will diminish as the line widths broaden, but has been implicated [8,26] in enhanced $|\chi^{(3)}_{ISO}|$ determined [27] for a polymer of polydiacetylene in comparison with the monomeric repeat unit model. The concentration dependence of $|\chi^{(3)}_{EFF}|$ provides one means to evaluate a resonance contribution to $|\chi^{(3)}_{EFF}|$, as $|\chi^{(3)}_{EFF}|/\varphi$ is expected to be independent of φ in the absence of resonance effects [26].

CONCLUSIONS

The third-order nonlinear optical properties of lyotropic liquid crystal poly(1,4-phenylene-2,6-benzobisthiazole), PBT, solutions studied by third harmonic generation measurements reveal coupling between the mean field nematic director **n** and the incident fundamental polarization $\mathbf{E}_0$. Different geometries, with respect to the relative orientation of $\mathbf{E}_0$ and **n**, provided different harmonic Maker Fringe Patterns, with the largest response obtained with $\mathbf{E}_0$ and **n** at about thiry degrees to each other. These data are compared using refractive index measurements, independently achieved on these materials, and necessary for Maker Fringe analysis. This behavior is not presently understood with simple models, but may imply that a transition within a single repeat unit dominates the response.

REFERENCES

1. *Nonlinear Optical Properties of Organic Molecules and Crystals*, Ed. by S. Chemla, J. Zyss, Academic Press, Vol. 1 and 2 (1987).
2. Y. R. Shen, *The Principle of Nonlinear Optics*, J. Wiley, New York (1984).
3. A Yariv, *Quantum Electronics*, J. Wiley, New York (1989).
4. *Nonlinear Optical Properties of Polymers*, Ed by A. J. Heeger, J. Orenstein, and D. R. Ulrich, Matl. Res. Soc Symp. Proceed. Vol 109 (1988).
5. *Optical and Electronic Properties of Polymers*, Ed, by J. M. Torkelson and J. A. Emerson, Matl. Res. Soc Symp. Proceed. Vol 214 (1991).
6. P. N. Prasad and D. J. Williams, *Introduction to Nonlinear Optical Effects in Molecules and Polymers*, J. Wiley, New York, 1991.
7. J. Zyss and D. S. Chemla, Chapt. II-1 in ref. 1.
8. F. Kajzar and J. Messier, Chapt. III-2 in ref. 1.
9. D. Pugh and J. O. Morley, Chapt. II-2 in ref. 1.
10. D. N. Rao, J. Swiatkiewicz, P Chopra, S, K. Choshal and P. N. Prasad, *Appl Phys. Lett.* **48**, 1187 (1986).
11. a) H. Mattoussi, P. G. Kaatz, G. D. Patterson, and G. C. Berry, in ref. 5.;
    b) H. Mattoussi and G. C. Berry,*ACS Polym. Preprints*, ACS Meeting, New York, August 25-30, 1991,in press.
12. H. Vanherzeele, J. S. Meth, S. A. Jenekhe and M. F. Roberts,*Appl. Phys. Lett.* **58**, 663 (1991).
13. G. C. Berry, *Disc. Faraday Soc.* No. **79**, 141 (1985); *Mol. Cryst. Liq. Cryst.* **165**, 333 (1988).
14. M. Srinivasarao and G. C. Berry, *J Rheology* 35, 379 (1989).
15. A. F. Garito and C. C. Teng, *Proc. Soc. Photo-Opt. Instrum. Eng.*613,146 (1986).
16. a) Berry, G.C. and Eisaman, P.R., *J. Polym. Sci, Polym. Phys. Ed.* **12**:2253 (1974);
    b) Lee, C.C., Chu, S.G. and Berry, G.C., *J. Polym. Sci., Polym. Phys. Ed.* **21**: 273 (1983)
17. H. Mattoussi, M. Srinivassarao, P. G. Kaatz and G. C. Berry, *Macromolecules*, submitted.
18. S. K. Kurtz, in *Quantum Electronics*, Ed by H. Rabin and C. L. Tang, Vol. 1, Part A, Academic Press, N.Y. (1975), Chapt. 3 and references therein.
19. F. Kajzar, J. Messier, *Phys. Rev. A*, **32**, 2353 (1985).
20. Flory, P.J., *Adv. Polym Sci* **59**,1 (1984).
21. L. Onsager, *Ann. N.Y. Acad. Sci.* **51**,627 (1949).
22. G. D. Boyd, H. Kasper, and J. H. McFee, *IEEE J Quant Electron* QE-7, 563 (1971).
23. A. F. Garito, J. R. Heflin, K. Y. Wong and O. Zamani-Kharmiri, in Ref. 4, p. 91.
24. J. Ducuing, in *Nonlinear Spectroscopy, ProcIntl School Physics*, ed by N. Bloembergen, Academic Press, New York, 1976, p. 959.
25. P. G. Kaatz, *Optical Third Harmonic Generation From Isotropic Multilayer Media*, Ph. D. Dissertation, Carnegie Mellon University, 1991.
26. F. Kajzar and J. Messier, *Thin Solid Films* **132**, 11 (1986).
27. C. Sauteret, J.-P. Hermann, R. Frey, F Pradère, J. Ducuing, R. H. Baughman and R. R. Chance, *Phys Ref. Lett.* **36**,956 (1976).

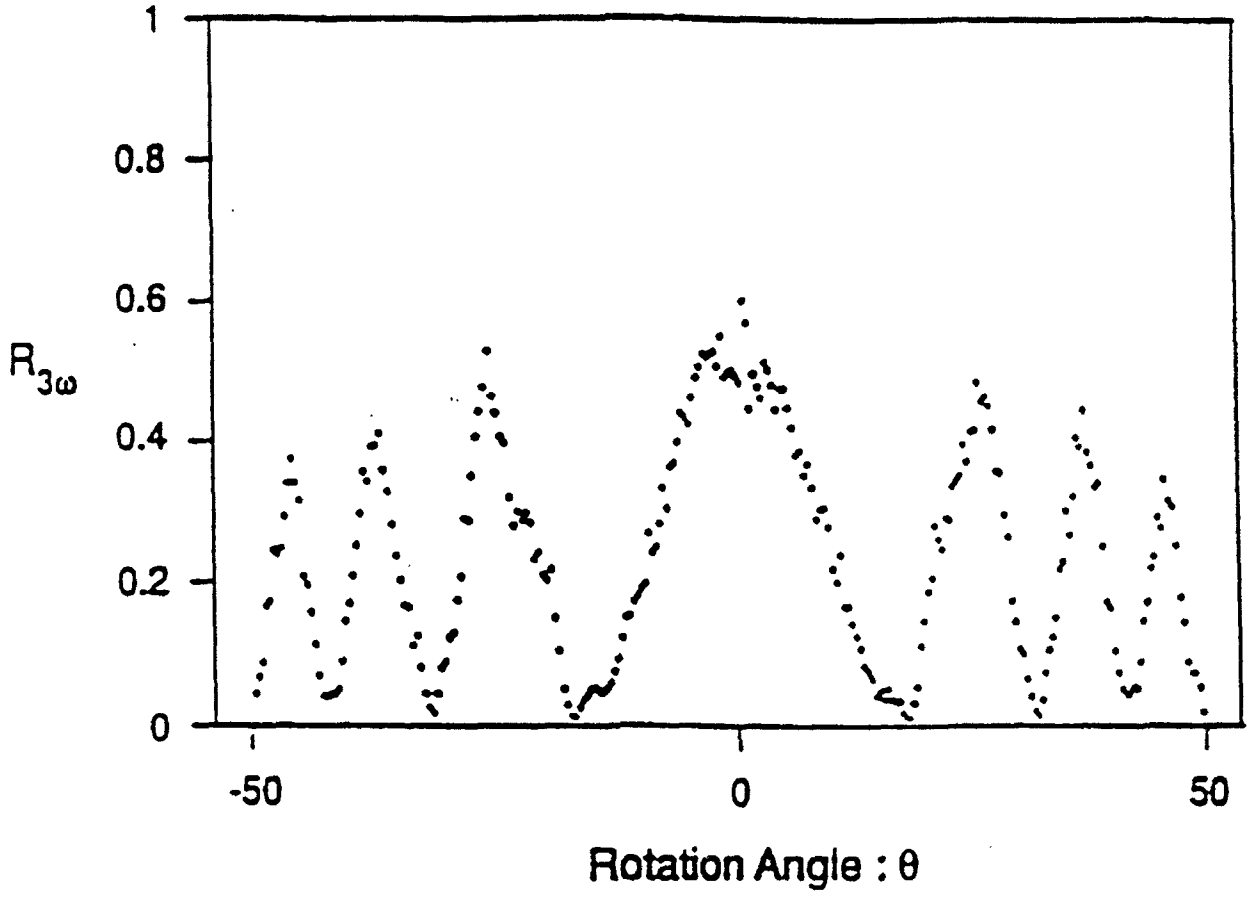

Fig. 1 Maker Fringe Patterns for a Nematic solution of PBT, with parallel polars and the incident polarization orthogonal to the director (e.g., arrangement V-H-V or H-V-H)

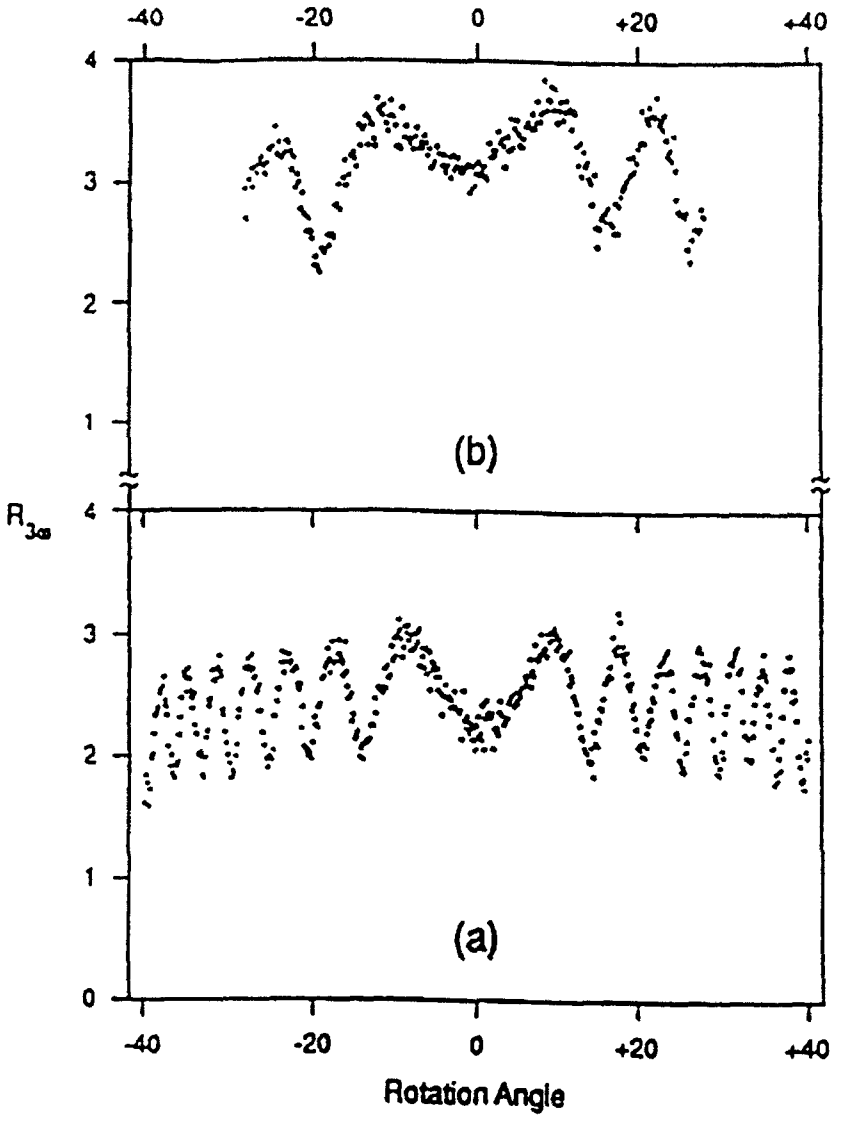

Fig. 2 Maker Fringe Patterns for a Nematic solution of PBT, with parallel polars and the incident polarization parallel to the director arrangement V-V-V (a) and H-H-H (b).

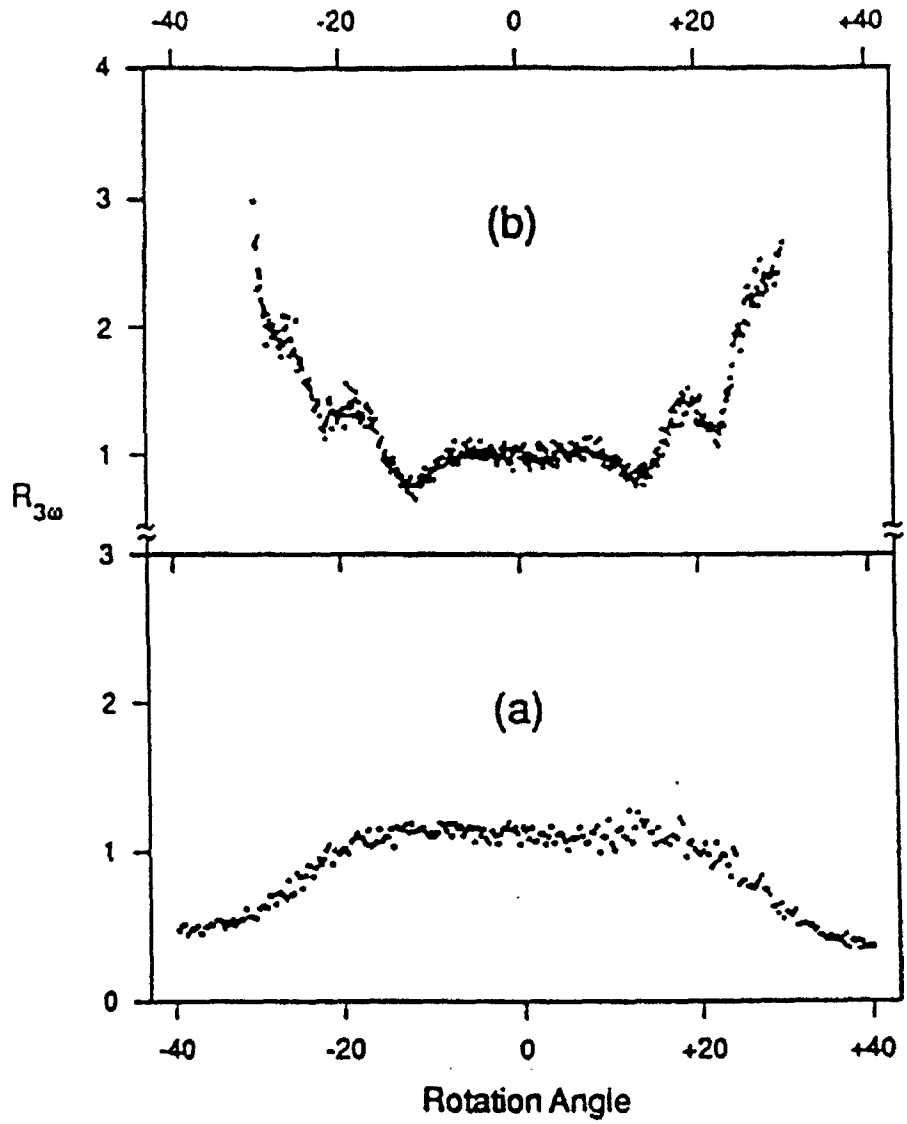

Fig. 3 Maker Fringe Patterns for a Nematic solution of PBT, with crossed polars and the incident polarization parallel to the director arrangement H-V-V (a) and V-H-H (b).

PART 2:REFRACTIVE INDICES DISPERSION AND ORDER OF LYOTROPIC LIQUID CRYSTAL POLYMERS

H. Mattoussi , M. Srinivasarao and Guy C. Berry

ABSTRACT

Refractive index measurements of polymer liquid crystals in the nematic phase are described. The technique used, applicable for any birefringent uniaxial medium, makes use of the birefringence to generate interference between the extraordinary and ordinary waves created after an incident plane polarized wave enters the crystal. The procedures are used to measure the ordinary and extraordinary refractive indices n_O and n_E, respectively, of nematic solutions of the rodlike poly(p-phenylene benzobisthiazole), PBT, for wavelengths from the visible to near infrared radiations. The measured birefringence is high, e.g., $|n_E - n_O|$ varies from 0.05 to 0.09 at 632.8 nm for polymer concentrations from $4x10^{-4}$ to $10x10^{-4}$ (g/cm^3). The birefringence is highly dispersive, and the dispersion is anisotropic: n_E has a more pronounced dispersion than n_O. The dispersion of the refractive indices (and consequently the birefringence) are correlated to the dichroism of these ordered media, as well as to the nonlinear optic properties subsequently achieved on these materials. The birefringence and its dependence on solute concentrations is discussed, with implications on the order parameter of these nematic solutions.

INTRODUCTION

The optical characterization of uniaxial, and nematic liquid, crystals requires the measurements of two refractive indices, the ordinary n_O and extraordinary n_E, defined, respectively, for plane waves traveling in the medium with polarization perpendicular or parallel to the optic axis of the system. Conventional thermotropic low molecular weight (lmw), and polymeric nematic liquid crystals have, in general, positive birefringence: $n_E - n_O > 0$, as opposed, for example, to discotic liquid crystals. [ref] On one hand, measurements of the birefringence $n_E - n_O$ of uniaxial lmw or polymeric liquid crystal media may be correlated to the order in these systems. [1-4] On the other hand, accurate measurements of the refractive indices n_O, n_E, n_{iso}(isotropic), and their dispersion are used to analyze harmonic generation signals, and the coupling between orientation and nonlinear optical (NLO) properties of such media. [5]

Poly(p-phenylene benzobisthiazole), PBT, is known to be rodlike. [6-8] Its solutions exhibit an isotropic to nematic transition if the rod concentration exceeds a temperature

dependent critical value c^*. This value is directly related to the aspect ratio L/D of the chain, where L and D designate the length and diameter of the rod, respectively. [9-12] Such media are known to have a moderate to high order parameter, S > 0.7 for instance. [13-16]

Because of its conjugated backbone, the nonlinear optical (NLO) properties of PBT are of great interest. [17] Studying such properties in the nematic phase is promising because of the high order of such solutions. As dissolution of this compound in strong acids is accompanied by protonation of the chain, [6-8,18] the NLO properties of PBT in solution will differ from those of the undiluted polymer. Measurement of the nonlinear optical susceptibilities $\chi^{(i)}(i = 2, 3)$, using a common technique, optical harmonic generation, requires accurate knowledge of the refractive index n of the medium and its dispersion n = n(ω or λ). [19-21] The dispersion must be known over a wide range of wavelengths, from UV-Visible to near infrared, for second and third harmonic generation (SHG and THG) techniques.

Here, we present refractive index measurements of nematic PBT solutions for several wavelengths: 500 nm < λ < 2000 nm. Two related methods have been used, involving transmission of polarized light: (1) Rotation of a plane parallel sample, and (2) conoscopic microscopy. The second method has been applied only for visible wavelengths. In the first section, analysis of the methods is given, followed by a description of the experimental arrangements. Then a brief description of the materials, the solutions, and the nematic monodomain preparation is given. In the last section, the discussion involves correlation between the birefringence and the order parameter in these nematic solutions, the dispersion of the refractive indices and its relation to the dichroism of these ordered media, and also some implications on NLO properties of nematic PBT solutions.

EXPERIMENTAL

Theoretical Background. Use of the medium birefringence to generate interference of light between the extraordinary and ordinary waves propagating in a crystal is a known procedure for optical characterization and identification of uniaxial materials. A plane light wave incident on a uniaxial crystal with its polarization at some angle to the optic axis of the medium may be decomposed into two secondary waves, traveling with speeds v'' = c/n'' (extraordinary) and v' = c/n' (ordinary), where n'' and n' are the extraordinary and ordinary refractive indices for the waves traveling in the crystal, and at an average direction eventually different from the principal axis of the medium, c is

PART 2:REFRACTIVE INDICES DISPERSION AND ORDER OF LYOTROPIC LIQUID CRYSTAL POLYMERS

H. Mattoussi , M. Srinivasarao and Guy C. Berry

ABSTRACT

Refractive index measurements of polymer liquid crystals in the nematic phase are described. The technique used, applicable for any birefringent uniaxial medium, makes use of the birefringence to generate interference between the extraordinary and ordinary waves created after an incident plane polarized wave enters the crystal. The procedures are used to measure the ordinary and extraordinary refractive indices n_O and n_E, respectively, of nematic solutions of the rodlike poly(p-phenylene benzobisthiazole), PBT, for wavelengths from the visible to near infrared radiations. The measured birefringence is high, e.g., $|n_E - n_O|$ varies from 0.05 to 0.09 at 632.8 nm for polymer concentrations from $4x10^{-4}$ to $10x10^{-4}$ (g/cm^3). The birefringence is highly dispersive, and the dispersion is anisotropic: n_E has a more pronounced dispersion than n_O. The dispersion of the refractive indices (and consequently the birefringence) are correlated to the dichroism of these ordered media, as well as to the nonlinear optic properties subsequently achieved on these materials. The birefringence and its dependence on solute concentrations is discussed, with implications on the order parameter of these nematic solutions.

INTRODUCTION

The optical characterization of uniaxial, and nematic liquid, crystals requires the measurements of two refractive indices, the ordinary n_O and extraordinary n_E, defined, respectively, for plane waves traveling in the medium with polarization perpendicular or parallel to the optic axis of the system. Conventional thermotropic low molecular weight (lmw), and polymeric nematic liquid crystals have, in general, positive birefringence: $n_E - n_O > 0$, as opposed, for example, to discotic liquid crystals. On one hand, measurements of the birefringence $n_E - n_O$ of uniaxial lmw or polymeric liquid crystal media may be correlated to the order in these systems. [1-4] On the other hand, accurate measurements of the refractive indices n_O, n_E, n_{iso}(isotropic), and their dispersion are used to analyze harmonic generation signals, and the coupling between orientation and nonlinear optical (NLO) properties of such media. [5]

Poly(p-phenylene benzobisthiazole), PBT, is known to be rodlike. [6-8] Its solutions exhibit an isotropic to nematic transition if the rod concentration exceeds a temperature

the speed of light in vacuum. When these waves recombine and interfere at the exit they have a light path difference δ (since $n'' \neq n'$). [22-24] A polarizer (P) may be used to define the incident polarization and an analyzer (A) to select the outgoing one, with an angle ψ between P and A. Let φ be the angle between the optic axis and the polarizer (or the incident polarization). A simple case used in the two methods discussed below has the optic axis n in the plane of the sample, and $\varphi = \pi/4$, as shown in Fig. 4a. The transmitted intensity I is then given by [22-24]:

$$I = I_{Max} \{ \cos^2 \psi - \sin 2\varphi \sin 2(\varphi - \psi) \sin^2 (\pi\delta/\lambda) \} \qquad (1)$$

where I_{Max} is the maximum possible transmission (I_{Max} depends on the transmission and reflection coefficients), and λ is the incident wavelength. [22-24] The oscillation of I with δ is enhanced by setting $\psi = \pi/2$ and $\varphi = \pi/4$ (or $-\pi/4$), see Fig. 4, so that:

$$I = I_{Max} \sin^2(\pi\delta/\lambda) \qquad (2)$$

Because of the anisotropy of the medium, when an incident light beam enters the medium with an incident angle ϑ, the extraordinary and ordinary waves inside the crystal have refraction angles, ϑ'_E and ϑ_O', respectively. Consequently, the waves travel with light path lengths, d_E' and d_O'. For the conditions described in Fig. 4 (planar geometry), the optical path difference δ is given by [22-24]:

$$\delta = d_E' (n'' - n_g \sin\vartheta \sin\vartheta'_E) - d_O' (n' - n_g \sin\vartheta \sin\vartheta'_O) \qquad (3)$$

with

$$d_E' = \frac{d}{\cos\vartheta'_E} \qquad \text{and} \qquad d_O' = \frac{d}{\cos\vartheta'_O} \qquad (4)$$

where d is the physical thickness of the sample, n''_g is the glass (cell wall) refractive index, and ϑ'_E and ϑ_O', are related to ϑ through Snell's law:

$$n'' \sin\vartheta'_E = n' \sin\vartheta'_O = n_{air} \sin\vartheta \qquad (5)$$

The refractive indices n'' and n' are angle dependent, and functions of the refractive indices n_O and n_E along the principal optical directions of the crystal, see below. [22-24]

The birefringence $|n_E - n_O|$ is always small compared to the refractive indices n_O and n_E ($|n_E - n_O| << n_O, n_E$). This allows the use of the approximation $\vartheta'_E \approx \vartheta'_O \approx \vartheta'$ in Eqn. 3 and 4, and permits an analytical expression for n'' – n'. [22-24] Thus, for small $|n_E - n_O|$

$$d_E' \approx d_O' \approx d' = d/\cos\vartheta' \tag{6}$$

and

$$\delta = \frac{d\,(n''_E - n_O)}{\cos\vartheta'} \sin^2\beta \tag{7}$$

where, using Eqn. 5 for the angles ϑ and ϑ':

$$\langle n_s \rangle \sin\vartheta' = n_{air} \sin\vartheta \tag{8}$$

with β is angle between the direction of propagation of the light beam and the optic axis **n** (see Fig. 4b,c). The angles ϑ' and β may be related trigonometrically. [22-24] For the cases with rays propagating in planes perpendicular or parallel to **n**, $\beta = \pi/2$ and $\beta = \pi/2 - \vartheta'$ respectively (see below). These cases correspond to the configurations for which **n** is either normal to or within the plane of incidence, respectively. The latter is defined as the plane containing the light beam and the normal to the sample surface (**s** in Fig. 5). The refractive index $\langle n_s \rangle$ for the average wave, may be written as a function of β (hence ϑ') and φ to give

$$\frac{1}{\langle n_s(\varphi,\beta)\rangle^2} = \frac{\sin^2\varphi}{{n_O}^2} + \cos^2\varphi\left(\frac{\cos^2\beta}{{n_O}^2} + \frac{\sin^2\beta}{{n_E}^2}\right) \tag{9}$$

The two cases introduced above, corresponding to $\beta = \pi/2$ (**n** normal to the plane of incidence) and $\beta = \pi/2 - \varphi'$ (**n** within the plane of incidence), are of great interest and simplicity. Together with the conditions for the angle φ ($+\pi/4$ or $-\pi/4$), they will be refered to as: geometry 1 for $\beta = \pi/2$ and $\varphi = \pi/4$, and geometry 2 for $\beta = \pi/2 - \vartheta'$ and $\varphi = -\pi/4$. For geometry 1 (**n** normal to the plane of incidence) Eqn. 7 becomes

$$\delta = \frac{d\,(n_E - n_O)}{\cos\vartheta'} \tag{10}$$

where ϑ' is given by Eqn. 8, with

$$\frac{1}{\langle n_s \rangle^2} = \frac{1}{2}\left(\frac{1}{n_O^2} + \frac{1}{n_E^2}\right) \tag{11}$$

The extraordinary and ordinary waves travel with respective refractive indices that are independent of the propagation angle ϑ', and the variation in δ reflects that of $d'(\vartheta')$ (Eqn. 6). For geometry 2 (n parallel to the plane of incidence), Eqn. 7 becomes

$$\delta = d\,(n_E - n_O)\cos\vartheta' \tag{12}$$

where ϑ' is given by Eqn. 8, with

$$\frac{1}{\langle n_s(\vartheta') \rangle^2} = \frac{1}{2}\left(\frac{1}{n_O^2} + \left(\frac{\cos^2\vartheta'}{n_E^2} + \frac{\sin^2\vartheta'}{n_O^2}\right)\right) \tag{13}$$

The two waves travel in the crystal with refractive indices dependent on ϑ'. The difference between the refractive indices for geometries 1 and 2 (Eqn. 11 and 13, respectively), may be written as

$$\frac{\langle n_s \rangle^2}{\langle n_s(\vartheta') \rangle^2} \approx 1 + \frac{n_E - n_O}{n_E}\sin^2\vartheta' \tag{14}$$

Since $|n_E - n_O| << n''_{E,O}$, and $\sin\vartheta' < 1$, $\langle n_s(\vartheta') \rangle$ is always close to $\langle n_s \rangle$. For example, the relative difference in Eqn. 14 is about 10% for a birefringence of $n_E \approx 1.5$, and at an angle $\vartheta' = \pi/2$; it is smaller for lower angles. The corresponding difference for the refractive indices $|\langle n_s(\vartheta') \rangle - \langle n_s \rangle| / \langle n_s(\vartheta') \rangle$ is about 5%.

Two additional assumptions lead to a simple analytical approximation for δ: when the inequalities $|n_O - n_E| << n_E, n_O$ hold, $\langle n_s \rangle$ can be approximated by the refractive index $\tilde{n}$ of the equivalent isotropic medium, defined as:

$$\tilde{n} = \frac{n_E + 2n_O}{3} \tag{15}$$

This approximation is reasonable when $|n_O - n_E|$ is small, eg., for geometry 1:

$$\frac{\langle n_s \rangle^2}{\langle n_s(\vartheta') \rangle^2} \approx 1 + \frac{3}{5}\frac{|n_E - n_O|}{n_O} \tag{16}$$

Thus, $\langle n_s \rangle$ and $\tilde{n}$ are close, even for a fairly large birefringence. For example, for the conditions described above for $\langle n_s \rangle$ and $\langle n_s(\vartheta') \rangle$ ($|n_E - n_O| \approx 0.2$) and the corresponding difference $\{\langle n_s \rangle - \tilde{n}\}/\tilde{n}$ is about 4%. Usually, the error committed by setting $\langle n_s \rangle$ and $\langle n_s(\vartheta') \rangle$ equal to $\tilde{n}$ in the data analysis for the birefringence is very small: it is less than 10% for an average value $\langle n_s \rangle \approx 1.5$ and at $\vartheta' = \pi/2$ (see Eqn. 17 and 18), and decreases for smaller angles.

A scan of the transmitted intensity as function of the angle of incidence ϑ provides an oscillating function. The minima occur at values ϑ_i for which the corresponding light path difference δ_i is an integer multiple of λ:

$$\delta_i = m_i\lambda = d\left(1 - \left(\frac{\sin\vartheta_i}{\langle n_s \rangle}\right)^2\right)^{1/2} |n_E - n_O| \qquad ;\text{Geom. 1} \qquad (17)$$

and

$$\delta_i = m'_i\lambda = d\left(1 - \left(\frac{\sin\vartheta_i}{\langle n_s(\vartheta_i) \rangle}\right)^2\right)^{1/2} |n_E - n_O| \qquad ;\text{Geom. 2} \qquad (18)$$

Experimentally, if d is known, either geometry can be used to determine the birefringence $|n_E - n_O|$, with $\langle n_s \rangle$ or $\langle n_s(\vartheta_i) \rangle$ replaced by $\tilde{n}$. However, a fit for the minima in the intensity curve I vs ϑ_i using the full expressions for $\langle n_s \rangle$ (or $\langle n_s(\vartheta_i) \rangle$), is required if values of the individual refractive indices are needed (see below). In the following, two methods are described to vary the propagation angle ϑ' (hence δ), with subsequent analysis of the transmitted intensity, to estimate the birefringence or/and the refractive indices of the material. More precisely, analysis of the intensity, using approximate solutions for δ, including the replacement of $\langle n_s \rangle$ by $\tilde{n}$, provides an estimate of $|n_O - n_E|$, whereas use of the full expressions can lead to an estimate of both n_O and n_E.

Method 1: Rotation of a Plane Parallel Slab. In this method, the variation of the phase difference is monitored as the path length in the crystal is varied by rotation of the sample with respect to the incident beam. The mean field director **n** is always in the plane of the sample. The axis of rotation is kept normal to the plane of incidence (Fig. 5). Geometry 1 corresponds to the conditions with the axis of rotation and the nematic director parallel, whereas geometry 2 corresponds to the case where they are perpendicular (Fig. 4a and 5a). The optical path difference δ is given by Eqn. 10 or 12,

and $\langle n_s \rangle$ is given by Eqn. 11 or 13, for the two cases, respectively. Rotation of the sample is accompanied by variation of β (hence ϑ') for geometry 2, but not for the geometry 1.

In practice, we proceed as follows: An estimate of $| n_E - n_O |$ is deduced from an experiment using geometry 1, together with the assumption $\langle n_s \rangle = \tilde{n}$. The latter is estimated from refractive index of the solvent and the increment $(\partial n/\partial c)$ for PBT solutions. [6-7] This $| n_O - n_E |$ is then used to fit the data for the same geometry, using Eqn. 10 and 11 for δ_i and $\langle n_s \rangle$, respectively, to obtain both n_E and n_O. The latter values may be checked by fitting the experimental data for geometry 2 to the full expressions for δ_i and $\langle n_s(\vartheta') \rangle$ (Eqn. 12 and 13). The values taken for n_E and n_O are those which provide the best fit for the experimental data for both geometries. Limiting the numerical fit to the experimental data for the geometry 1, which is simpler because $\langle n_s \rangle$ is independent of ϑ', will usually provide values for the individual refractive indices. However, it is useful to apply both geometries when initial estimate for n_E and n_O are poorly defined.

Method 2: Conoscopy . In the conoscopic mode, a crystal is examined in highly convergent light between crossed polars. [22-24] Because of the convergent nature of the beam, the optical properties of the crystal are observed simultaneously at many propagation angles in the medium. A schematic description of this method is shown in Fig. 4c.The path difference δ, is a function of the angle made by this ray on the cone of light. Consequently, when the transmitted beam is brought to interference in the focal plane of a lens, every point in this plane is associated with a direction of parallel rays entering and leaving the crystal (a finite angle on the cone).

For a planar nematic monodomain (**n** laying in the sample plane), the parameter δ is expressed as a function of the angles that a ray on the cone of light forms with respect to the cone axis, and to the optic axis **n**, ϑ' and β, respectively. Because the cone axis is taken normal to the sample surface, the angle of propagation of ray on that cone is also the angle of incidence. For small birefringence, δ is given by Eqn. 7. [22-24] For details about how the interference figure is formed for such media, see, e.g., references [23,24]. We simply recall that for a sample between crossed polars (P and A), with its optical axis at an angle $\pi/4$ with respect to P and A, the interference figure is a set of hyperboli isochromatic fringes centered around the cone axis if **n** is orthogonal to the microscope optic axis. [22-24] The interference figure reflects the symmetry of the medium: point inversion and mirror reflection around **n**. The set of fringes rotates with **n** as the latter is rotated within the the sample plane, and disappears when **n** is parallel to either P or A. [25] Scanning the corresponding values of ϑ' on the cone of light and within the focal

plane, reveals oscillations of the intensity as predicted by Eqn. 2. A simplification of the expression for δ (Eqn. 7) arises for all directions of propagation within planes corresponding to geometries 1 and 2, to give Eqn. 10 and 12, respectively. A more complex formulation is required if an arbitrary direction of propagation is chosen, and an extra dependence on β emerges. [25] In practice, the angle ϑ' is determined by referring to the numerical aperture of the lens, so that each point on the conoscopic figure can be related to an angle ϑ'. In principle, both geometries ($\beta = \pi/2$ and $\beta = \pi/2 - \vartheta'$) can be used to estimate the birefringence, given the sample thickness d, and replacing $\langle n_s \rangle$ by $\tilde{n}$. Only the first case $\beta = \pi/2$, where δ and $\langle n_s \rangle$ are given by Eqn. 10 and 11, respectively, is used in the present study, to provides values for the birefringence.

Experimental Arrangements 1.Rotating Sample. The experimental set-up is shown schematically in Fig. 5. For the visible radiation, a cw laser (Spectra Physics) was used as the light source, (Fig. 5a). Two wavelengths were used: $\lambda = 514.5$ nm with an Ar–ion laser and $\lambda = 632.8$ nm with a He–Ne laser. A Nicol prism (CVI Laser Corp.) was used to provide a polarized incident light beam. A rhomb rotater (Karl Lambrecht Inc.) was used as the polarizer (P), and a polarizing film was used as an analyzer (A), with an angular resolution of 0.1ϑ. A silicon photodiode connected to a chart recorder was used to record the transmitted intensity.

For the infrared (I.R.) region, the light source was a pulsed Nd: YAG laser (Fig. 5b). It provides an intense nanosecond pulse at $\lambda = 1064$ nm. A Raman cell was used as the source for the other I.R. wavelengths. [26] Pumped with the incident YAG signal, pulsed signals at $\lambda = 1542$ nm and $\lambda = 1907$ nm (Stokes components) were generated from methane and hydrogen gases, respectively. The pulse duration, the incident radiation wavelength, and the quantum efficiency of the photomultiplier caused a problem in detection. To circumvent these limitations, the I.R. beam exiting the crystal was used as a source to generate optical harmonic(s) on passage through a suitable material (component S_1 in Fig. 5b). [19-21,26,27] The signal at 2ω or 3ω (for second and third harmonic generation processes) always falls within the UV–visible region and is therefore easy to detect. In addition to the polarizer and analyzer used for experiments with visible radiation, an IR bandpass filter (F_2 placed after the sample) is used to select the signal at · after the sample, eliminating harmonic signal generated from the sample, which also oscillates with ϑ, though with different dependence on ϑ (i.e., Maker Fringes). [19-21] Two extra filters (F_3), a visible bandpass and an interference filter, are needed to select the signal at 2ω (or 3ω) after the harmonic generation sources (Fig. 5b). The signal at 2ω (or 3ω) is detected using a photomultiplier tube, then digitized through the use of an ADC system [CAMAC]. The sample signal is normalized by the signal for

the reference to account for fluctuations in the pulsed source intensity (see Fig. 8b). Since the harmonic signals are proportional to a power of the incident intensity, e.g., $I_{2\omega} \propto (I\omega)^2$, and $I_{3\omega} \propto (I\omega)^3$, these signals reproduce exactly the periodicity of I_ω on the rotation angle ϑ. [19-21] Consequently, the data analysis for the variation of intensity with the angle of incidence ϑ, is identical to that discussed above. The second harmonic process was found to provide sharper minima, and consequently better angular resolution, because of the dependence on I_ω (I_ω^2 instead of I_ω^3).

2. Conoscopy. An optical microscope (Leitz) equiped with a set of polars placed before and after the sample is used in this method. The same arrangement is often used to examine liquid crystal samples. [12,28] However, an extra set of lenses is required for conoscopic use. A short focal lens is used before the sample to provide a converging light beam with a large cone angle (Numerical Aperture: $\sin \vartheta''_{max} = 0.6$). Another lens (Bertrand lens) is required to bring the interference figure to the plane of observation (Fig. 5c). Experimentally, the distance between two fringes is measured using a micrometer mounted on the microscope. This distance is converted to the corresponding angles on the cone, using the numerical aperture of the lens placed before the sample. Details on the experimental arrangement can be found in general review(s) on optical microscopy. [29-31] The spacing between fringes could also be measured from a photographic picture or the screen of a videorecording of the interference figure, knowing the experimental conditions.

Materials And Sample Preparation. The polymer liquid crystal used for this present study is formed by solutions of poly(p-phenylene benzobisthiazole), PBT. The material was provided as solutions in polyphosphoric acid (PPA) by SRI International (Stanford CA) through the courtesy of Dr. J. F. Wolfe. The synthesis procedures are described elsewhere. [6-1,18] The PPA solution was diluted in methane sulfonic acid (MSA), precipitated in methanol, and thoroughly washed with water, freeze-dried, and stored in a dry atmosphere.

Freshly distilled MSA was used to prepare the solutions. Solution preparation was carried out under nitrogen atmosphere to avoid contamination by atmospheric moisture. The solutions were stirred (using a magnetic stirrer) for several days, until homogeneous media were formed. This process is slow because of the high viscosity of these solutions ($\eta > 1000$ poise). We used PBT with weight average molecular weight $M_w = 34{,}000$, determined by light scattering measurements. [7,11] This corresponds to a weight average rod length of 160 nm, and an index of polymerization of 140. An aspect ratio of L/D "Ñ" 300 (where L stands for the rod length and D is the nominal diameter) provides

a critical concentration for the isotropic to nematic transition of about w ≈ 0.03 wt (c ≈ 4.44×10^{-2} (g/cm^3)) in MSA solutions. [6-12]

Liquid crystal monodomains were obtained using flat cells of 200, 300, and 350 Øm thickness with good optical quality ($\lambda/4$ surface flatness) provided by Hellma Cells Inc. The same cell(s) and, consequently, the same samples were used for NLO harmonic generations measurements. Nematic monodomains were prepared as follows. The solution was extruded into the sample through a luer joint. Prealigned rods adsorb on the surface walls, and orientational order propagates through the bulk of the sample on subsequent annealing. [6-12] Nevertheless, this process is not always sufficient to provide a monodomain structure. Good quality monodomains, useful for optical purposes, are obtained by applying a strong magnetic field (H ≈ 4 Tesla) to freshly prepared samples for several hours, with H parallel to the sample walls and to the initial flow direction. The monodomains thus reached are stable indefinitely (provided they are kept dry). All measurements were done on monodomains which had been outside the magnetic field for several hours. Consequently, no direct effects of the aligning field on the present data are expected, since the sample had previously reached equilibrium outside the field before the measurements were taken. The alignment quality of the planar sample subsequently obtained was checked by looking at the extinction properties of the transmitted white light between crossed polars: full extinction occurs when n is parallel to either analyzer (A) or polarizer (P), as done for nematic lmw liquid crystals. [1-4] Another check was provided by the conoscopic figures obtained for these mondomains (Fig. 9b). As outlined in the previous section for method 2, the point inversion and mirror reflection around In! are observed. This was always compared against conoscopic figures given by a conventional uniaxial crystal (quartz) used as a reference [9] The quartz crystal is a flat slab of 4190 μm thickness, with its optical axis laying within the sample plane. It served for reference measurements for both methods used in the present study.

RESULTS

A typical interference figure for a rotating plane parallel sample is given in Fig. 6, showing the oscillatory function predicted by Eqn. 2 for I(ϑ). The angles ϑ_j for the minima, as well as their number for a given rotation interval, depends on the geometry (n parallel or perpendicular to the rotation axis), the wavelength λ, the sample thickness d, and the medium birefringence. More oscillations occur for smaller λ, larger d and/or $|n_E - n_O|$. Similar plots for the intensity $I_{2\omega}$ (and $I_{3\omega}$ vs. ϑ for infrared radiation (pulsed source) are shown in Fig. 7. Each point on the graph corresponds to a value of the angle

ϑ, and to an intensity averaged over 10 pulses. Fig. 7a,b,c refer to the PBT monodomain, whereas Fig. 7d,c correspond to the quartz crystal. As mentioned above, better resolution for the minima location is obtained when second harmonic generation (SHG) is used (compare Fig. 7a, b, d and Fig. 7c,d). However, a third harmonic generation process was needed for λ = 1907 nm, as $\lambda(2\omega)$ = 953.5 nm falls within the I.R. region, and is, therefore, not detected by the photomultiplier used.

Conoscopic interference figures are shown in Fig. 8 for a nematic planar monodomain (solution with w ≈ 0.0483 (wt) or c ≈ 0.0715 (g/cm^3)) together with the corresponding interference pattern for the quartz planar crystal, at the He-Ne red line (λ = 632.8 nm). We checked to insure that the interference figure rotates with the mean field director as the sample is rotated within its plane, P and A being fixed and crossed. [12,25] As expected, the fringe spacing is invariant to such an operation, whereas the contrast between the dark and bright fringes varies with rotation of **n** with respect to its initial direction (**n** at 45° with respect to P), or when the angle between P and A is changed, keeping **n** fixed. The fringes disappear when **n** is parallel to either A or P (see the previous section).

Values for the birefringence $|n_E - n_O|$, using the approximate expression for δ (Eqn. 9 and 10) and $\langle n_s \rangle = \tilde{n}$ to fit the minima in I vs. ϑ curves for geometries 1 and 2 (Method 1), are reported in Table 1 for the different wavelengths used. We also report, in the same table, values for $|n_E - n_O|$ using Method 2 and Eqn. 10 (with $\langle n_s \rangle = \tilde{n}$) for visible He-Ne radiation, λ = 632.8 nm. The corresponding values measured for the quartz slab using the same procedures are also given, together with those reported in the literature.[32] For the quartz reference slab, it is important to notice the agreement between the values of $|n_E - n_O|$ measured using method 1, with its two geometries, and those reported in the literature. In addition, the values deduced for a PBT monodomain using the approximate fit for each geometry are also in agreement for both methods, showing the usefulness of the approximations made for the estimation of the birefringence. Nevertheless, the values provided by geometry 2 (Method 1) are slightly larger than those obtained with geometry 1. This can be attributed to the approximation used for $\langle n_s \rangle$, and neglect of its dependence on ϑ' (Eqn. 13).

The use of the full expression for $\langle n_s \rangle$ (Eqn. 11, geom. 1) in the data analysis (numerical fit) provides values for the individual refractive indices n_O, n_E and the corresponding $|n_E - n_O|$ as summarized in Table 2. A fit for the geometry 2, and Eqn. 13 for $\langle n_s(\vartheta') \rangle$ provided similar values for the refractive indices. The final values for the birefringence $|n_O - n_E|$, deduced from the numerical fit, are slightly smaller than those deduced from

the "approximate" analysis for both geometries 1 and 2. However, they are in much better agreement with those provided by the anaysis for geometry 1: $|n_O - n_E|$ is about 5% smaller than what has been deduced previously (approximate analysis in geom. 1) for all wavelenghts.

DISCUSSION

The birefringence shows pronounced dispersion for visible wavelengths: $|n_E - n_O|$ increases by a factor of about 2.5 when λ decreases from 1 μm to 0.5 μm, whereas its increase is less than 20% in the range $1 < \lambda < 2$ μm (see Fig. 9). The dispersion of $|n_E - n_O|$ for the lower wavelengths is slightly more pronounced than reported for conventional liquid crystals (pure materials): $|n_E - n_O|$ increases by a factor of 2 for MBBA for λ in the visible spectrum, for instance. [33] However, the analysis of the variation of the individual refractive indices n_E and n_O shows that the dispersion is more pronounced for the extraordinary refractive index only at wavelengths in the visible spectrum (Fig. 10). Isotropic solutions of PBT in MSA are known to have a modest absorption band centered around 436 nm, and their ordered nematic monodomains are dichroic, with an enhanced dichroism for smaller wavelengths in the visible spectrum. [12] For instance, the transmission coefficient of a plane polarized light is about two times larger for polarization normal to **n** ($\mathbf{E} \perp \mathbf{n}$) than the case where **E** and **n** are parallel ($\mathbf{E} \parallel \mathbf{n}$), at the green line ($\lambda$ = 514.5 nm) and for a nematic monodomain of 300 Øm thickness and a polymer concentration w = 0.055 wt. [12] Therefore, the strong dispersion of $|n_E - n_O|$ for small λ, may be mainly attributed to the effects on n_E, and a meaningful discussion of the dispersion ought to consider each refractive index separately.

For many organic molecules, the dispersion may be represented by an empirical expression (similar to the Cauchy formula), based on a calculation using the Lorentz oscillator. For frequencies ν far from an absorption band centered around ν_m, this relation reduces to [23,24,34]

$$R = n^3 - 1 \approx \frac{K\nu_m^2}{\nu_m^2 - \nu^2} \qquad (19)$$

where $K\nu_m^2$ is an average oscillator strength. The latter results from an integration over all contributing individual oscillators in the molecule, and is related to the absorption coefficient of the medium. Eqn. 19 predicts a straight line for a fit of $(1/R)$ vs. ν^2. Such a relation has been used fairly successfully to interpret the dispersion of the refractive

index data for many dense systems and at wavelengths far from the absorption peak ν_m. [34] For uniaxial materials, Eqn. 19 may be used for refractive indices n_E and n_O, with constants ν_m and K for each. Plots for the experimental values for (1/R) as a function of ν^2 are shown for both n_E and n_O in Fig. 11. Agreement with Eqn. 19 is observed for both cases over the range of wavelengths scanned, giving $\nu_m \approx 12 \times 10^{14}\ s^{-1}$ (or ($\lambda_m \approx$ 250 nm) for n_E, $\nu_m \approx 15 \times 10^{14}\ s^{-1}$ (or ($\lambda_m \approx$ 200 nm) for n_E, and K = 0.27 for both n_E and n_O. The emergence of two separate absorption frequencies, $(\nu_m)_E$ and $(\nu_m)_O$, in the UV region of the spectrum, suggests that PBT ordered solutions have two close by spaced absorption lines at lower wavelengths. This may be the reflected in the dichroism of these monodomains observed for visible radiation. The $K\nu_m^2$ value for n_E and n_O, which are associated with dichroism in the absorption properties for these monodomains in the UV, suggest a higher absorption coefficient for the ordinary case. By contrast, around the absorption maximum in the visible (436 nm) the extraordinary is more strongly absorbed, but with an extinction coefficient less than that in the UV. Apparently the latter dominates the dispersion of the refractive indices.

The present dispersion data and their strong anisotropy have direct implication on the NLO data for these ordered solutions using third harmonic generation (THG) technique. An important parameter in such measurements, crucial for the signal analysis, is the coherence length, defined, at normal incidence as: [19-21]

$$\ell_c(\vartheta=0) = \frac{\lambda_\omega}{2m\,|n_{3\omega} - n_\omega|} \qquad (20)$$

where m is 2 or 3 for second or third harmonic generations respectively. It characterizes the distance below which the interference of the harmonic signal is constructive. The dispersion is also involved in the estimation of the nonlinear optical coefficient $\chi^{(m)}$, where the factor $\chi^{(m)}/[n_{3\omega}^2 - n_\omega^2]^2$ is the one actually extracted from the harmonic signal. [19-21] The data for the dispersion of both n_E and n_O in the analysis of THG data collected for ordered PBT solutions discussed in Part 1 of this report.

The order parameter S, defined as: [1-4]

$$S = \left\langle \frac{3\cos^2\Omega - 1}{2} \right\rangle \qquad (21)$$

characterizes the "degree" of alignment of the rods in nematic media. Here Ω is the angle made by the rods with respect to the mean field direction, and the bracket designates an

ensemble average. In lyotropic media, such as PBT nematic solutions, S is mainly dependent on the solute concentration, but also on the temperature. The order can be related to the optical properties of the medium, thus to the birefringence, $|n_E - n_O|$, as has been done for conventional low molecular weight liquid crystals. [1-4,36,37] Over the concentration range of interest here, this relation reads:

$$|n_E - n_O| \approx |n_E - n_O|_{mol} S \Phi \qquad (22)$$

where Φ is the solute volume fraction, and the "molecular birefringence $|n_E - n_O|_{mol}$ may be approximated by

$$|n_E - n_O|_{mol} \approx \frac{2\pi(n_s^2 + 2)}{3n_s} \frac{N_a \rho |\gamma_{||} - \gamma_\perp|}{M} \qquad (23)$$

with ρ the solvent density, and $\gamma_{||} - \gamma_\perp$ the difference between the principal molecular polarizabilities parallel and perpendicular to the rod axis, respectively. The parameter $|n_E - n_O|_{mol}$ is equal to the measured birefringence for both S and Φ equal to 1. Eqn. 23 is based on the expression:

$$\frac{4}{3} N\alpha_j \approx \frac{(n_j^2 - 1)}{\langle n^2 \rangle + 2}; \qquad j = E,O \qquad (24)$$

for the extradinary and ordinary components of the polarizability, with

$$\langle n^2 \rangle = \frac{n_E^2 + 2n_O^2}{3} \qquad (25)$$

Values of the birefringence $|n_E - n_O|$ for $\lambda = 632.8$ nm, where absorption is small, are reported for a few concentrations in Table 3. The corresponding plot is shown in Fig. 12, and a linear curve results, for which

$$|n_E - n_O| \approx 1.46 S (\Phi - 0.002); \qquad \text{for } \Phi > 1.1\Phi^* \qquad (22)$$

On the basis that S should not decrease with increasing Φ, the data in Fig. 12 give S at Φ^* equal to $1 - 0.002/\Phi^*$, or 0.94, and $|n_E - n_O|_{mol} = 1.46$ [6,7]. By comparison, an analysis for $|n_E - n_O|_{mol}$ for PBT in MSA based on $|\gamma_{||} - \gamma_\perp|$ determined in dilute solution gives $|n_E - n_O|_{mol} = 1.55$. [6,7,9,10,39]

The behavior in Fig. 12 suggest that S is close to 0.94 over the entire range of concentration studied. This is particularly high since the smallest concentration studied is very close to the critical value Φ^*, for the threshold of the isotropic to nematic transition, e.g., $\Phi/\Phi^* \approx 1.1$. The result, S constant, over a fairly wide range of concentations ($1 < (\Phi/\Phi^*) < 2.5$), is new. The order parameter has been found to depend on φ for other lyotropic media, and the value of S at Φ slightly above Φ^* is smaller than that reported here. [b13-16] For example S = 0.75 was reported for aqueous TMV solutions with $\Phi/\Phi^* \approx 1.05$ with S reading 0.95 for $\Phi/\Phi^* = 1.5$, whereas a value of about 0.7 was reached for PBLG at $\Phi/\Phi^* \approx 1.2$ with S = 0.8 for $\Phi/\Phi^* = 1.8$. [13-16] The charged, rodlike nature of PBT, and the high aspect ratio ($L/D \approx 300$) may enhance the order in the solutions. [40,41]

The birefringence measured for PBT ordered solutions is high. For example, it is much higher than that reported for ordered solutions of poly(π-benzyl glutamate), PBG, poly(π-benzyl-L-glutamate), PBLG, or tobacco mosaic virus, TMV at similar concentrations, e.g., for $\Phi/\Phi^* < 2.5$, $|n_E - n_O| \leq 0.005 \times 10$ for both TMV and PBLG for example. [13-16] These smaller values for PBLG, TMV, etc., may be attributed in part to the helocoidal structure of these molecules. The normalized birefringence for pure PBT material $|n_E - n_O| / \Phi$ obtained here are, however, higher than $|n_E - n_O|$ for some conventional thermotropic liquid crystals such as PAA or MBBA for example, where $|n_E - n_O|$ reaches values about 0.3 - 0.4 for the latter for temperatures far from the clearing point; a weaker order parameter characterizes these media: $S \approx 0.5 - 0.6$. [33,42-47] .

CONCLUSION.

The results reported above exhibit an unexpected insensitivity of the order parameter S on the volume fraction Φ of the rodlike solute PBT over the range $1.1 < \Phi/\Phi^* < 2.5$. Furthermore, S is deduced to be surprisingly close to unity over the entire concentration range studied. Here, S is deduced from the dependence of the birefringence $|n_E - n_O|$ on Φ, and therefore requires a number of assumptions discussed in the preceding. It would be desirable to confirm the conclusions reached here on the variation of S with Φ using an independent technique, e.g., measurement of the diamagnetic susceptibility. A possible reason for the unexpected behavior may be related to the way in which the aligned solutions were formed, making used of an aligning magnetic field on a nematic solution confined between parallel plates. Studies are in progress to assess whether S might be increased from its normal equilibrium value for the bulk nematic PBT solution under such conditions. If not, it will be of interest to consider whether other special factors might contribute to the observed behavior for $|n_E - n_O|$, and the deduced

behavior for S. Candidate factors would include the effects of electrostatic interactions among the protonated PBT solute chains.

The dispersion of the birefringence $|n_E - n_O|$ over the spectral range studied (514 to 1907 nm) is not considered to be abnormal, but is due to the different dispersions of the ordinary and extraordinary refractive indices. Thus, although both can be fitted by the same expression over the range studied, one of the two adjustable parameters in that expression differs for n_E and n_O. These parameters lie in the range normally experienced with organic molecules in both cases. Measurements in the visible spectral range show that nematic solutions are strongly dichroic, with light polarized along the extraordinary axis being more strongly absorbed than that polarized along the ordinary axis. [12] Nevertheless, naive interpretation of the parameters used to fit the dispersion data suggest a larger extinction coefficient for light polarized along the ordinary axis for wavelengths in the ultraviolet range. Owing to the magnitude of the extinction coefficient for the latter wavelengths, and the thickness of the samples, no direct information is available as yet on the dichroism in the ultraviolet for nematic solutions of PBT. Although not novel in concept, we are unaware of previous reports in which the procedures used here to measure n_E and n_O over a wide range of wavelengths has been so implemented. .

REFERENCES

1. de Gennes, P. G., *The Physics of Liquid Crystals*, Clarendon Press, Oxford (UK) (1974).
2. Stephen, M. J., Straley, J. P., *Rev. of Mod. Phys.* **46**, 617 (1974).
3. Chandrasekhar, S., *Liquid Crystals*, Cambridge University Press, Cambridge (1977).
4. De Jeu, W. H. *Physical Properties of Liquid Crystalline Materials"*, Gorden and Breach Science Publishers, New York (1980).
5. Mattoussi, H., Berry, G. C., *Polym Press,* (Am. Chem. Soc., Div. Polym. Polymer Sci) preprints **32 (3)**, 690 (1991)
6. Lee, C. C., Chu, S. G., Berry, G. C., *J. Polym. Sci. Polym. Phys. Ed.*, **21**, 1573 (1983).
7. Metzger Cotts, P., Berry, G. C., J. *Polym. Sci. Polym. Phys. Ed.*, **21**, 1255 (1983).
8. Furukawa, R., Berry, G. C., *Pure & App. Chem.*, **57**, 913 and Ref. therein (1985).
9. Venkatraman, S., Ph.D. Dissertation, Carnegie Mellon Univ., (1981).
10. Tsai, H-H., Ph.D. Dissertation, Carnegie Mellon Univ., (1983).
11. Sullivan, V., Ph.D. Dissertation, Carnegie Mellon Univ., (1990).
12. Srinivasarao, M., Ph.D. Dissertation, Carnegie Mellon Univ., (1990).
13. Murthy, N. S., Knox, J. R., Samulski, E. T., *J. Chem. Phys..*, **65**, 4835 (1976).
14. Oldenbourg, R., Wen, X., Meyer, R. B., Caspar, D.L.D., *Phys. Rev. Lett.*, **61**, 1851 (1988).
15. Leadbetter, A. J., In *The Molecular Physics of Liquid Crystalss*, Ed. by Luckhurst, G. R., and Gray, G. W., Academic Press, N.Y. (1979).
16. Dupre, D. P., and Lin, F. M, *Mol. Cryst. Liq. Cryst.*, **75**, 217 (1981).
17. Rao, D. N., Swiatkiecz, J., Chopra, P., Ghoshal, S. K., Prasad, P. N., *App. Phys. Lett.*, **48**, 1187 (1986).
18. Wei-Berk, C., Berry, G. C., *J. App. Polym. Sci., Polym. Phys. Ed.*, in press.
19. Kurtz, S. K., In *Quantum Electronics*, Rabin, H., and Tang C. L., Eds., **Vol. 1**, Part A, Ch. 3, Academic Press, N.Y. (1975).
20. Shen, Y. R., *The Principles of Nonlinear Optics*, J. Wiley, N.Y. (1984).
21. Yariv, A. *Optical Electronics*, Holt, Rinehart and Winston, **3rd ed.**, New York (1985).
22. *Oeuvres Completes d' Auguste Fresnel*, De Senarmont, H., Verdet, E., Fresnel, L., Publishers, **Vol. 1**, Imprimerie Imperiale, Paris (1866).
23. Born, M., Wolfe, E., *Principles of Optics*, **6th ed.**, Pergamon Press, Oxford (U.K.), (1980).
24. Bruhat, G., *Optique*, Masson & Cie Editeurs, **5th ed.**, Paris (1965).
25. Cladis, P. E., *Phys. Rev. Lett.*, **28**, 1629 (1972).
26. Kajzar, F., Messier, J., *Phys. Rev. A*, **32**, 2353 (1985).

27. *Nonlinear Optical Properties of Organic Molecules and Crystalss*, Chemla, D. S., Zyss, J., De Senarmont, H., Verdet, E., Fresnel, L., Publishers, **Vol. 1 & Vol. 2** , Academic Press, N.Y. (1987).
28. Demus, D., Richter, L., *Texture of Liquid Crystals*, Springer and Verlag, Leipzig, Ref. 1. (1978);
29. Don Bloss, F., *An Introduction to Methods of Optical Crystallography*, Holt, Rienhart and Winston, New York (1961).
30. Ditchburn, R. W., *Light*, Interscience Publishers (1963)
31. McCrone, W. H., McCrone, L. B., Delly, J. G., *Polarized Light Microscopy*, McCrone Research Institute, Chicago (1987).
32. Wolfe, W. L., In *Handbook of Optics*, Optical Society of America, Driscoll, W. G., Vaughan, W., Eds., Mc Graw Hill, Section 7, (1978).
33. Kuczynski, W., Stryta, B., *Mol. Cryst. Liq. Cryst.*, **31,** 267 (1975).
34. Kauzmanm, W., *Quantum Chemistry. An Introduction*, Academic Press Inc., NY, Chap. 15, (1957).
35. Mattoussi, H., and Berry, G. C., to be submitted for Publication.
36. Chang, R., *Mol. Cryst. Liq. Cryst.*, **30,** 155 (1975).
37. a. Chatelain, P., *Bull. Soc. Fr. Mineral Crist.*, **50,** 280 (1937), and **78,** 262 (1955).
    b. Chandrasekhar, S., Krishnamurti, D., Madhusudana, N. V., *Mol. Cryst. Liq. Cryst.*, **8,** 45 (1969).
38. Vuks, M. F., *Opt. Spec.*, **20,** 361 (1964).
39. Tvetskov, V. N., Eskin, V. E., Frenkel, S. Y., *Structure of Macromolecules in Solutions*, English Translation, National Lending Library for Science and Technology, Boston , **Vol. 1,** (1971).
40. Onsager, L., *Ann. N.Y. Acad. Sci.*, **51,** 627 (1949).
41. Flory, P. J., Ronca, G., *Mol. Cryst. Liq. Cryst.*, **54,** 289 and 311 (1979), and Ref. therein.
42. Chatelain, P., Germain, M., *C. R. Aca. Sci.*, Paris, **259,** 127 (1964).
43. Chandrasekhar, S., Madhusudana, N. V., *J. Phys*, Coll. C4. (Les Ulis), **30,** 24 (1969).
44. Brunet-Germain, M., *C. R. Aca. Sci.*, Paris, **B?71,** 1075 (1970), *Mol. Cryst. Liq. Cryst.*, **11,** 289 and Ref. therein (1970).
45. Balzarini, D. A., *Phys. Rev. Lett.*, **25,** 914 (1970).
46. Hanson, E. G., Shen, Y. R., *Mol. Cryst. Liq. Cryst., 36,* 193 (1976).
47. Laurent, M., Journeaux, R., *Mol. Cryst. Liq. Cryst.*, **36,** 171 (1976).

Table 1: Birefringence for PBT Monodomans and Quartz Crsytal

	$\lvert n_E - n_O \rvert$						
	Method 1 (Sample Rotation)				Method 2 (Conoscopy)		
	GEOMETRY 1		GEOMETRY 2				
wavelength λ/nm	PBT d = 370μm c = 0.0813 g/cm³	Quartz d = 4190μm	PBT d = 370μm c = 0.0813 g/cm³	Quartz d = 4190μm	PBT d = 370μm c = 0.0758 g/cm³	Quartz d = 4190μm	Quartz Lit.
514.5	0.125 ±0.002		0.137±0.002				0.00924
632.8	0.0788±0.005	0.0091	0.083±0.005	0.0093	0.072	0.009	0.00911
1064	0.0492±0.000	0.0087	0.051±0.0002	0.0088			0.00878
1542	2	0.0084		0.00857			0.00849
1907	0.0452±0.000	0.0082					0.0082
	5						
	0.045 ±0.001						

Table 2: Refractive Indices n_E and n_O, and the Birefringence $\lvert n_E - n_O \rvert$

	PBT in MSA c = 0.08 gm/cm³			Quartz		
wavelength λ/nm	n_O	n_E	$\lvert n_E - n_O \rvert$	n_O	n_E	$\lvert n_E - n_O \rvert$
514.5	1.5270	1.6480	0.1210			
632.8	1.4990	1.5770	0.0780	1.54330	1.55244	0.00914
1064	1.4389	1.4888	0.0499	1.53430	1.54304	0.00874
1542	1.4340	1.4801	0.0461	1.52860	1.53708	0.00848
1907	1.4294	1.4743	0.0449	1.52080	1.52902	0.00822

Table 3: Birefringence $\lvert n_E - n_O \rvert$ of PBT in MSA

100c/g cm^{-3}	$\lvert n_E - n_O \rvert$	Method

4.93	0.047	Rotating sample; Geo. 1
4.93	0.046	Conoscopy
6.30	0.059	Conoscopy
7.15	0.0676	Rotating sample; Geo. 1
7.15	0.067	Conoscopy
7.58	0.078	Conoscopy
8.13	0.0788	Rotating sample; Geo. 1
9.88	0.094	Conoscopy

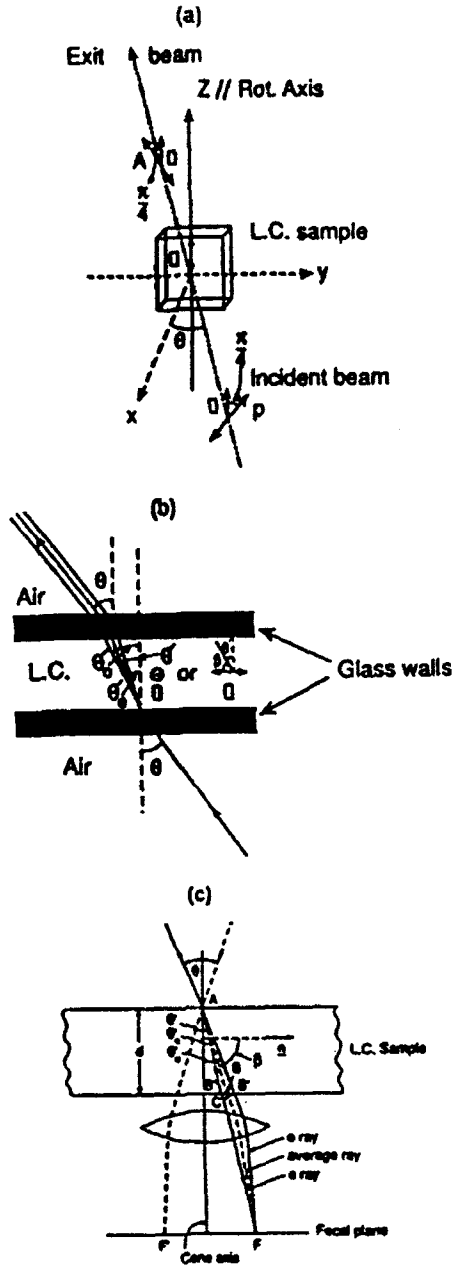

Fig. 4 Schematic description of the sample and the polarizations configuration for the interference process. (a) Geometry 1 ($\varphi = \pi/4$) in the first method , a perpspective view is given. (b) Light path(s), ordinary and extraordinary, in the crystal with the corresponding refraction angles ϑ'_E and ϑ'_O. (c) Schematic diagram for the diverging beam with the different waves in the crystal for the second method; **n** is kept within the plane and normal to the cone axis.

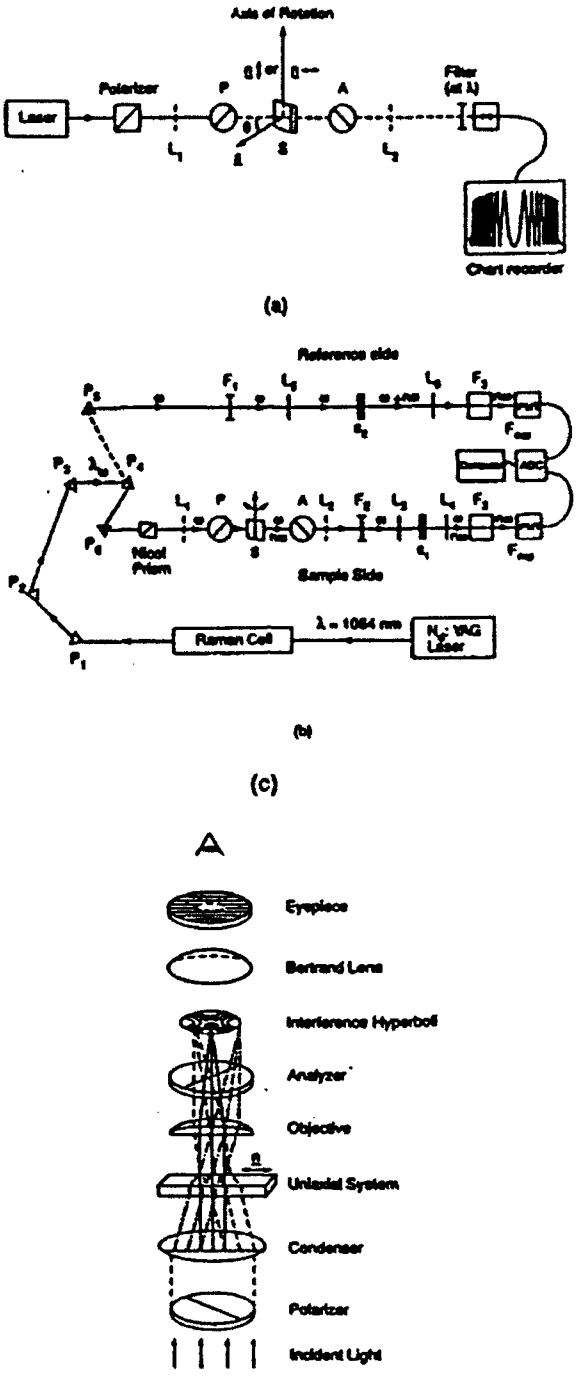

Fig. 5 Experimental arrangement for the rotation of a plane parallel sample and conoscopic, methods: (a) Visible radiation, n is always within the sample plane. (b) Harmonic Generation apparatus for the incident I.R. radiation. Weakly converging lenses L_1 and L_2 may help reaching a better definition of the light beam in the sample, and therefore for ϑ. (c) Schematic diagram for the conoscopy mode.

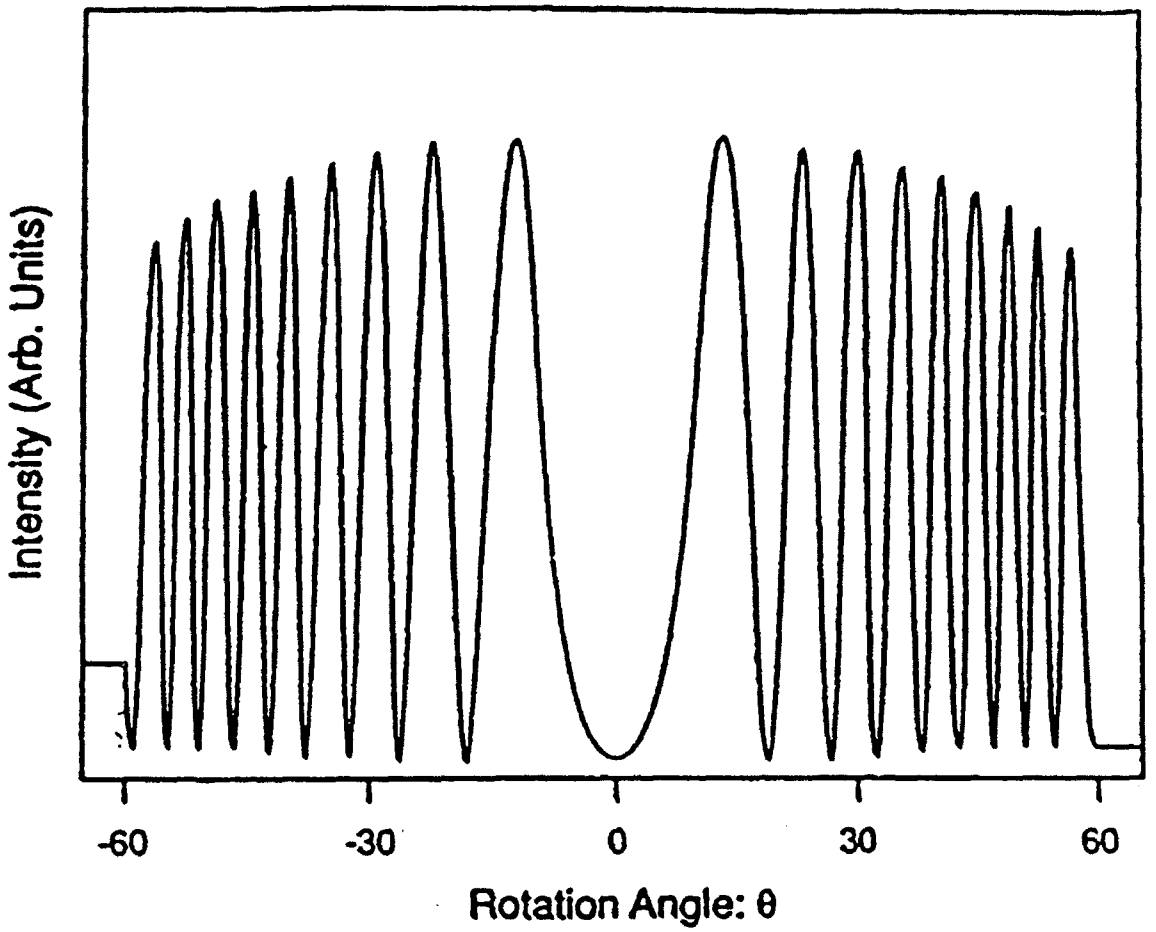

Fig. 6 Transmitted Intensity as function of the rotation angle ϑ for the visible radiation case: λ = 632.8 nm (He–Ne red line), d = 200 μm, c = 0.0715 (g/cm^3).

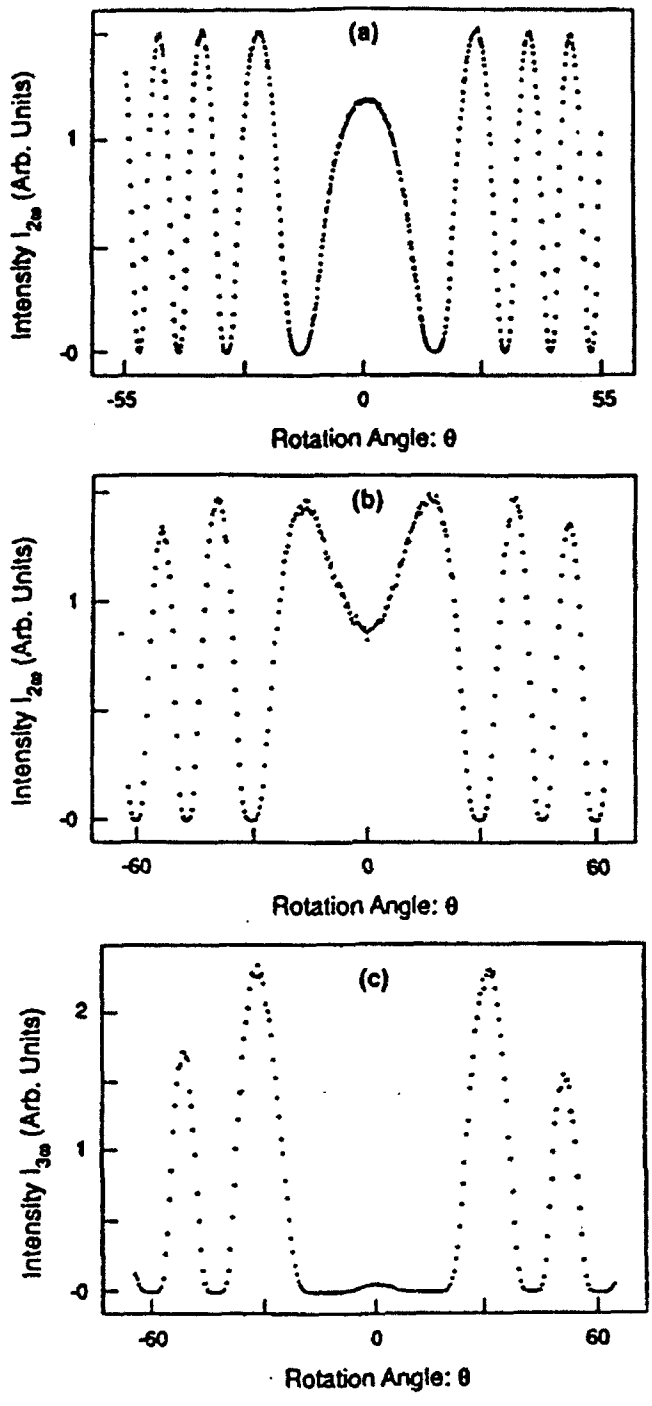

Fig. 7 Harmonic Generation (HG) signal as function of the rotation angle from PBT monodomain (c = 0.0813 (g/cm^3), and d = 350 μm): (a) SHG signal at λ_ω = 1064 μm. (b) SHG signal at λ_ω = 1542 nm; (c) THG signal at λ_ω = 1907 nm.

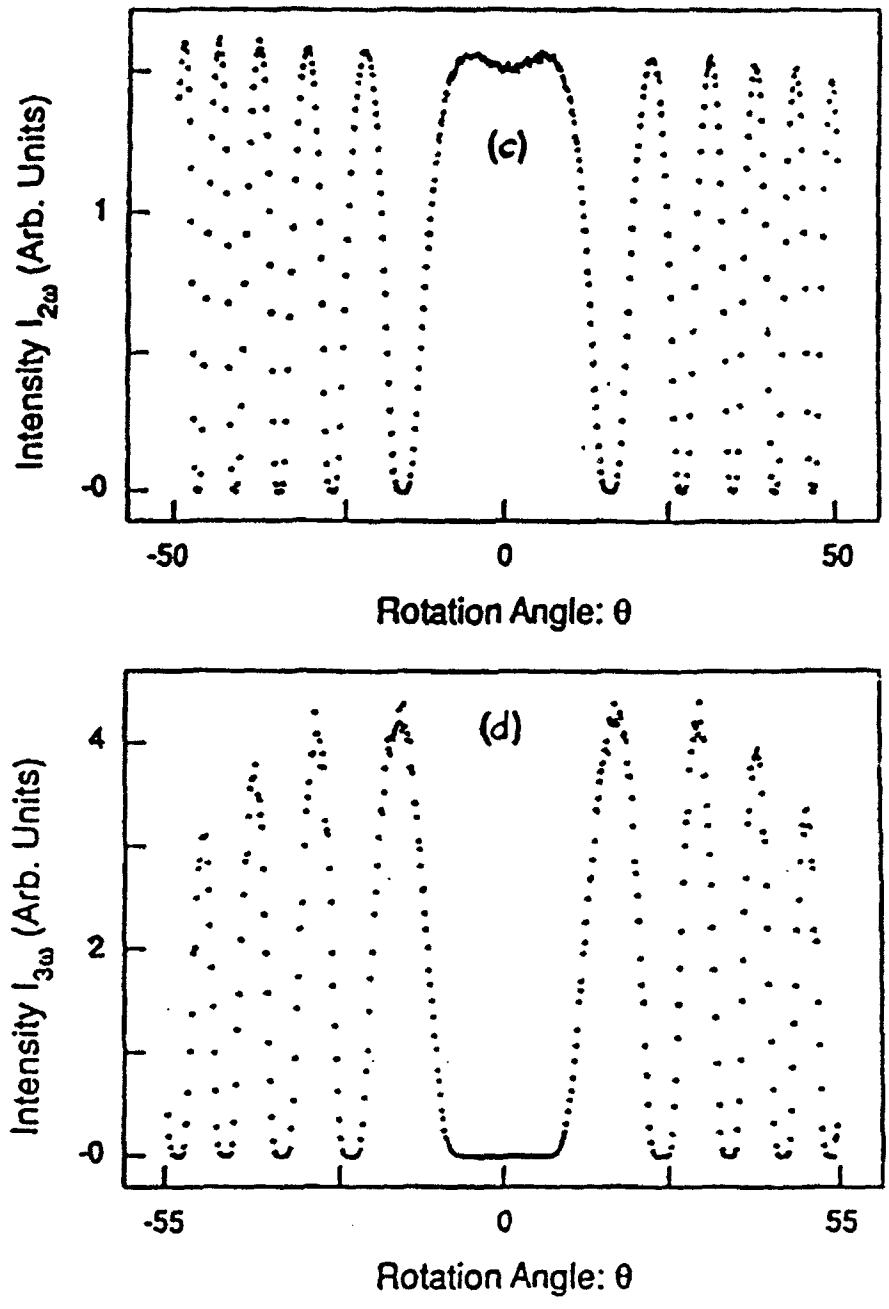

Fig. 7 Plots for SHG and THG signals from the quartz reference (c) SHG at $\lambda_{2\omega}$= 532 nm; (d) THG at $\lambda_{3\omega}$= 514 nm. The minima for THG pattern are broader than observed for SHG case.

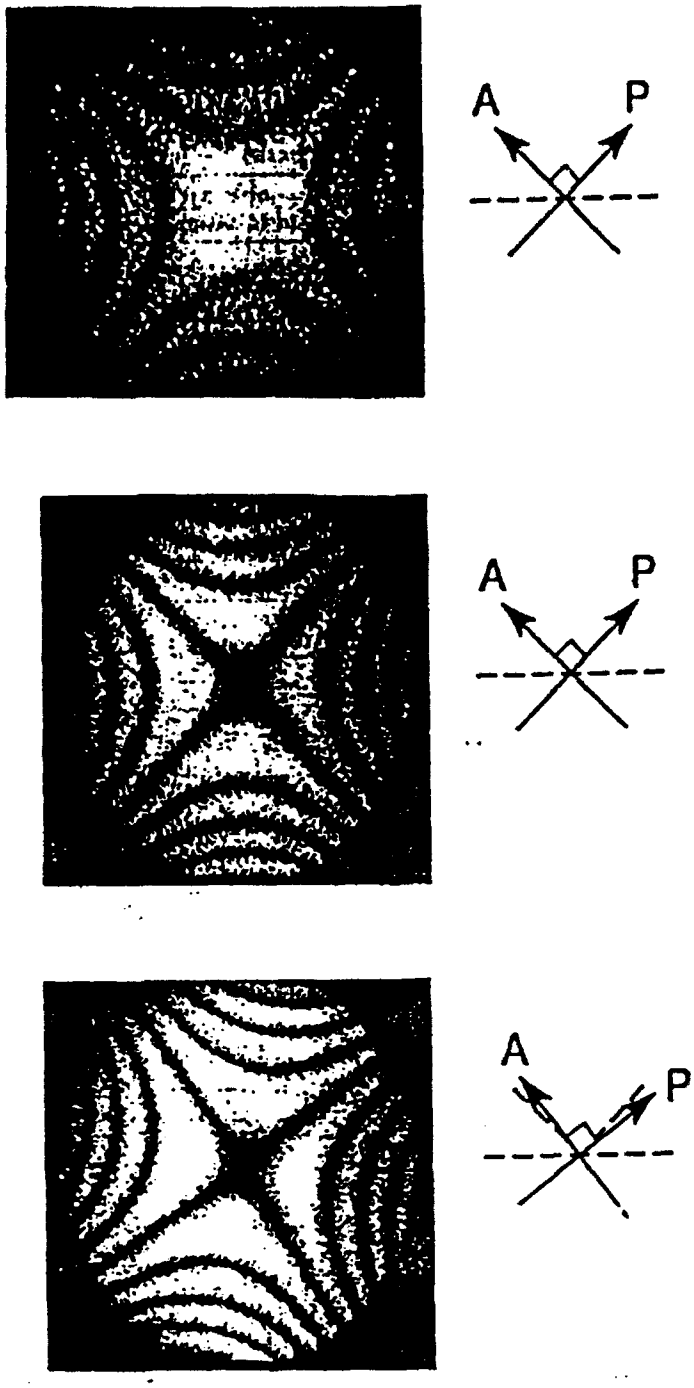

Fig. 8 Conoscopic interference figures for a PBT monodomain (c = 0.075 (g/cm^3) #and d = 300 μm), together with the Quartz reference (top and middle figures, respectively); crossed polars and n at π/4 with respect to P and A. Bottom figure correspond to a tilted crystal within its plane; the interference figure is slightly rotated within its plane.

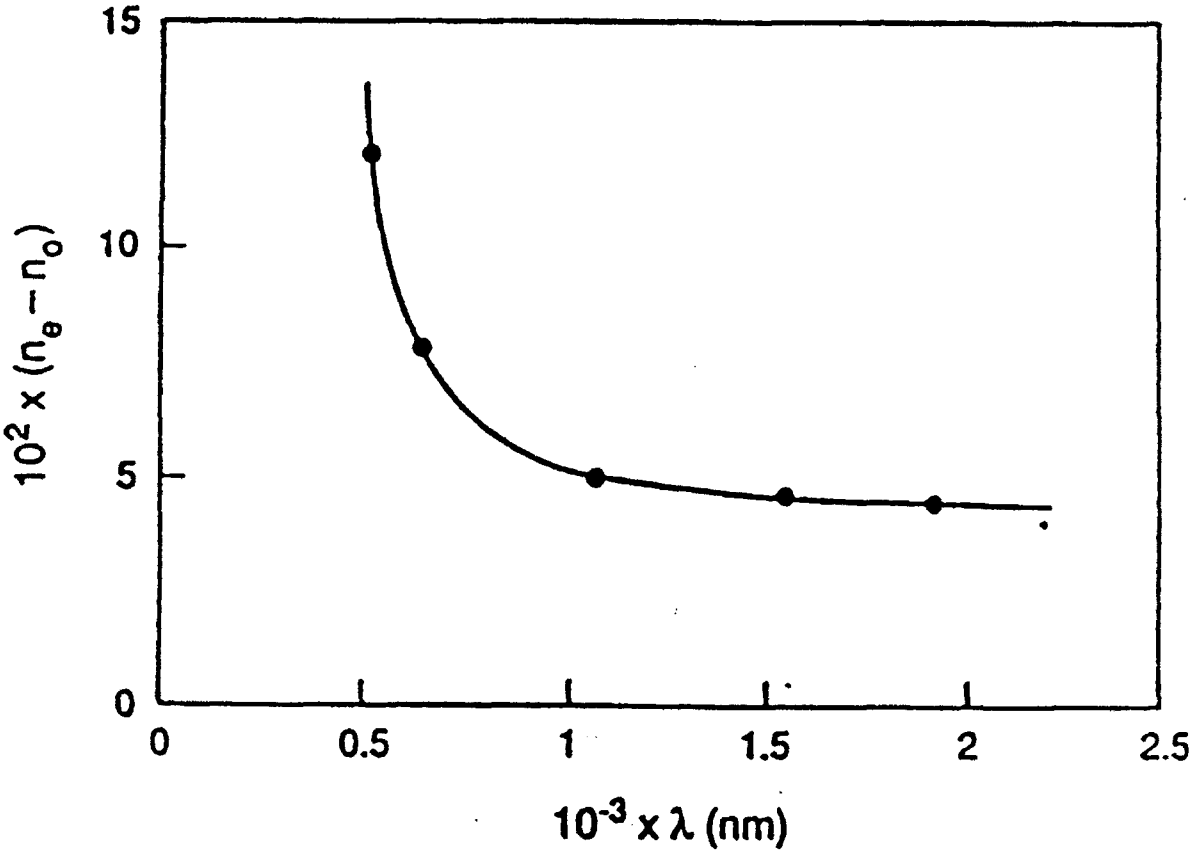

Fig. 9 Plot for the birefringence $|n_E - n_O|$ vs. λ; for a monodomain with $c = 0.0813$ (g/cm^3) and a sample thickness $d = 350\ \mu m$.

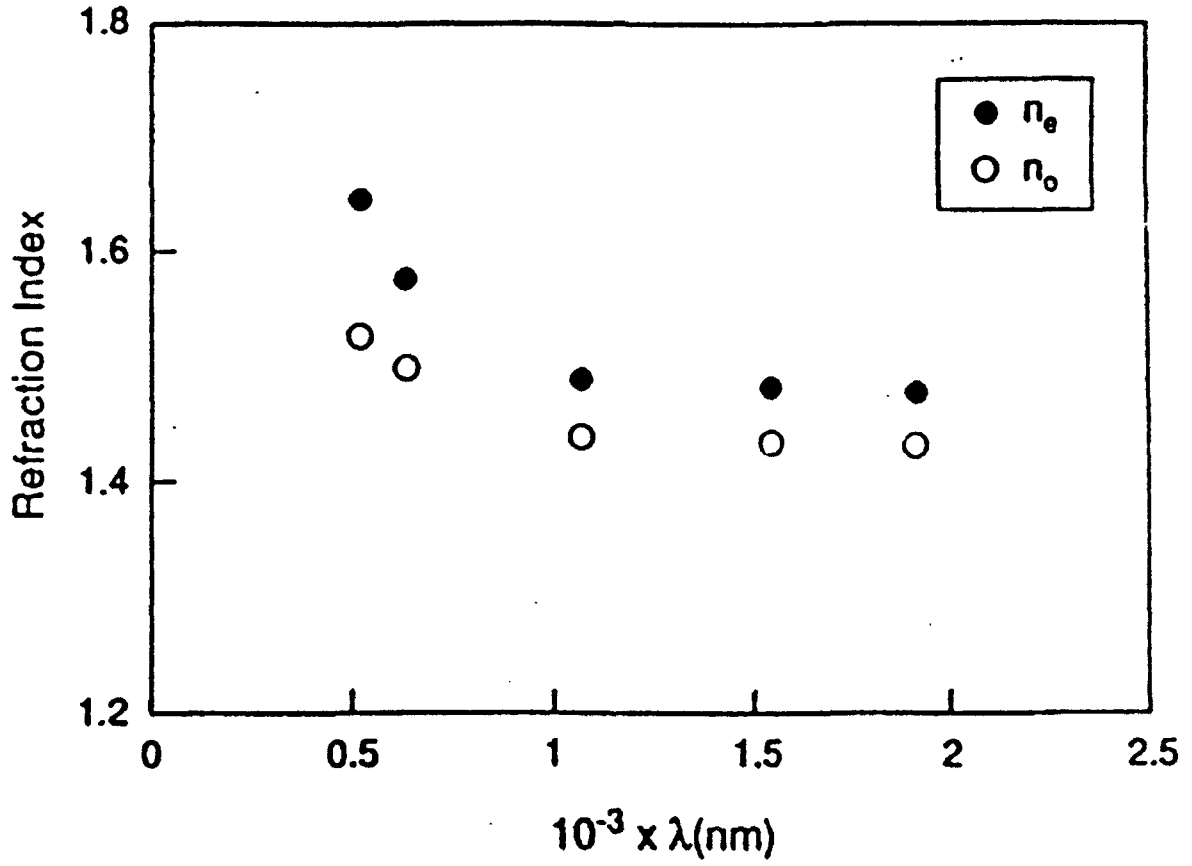

Fig. 10 Plot for the absolute refractive indices vs. λ: Top curve is for n_E whereas the bottom curve is for n_O.

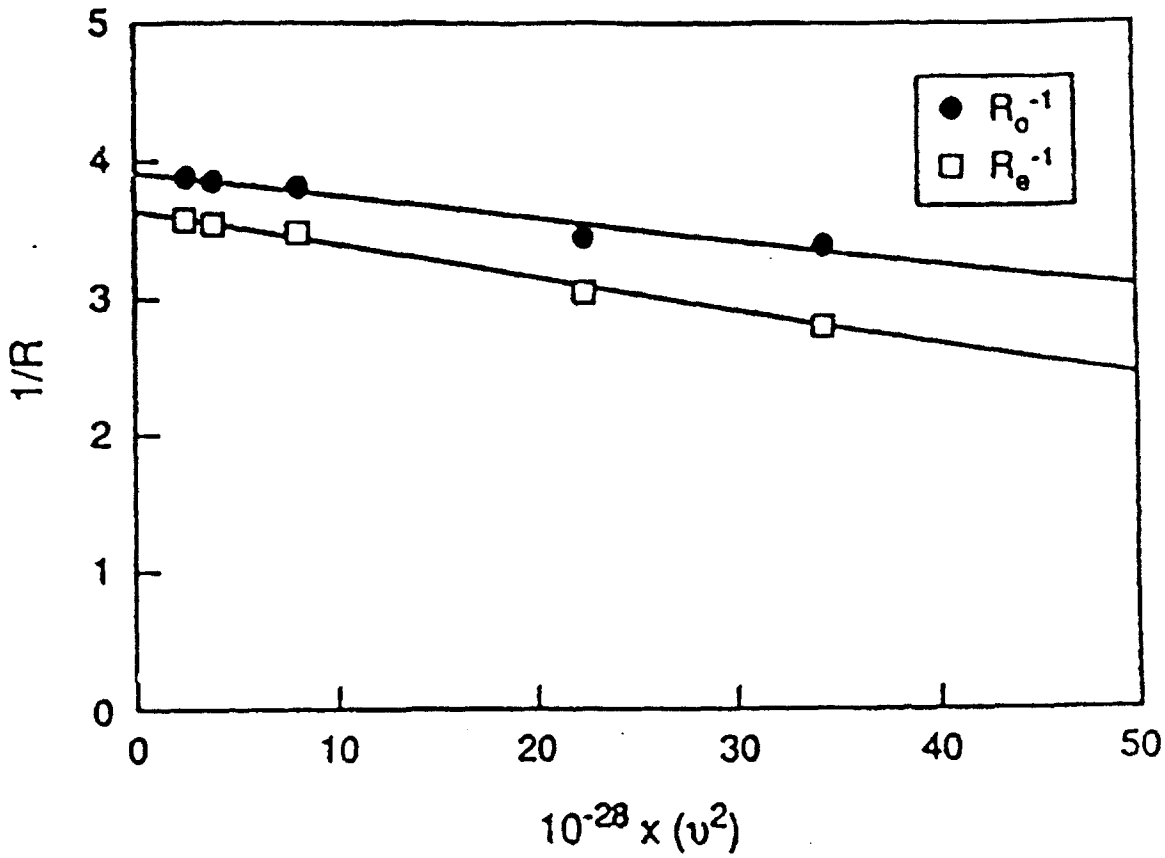

Fig. 11 Plot of 1/R vs. ν^2 for both refractive indices: ordinary and extraordinary.

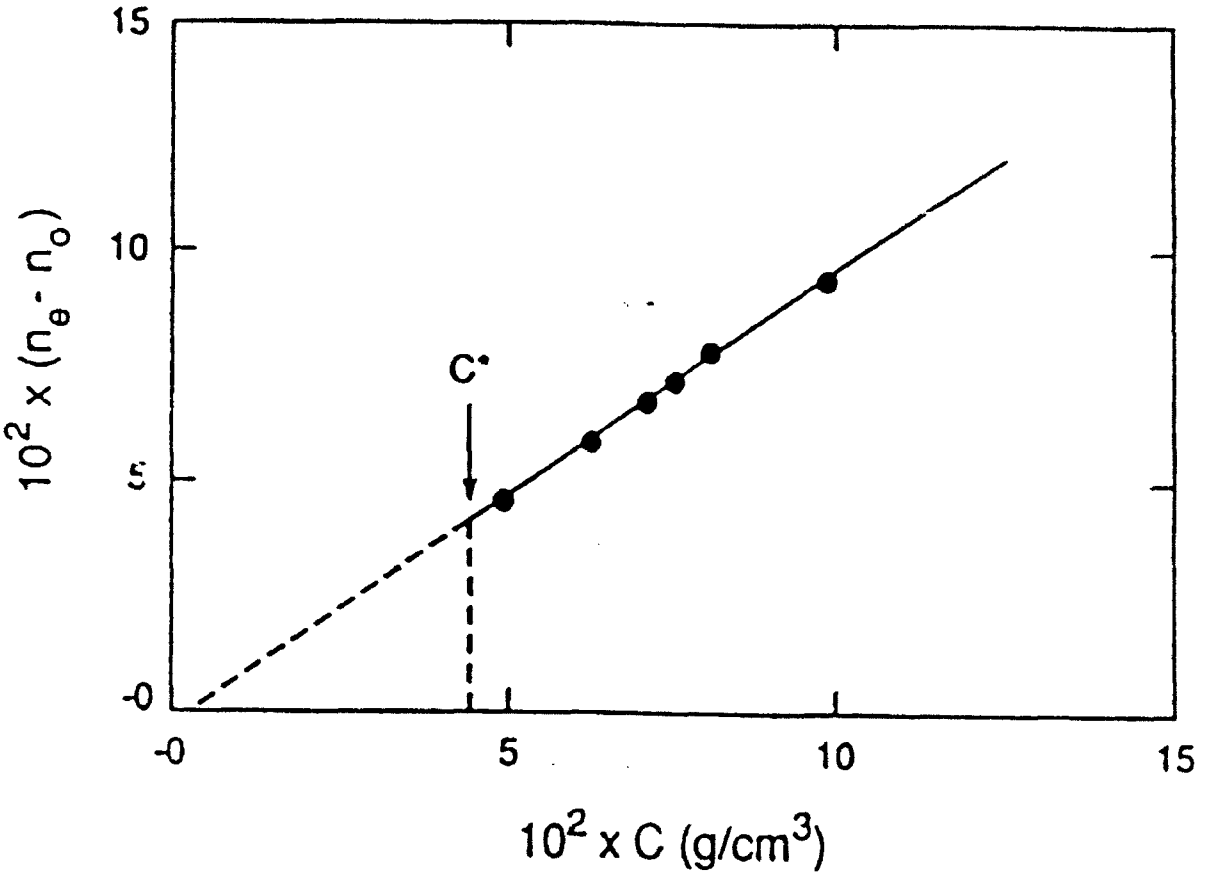

Fig. 12 Plot of the birefringence $|n_E - n_O|$ as function of the concentration c. The value of c scanned are within the range sligthly above the critical concentration indicated by the arrow.

PART 3: RHEOLOGICAL PROPERTIES OF BLENDS OF RODLIKE CHAINS WITH FLEXIBLE OR SEMIFLEXIBLE CHAINS

V. J. Sullivan, C. S. Kim and G. C. Berry

ABSTRACT

Rheological and rheo-optical properties are studied for homogeneous blends of the rodlike poly(1,4-phenylene-2,6-benzobisthiazole), PBT, and the flexible poly(hexamethylene adipamide), nylon-66, and homogeneous blends of the rodlike poly(1,4-phenylene-2,6-benzobisoxazole), PBO, and the semiflexible poly(2,5–benzoxazole), PabPO. The linear recoverable creep compliance shows that the distribution of retardation times is similar for all the blends studied, though shifted on the time scale by large variation in the viscosity among the blends. A single-integral (BKZ-type) constitutive equation is found adequate to represent the dependence on shear rate of the nonlinear steady-state viscosity, the recoverable compliance, and the flow birefringence (save for certain anomalous behavior at low shear rate in the latter case). Effects on the viscosity are discussed in terms of a simplified model forbehavior when a characteristic rheological time constant is longer for the rodlike than for the flexible chain component.

INTRODUCTION

Solutions of rodlike chains blended with a flexible chain may serve as precursors to so-called molecular composites, the latter being formed on solvent removal under certain conditions [1,2]. In many cases, as with the system studied here, the rheological properties of the component solutions differ markedly. Typically, the rodlike solution will exhibit much longer relaxation times and larger viscosity than the solution of the flexible chain at comparable chain lengths and polymer concentration, see below. Also, miscible systems will usually be only moderately concentrated owing to a tendency for phase separation with increasing concentration [3]. In fact, the aforementioned phase separation may often frustrate attempts to prepare a molecular composite free of domains rich in the rodlike component [4].

Homogeneous solutions of two separate systems in methane sulfonic acid, MSA, have been studied: the rodlike *trans*-poly (1,4-phenylene-2,6-benzobisthiazole), PBT, and the flexible poly (hexamethylene adipamide), nylon-66, and the rodlike *cis*-poly(1,4-phenylene-2,6-benzobisoxazole), PBO, and the semiflexible poly(2,5–benzoxazole), PabPO (PBX structures are given in Part 1 of this report.

As discussed in references [5-7] solutions of PBX are nematogenic, and exhibit many of the properties expected for rodlike chains, both for isotropic and nematic solutions. For example, for isotropic solutions, the linear (Newtonian) viscosity η
may be expressed in the form [8]

$$\eta/\eta_s = KN_A^2M[\eta](cL/M_L)^3f(cL/M_L)\Omega \quad (1)$$

where c is the polymer concentration (wt/vol), η_s is the solvent viscosity, N_A is Avogadros Number, M is the molecular weight and η the intrinsic viscosity of a rodlike chain of length L, $M_L = M/L$ is the mass per unit length, f is a crowding factor, discussed below, and $\Omega = \zeta/3\pi d\eta_s$, with ζ the local friction factor and d the chain diameter. The parameter K is of order 10^{-4} [6,8-10]. For low c,Ω is expected to be unity, but Ω may depend on temperature T and on c for larger c, see below [11]. For rodlike chains [12],

$$M[\eta] = \pi N_A L^3/24\ln(3L/2d) \quad (2)$$

making η markedly dependent on L, e.g., $[\eta] \propto L^{1.8}$ for L/d of interest here. Thus, rearrangement of Eqn. (1) gives

$$\eta/\eta = [\pi K/24\ln(3L/2d)](\nu L^3)f\Omega \quad (3)$$

where $\nu = cN_A/M$ is the molecular concentration. In prior [10] discussion of the viscosity of isotropic PBT solutions, use was made of the expression [13]

$$f = (1 - BcL/M_L\alpha_{NI}) \quad (4)$$

with B nearly unity, where $\alpha_{NI} = (cL)_{NI}/M_L$ is calculated with the values of c and L for the conditions necessary to form a stable nematic phase; α_{NI} is expected to be essentially a constant [14]. A different form, given by [15]

$$f = [1 - (B'cL/M_L\alpha_{NI})^{3/2}]^{-1} \quad (5)$$

with $B' < 1$ gives smaller f than Eqn. (4) for $c << c_{NI}$, but gives larger f than Eqn. (4) as c approaches c_{NI}, the two expressions being equal for some c/c_{NI}, dependent on B'/B.

By comparison, the dependence of η on M and c given by the preceding is more marked than is the case for flexible chain polymers, for which Ë may be expressed as [10,16]

$$\eta/\eta_S = (N_A c R_G^3/6m_a(c/\rho)^{1/2}E(cR_G^2/\rho R_{G,c}^2)(3\pi d\Omega) \quad (6)$$

where R_G is the root-mean square radius of gyration of the chain at concentration c, $R_{G,c}$ is a polymer dependent constant, ρ is the polymer density, and m_a is the molar weight per chain atom, with contour length l and friction factor ζ per chain atom. The entanglement function E is discussed elsewhere [17,18] -- a useful semiempirical expression takes the form $E(z) = (1 + z^{2.4\epsilon})^{1/\epsilon}$, where ϵ is an adjustable parameter [18]. (For large ϵ, $E(z) \approx z^a$ with $a \approx 2.4$ if $z > 1$ and zero otherwise). For a flexible chain, $R_G^2 = \hat{p}L/3$, with $\hat{p}$ the persistence length ($\hat{p} << L$ for a flexible coil). Rearrangement to a form similar to Eqn. (3) gives

$$\eta/\eta_S = (\pi d/2)(\hat{p}/3l)^{1+a}(c/\rho)^{1/2}N_A X_c)^{-a}(\nu L^2\alpha^2)^{1+a}\Omega \quad (7)$$

where use is made of the approximation $E(z) \approx z^a$ mentioned above, X_c is the Fox parameter $\rho R_{G,c}^2/m_a$ with $N_A X_c \approx 240$ nm^{-1} for a number of polymers [11], and α is the excluded volume expansion factor at concentration c [16] (not to be confused with $\alpha_{N\Pi}$ introduced above). Comparison of Eqns. (3) and (6) shows that η will generally be much less for flexible chains polymers than for rodlike chains at common ν and L.

As discussed elsewhere [6], isotropic solutions of PBT are observed to exhibit linear viscoelastic behavior under a recently small deformation, as is also the case with solutions of flexible chain polymers [8,18-21]. Thus, in either case, the creep compliance may be expressed in the form [18,20,21]

$$J(t) = R(t) + t/\eta \quad (8)$$

where the recoverable compliance R(t) reaches its asymptotic limit $R^{(S)}$, the steady-state recoverable compliance, for large t. ($R^{(S)}$ is often denoted J_e^o [21]). In the form

$$R(t) = R^{(S)} - [R^{(S)} - R^{(I)}]\,\delta\, r_\nu \exp(-t/\lambda_\nu) \quad (9)$$

the data for R(t) on PBT solutions require several retardation times λ_ν to represent R(t) [6,10]. Here, $R^{(I)}$ is the instantaneous compliance, and the weight factors r_ν sum to unity. Making use of the well-known convolution integral relating J(t) and the (linear) shear modulus G(t),

the data on η, $R^{(S)}$ and the r_ν and λ_ν set may be converted to an equivalent set of relaxation times τ_ν and their weight factors g_ν [7,19-21]:

$$G(t) = (R^{(I)})^{-1}\delta\, g_\nu \exp(-t/\tau_\nu) \tag{10}$$

where theg_ν sum to unity.

With isotropic polymers and their solutions, certain nonlinear properties can be represented by the use of a single-integral (BKZ-type) constitutive equation involving G(t) andωthe shear strain $\gamma(t)$ [7,19,22]:

$$\sigma_m(t) = -\int_0^\infty du \frac{\partial G(u)}{\partial u} [\gamma(t) - \gamma(t-u)]^m F[\gamma(t) - \gamma(t-u)] \tag{11}$$

for the shear stress $\sigma(t)$, m = 1, or thefirst-normal stress difference $\nu^{(1)}(t)$, m = 2. Here $F(\gamma)$ is a function known reasonably well [8,19,23]; theoretically, $F(\gamma)$ is the same for rodlike and flexible coil chains [8,23]. In fact, Eqn. (11) has been used with isotropic solutions of PBT in reference [6], as well as a variety of flexible chain polymers [19,24]. Thus, the dependence of the steady-state viscosity $\eta_\kappa = \sigma(\infty)/\kappa$ on shear rate κ and the recoverable compliance $R^{(S)}$ following steady-state flow at shear rate κ are well represented by Eqn. (11) with m = 1. Flow birefringence data were represented in reference [6] by Eqn. (11) with m = 2, combined with the stress-optic law [25] in the form (for $\Delta n_{13} >> \Delta n_{23}$)

$$\Delta n_{13}(t) = C'\, \nu^{(1)}(t) \tag{12}$$

where C' is a stress-optic constant and Δn_{13} is the flow birefringence in the 1-3 flow plane (e.g., for light propagated perpendicular to the flow plane for flow between parallel plates). The steady-state behavior of interest here given by Eqn. (11) can be summarized by the relations

$$\eta_\kappa/\eta_o = h(\beta\tau_c\kappa) \tag{13}$$

$$R_\kappa^{(S)}/R_o^{(S)} = r(\beta\tau_c\kappa) \tag{14}$$

$$M_\kappa/M_0 = m(\beta\tau_c\kappa) \quad (15)$$

where $\tau_c = R_0^{(S)}\eta_0$, and $1/\beta$ is a material specific constant generally in the range 2-4 [19] (see below). Here, $M_\kappa = \Delta n\lambda/(\eta_\kappa\kappa)^2$, and the subscript 0 indicates a limiting value for small κ. The subscript 0 will be suppressed when dealing with linear properties if no confusion should result. The functions h( ), r( ) and m( ) are discussed in detail elsewhere [19].

Relatively little is known about the rheological behavior of miscible blends of rodlike and flexible chain polymers. Nevertheless, it can be anticipated that the linear viscoelastic behavior embodied in Eqns. (8) - (10) will apply for recently small deformations. Similarly, Eqns. (11) - (15) should be applicable for the blend, using the functional form for $F(\gamma)$ found in common for rodlike and flexible chains. By contrast, the mixing laws for η and $R_0^{(S)}$ may be quite complex, as indeed is the case even for polydisperse solutions of either rodlike [6] or flexible chains [19].

EXPERIMENTAL

Materials. The PBT samples were supplied by SRI International, through the courtesy of J. F. Wolfe. The intrinsic viscosity in solution in MSA was 1400 cm^3/g for sample 53, and 3600 cm^3/g for sample 28. These polymers have been used in previous studies in this laboratory [5-7]. The nylon-66 used was a sample of Zytel 42, made by E. I. duPont de Nemours & Co. The intrinsic viscosity of the nylon-66 sample was found to be 425 cm^3/g in solution in MSA, and 185 cm^3/g in solution in 96% sulphuric acid; $[\eta]$ was determined by methods described elsewhere [26]. Methane sulfonic acid was distilled under a reduced pressure prior to use. Solutions were prepared employing techniques discussed in reference [5] to insure minimal contamination by moisture.

The PBO and PabB) samples were supplied by Dow Chemical C0., through the courtesy of W. F. Hwang. The intrinsic viscosity in solution in MSA was 1300 cm^3/g for the PBO sample, and 1400 cm^3/g for the PabBO sample.

Two sets of solutions of PBT and its blends with nylon were used in this study. A set of solutions of PBT-28 and PBT-28/nylon-66 blends, designated by the prefix A, was received through the courtesty of W. Adams, Air Force Wright Aeronautical Laboratories. These samples are designated by the code A - R/F, where R and F are the weight percents of the PBT and nylon-66, respectively. (e.g., the notation A-1.75/0 designates a solution with 1.75 weight

percent PBT-28, but no nylon-66). A similar notation is used for the mixtures of PBO and PabBO. The total polymer concentration in the mixture varied in this series, being adjusted to be slightly smaller than the concentration required to form an anisotropic solution. Thus, for example, F decreases with increasing R. A set of solution of PBT-53 and PBT-53/nylon-66 blends, designated by the code C-R/F was prepared in our laboratory. The latter were developed as sequences, each sequence containing a fixed weight percent R of PBT-53 in the solution for a range of nylon-66 weight percent F.

Weight fractions were converted to concentrations c or volume fractions φ where necessary by the assumption of volume additivity and the use of the specific volumes 0.69 cm^3/g for PBT [26], 0.92 cm^3/g for nylon-66 [27], and 0.675 cm^3/g for MSA, all at 25°C. The weight fraction is convenient as a measure of the concentration that is independent of temperature, whereas the mass per volume concentration c often is more natural for comparison of experiment and theory.

Rheological Measurements. With the exception of a few viscosity measurements on solutions of nylon-66 at low concentration made in suspended-level Ubbelhode viscometers, all rheological measurements were made using a custom rheometer described elsewhere [28], following methods discussed in detail in references [5–7]. In particular, the rheometer utilizes a cone-and-plate geometry, and permits measurement of J(t) and R(t), in creep and recovery experiments, or may be used to monitor the stress $\sigma(t)$ on imposition of a ramp strain at strain rate κ, including the steady-state stress used to compute η_κ, or the stress during relaxation following steady flow. The rheometer is well-sealed against contamination by moisture.

Rheo-optical measurements were made as described in reference [5], in an apparatus with glass parallel plates. The flow birefringence Δn_{13} is measured either in steady flow at shear rate κ, or during relaxation following steady flow. In these experiments the nylon-66 component contributes negligibly to the measured retardation, from which Δn_{13} is computed.

RESULTS

Phase Equilibria Ternary diagrams are given in Fig. 13 and Fig. 14, showing the compositions studied, as well as compositions found to be biphasic. The circles represent compositions prepared by direct dissolution of the polymers in the appropriate amount of solvent. The triangles represent solutions prepared by addition of nylon-66 to a previously prepared solution (usually the composition given by the circle or triangle with next lowest

nylon-66 concentration). The latter were not used for rheological studies. The diagrams also illustrates compositions for which the solutions were isotropic or nematic at 25°C. Apparent irregularities in the latter behavior evident in Fig. 13 will be discussed below.

Linear Viscoelasticity Results on the limiting viscosity η at low shear rate are given in the following for solutions in MSA of nylon-66, either PBT-28 or PBT-53, blends of the nylon-66 and PBT polymers, PBO, PabBO, and blends of PabBO and PBO. This section concludes with a paragraph on the transient recoverable compliance R(t).

The specific viscosity η_{sp}, equal to $\eta_{rel} - 1$, with $\eta_{rel} = \eta/\eta_s$, was studied over the concentration range $0.0016 < w < 0.24$ for solutions of nylon-66 in MSA at 297K. Here, the solvent viscosity $\eta_s$is 11.7 mPa.s at 297K, and $\partial \ln \eta_s / \partial T^{-1} = 2800$K. (The difference between η_{rel} and η_{sp} is negligible except for the lowest c). A semi-empirical expression based on Eqn. (6) found to represent the measured η_{sp} for nylon-66 solutions with $c < 0.2$ g/cm^3 is given below (see Eqn. 17). It is hoped that this expression might prove to be generally useful for nylon-66 solutions in the stipulated range of c. The viscosity average molecular weight M_w = 61,000 is computed from the intrinsic viscosity in 96% sulfuric acid using the relation $[\eta] = KM_v^{0.67}$, with K = 0.115 for $[\eta]$ in cm^3/g [27]. In the concentration range of interest, the excluded volume chain expansion factor is expected to vary appreciably with c [16,29]. In the following, this variation is estimated from the expression (for c small enough that $\alpha > 1$) [16]

$$\alpha^2 = \alpha^2_o(1 + ([\eta]c)^2)^{-0.125} \qquad (16)$$

where α_o is the expansion factor at infinite dilution. The latter is estimated as $([\eta]/[\eta]_o)^{1/3}$, where $[\eta]_o = KM_v^{0.5}$, with K = 0.227 for $[\eta]_o$ in cm^3/ for nylon-66 under Flory theta conditions [27]. Thus, α_o 1.96 in MSA for the nylon-66 sample used. Making use of Eqn. (16), the measured η_{sp} may be represented to within 4 percent for $c < 0.2$ g/cm^3 by the semi-empirical form (see Eqn. (6))

$$\eta_{sp} = 0.080(c/\rho)^{1/2} cM_w\alpha^2[1 + (cM_w\alpha^2/\rho M_c)^{2.4\varepsilon}]^{1/\varepsilon}\Omega \qquad (17)$$

at 297K,where $M_c = 4210$, $\rho = 1.087$ g/cm^3, and $\varepsilon = 2$. The factor in the square brackets represents E. For the range of c of principal interest here, $cM_w\alpha^2 < \rho M_c$, and consequently $\eta_{sp} \propto c^{1.4}$. The principal fitting parameters in Eqn. (17) are 0.080 Ω and M_c; the parameter ε is less critical, mostly influencing the function in the range $cM_w\alpha^2/\rho M_c < 1$. The empirical value for M_c is in good agreement with the estimate 4000 calculated with the "universal"

constant $N_A X_c = 240$ nm $^{-1}$, both being smaller than the estimate 5000 reported for the similar poly(ε-caprolactam), nylon-6, based on data on the melt at 263°C [11]. The factor Ω is esentially unity for c less than about 0.2 g/cm^3 (the range of c of interest here), but increases with increasing c for larger c. Accordingly, η_{rel} is only weakly dependent on temperature T for the lower c studied, but $\partial \ln \eta_{rel}/\partial T^{-1}$ increases with increasing T for the solutions with larger c. Studies over the relatively narrow temperature span 286 to 346K gave the result

$$\partial \ln \eta_{rel}/\partial T^{-1} = 7500w \qquad (18)$$

over the span $0.03 < w < 0.1$; $\partial \ln \eta_{rel}/\partial T^{-1}$ is larger than predicted by Eqn. (18), and increases with decreasing T for the highest w studied ($w = 0.24$). The data are too limited to permit further analysis of/in terms, say, of free volume parameters [11,21].

The viscosities of isotropic solutions of PBT-53 and PBT-28 (no nylon-66 component) and mixtures of PBO and PabBO are given in Tables 4 and 6, respectively, and presented in Fig. 15 and 16, respectively. In the latter, the data are in the form $\eta/\eta_s M_w[\eta]$ versus cL_w/M_L based on the use of Eqn. (1). Values of $L_w = M_w/M_L$, using M_w computed from $[\eta]$ using Eqn. (2), were found to be 118 and 200 nm for PBT-53 and PBT-28, respectively. The viscosity averaged chain length L_η computed with Eqn (2) was converted to a weight average L_w from the approximation [26] $L_\eta \approx L_w(L_z/L_w)^{1/2}$, assuming that $L_z/L_w = 1.5$The estimate for L_η isrelatively insensitive to d, which was set equal to 1 nm, e.g.,$\partial \ln L_\eta/\partial \ln d \approx -0.1$ [26] ($M_L = 220$ nm $^{-1}$ for PBT). The curves in Fig. 15 represent Eqn. (1) and (4), with $K = 1.13 \times 10^{-4}$ and $N_A(cL_w)_{NI}/BM_L) = 21.2$ nm^{-1} on the one hand, or Eqn. (1) and (5) with $K = 1.76 \times 10^{-4}$ and $N_A(cL_w)_{NI}/B'M_L) = 16.0$nm^{-1}, with $\Omega = 1$ in both cases for solutions of PBT. The former estimate for K is similar to that reported elsewhere [6], but the corresponding $N_A(cL_w)_{NI}/BM_L)$ is larger (by 45%). This may reflect a small extent of association of the chains in parallel arrays, resulting in increased M_L (in comparisonωwith $M_L = 220$ nm^{-1} for a single chain), with minor effect on $M[\eta]$ [26]. The constant K includes the effects of molecular weight dispersion, being proportional to $(L_{z+1}/L_z)^2(L_z/L_w)^3$ accordingωto one model [30]. Thus, the value of K reported here may be larger than would be observed with a solution of a monodisperse rodlike chain. The data in Fig 16 for solutions of PBO could be fitted similarly, with $K = 0.86 \times 10^{-4}$ and $B = 0.96$, as shown by the solid line given in the figure.

Studies of the temperature dependence of η_{rel} for solutions of PBT-53 in MSA over the span $0.01 < w < 0.026$ gave $\partial \ln(\eta_{rel})/\partial T^{-1} = 1265K$, independent of the polymer concentration. This weak dependence on temperature will be discussed below.

Viscosities of the isotropic solutions of the blends in series A are also given in Table 4 and Fig.15. In the latter, $\eta_{rel}(M_w[\eta])_R$ is plotted against $(cL_w)_R/M_L$, where the subscript R denotes the rodlike PBT component in the solution. Thus, $(cL_w)_R$ is the product of the concentration c_R of the rodlike polymer and its length L_w. Data on mixtures of PBO and PabBO are given in Table 6. The sometimes substantial enhancement in η for the solutions of the blends, relative to η for the comparable solution free of nylon-66 will be discussed in the next section. Similar, but smaller trends may be observed for the viscosities of the isotropic blends in series C given in Table 5. The temperature dependence of η for the solution of the blends in either series A or C was within experimental error of that for the comparable solution of PBT free of nylon-66.

Measurements of R(t) were possible with solutions of nylon-66 (free of PBT) having $w \geq 0.13$. The results for one case are given in Fig. 17 to illustrate the viscoelastic time-scale for the solution —$\tau_c = 3.30$ s for the data in Fig. 17. Data on R(t) were obtained for most of the blend solutions; results are shown in Figs. 17 and 18. As shown in Figs. 17 and 18, reduced plots of $R(t)/R_o^{(S)}$ versus t/τ_c superpose for the blends and the nylon-66 free solutions of PBT. In all cases, the data could be fitted to within experimental error by the use of Eqn. (9), and were analyzed to obtain the r_v - λ_v set needed to fit Eqn. (9) to the data. (Four contributions were usually required, with $0.1 < (\lambda_v/\tau_c) < 30$). Typical resulting fits are shown in Fig. 17 for series A samples.

Reduced linear viscoelastic data for solutions of PBO, PabBO and their mixtures are given in Figs. 19, 20 and 21, respectively. The use of compliances reduced by $R_o^{(S)}$ and the reduced time t/τ_c is seen to result in reduced curves over the concentration range studied.

Transient Nonlinear Viscoelasticity In reference [6] on isotropic solutions of rodlike PBT, and on solutions of flexible chain polymers [19,24], it has been found that the transient nonlinear viscoelastic behavior admits to a strain criterion such that the viscoelastic behavior is linear for strains $\gamma(t)$ less than a critical value γ', regardless of the stress or the rate of strain. Similar behavior was observed for the solutions of the blends. As shown in Figs. 17 and 18 for typical data, this behavior is conveniently revealed in plots of $\Delta\gamma(t) = \sigma[J_\sigma(t) - J_o(t)]$ versus $\gamma(t)$, where $J_\sigma(t)$ is the creep at stress σ and $J_o(t)$ is the linear creep compliance (which

is independent of σ). For $\gamma(t) < \gamma'$, $\Delta\gamma(t)$ is zero, with deviation from zero developing at common $\gamma(t) = \gamma'$ for any σ large enough that $\tau_c\kappa$ exceeds about unity under steady flow at shear rate κ. Since $\Delta\gamma(t)$ must be linear in $\gamma(t)$ for large $\gamma(t)$, a simple linear extrapolation is used to define γ', as shown in Fig. 21. The results gave γ' equal to 0.5 for A - 1.10/1.10 and 0.6 for C - 2.57/0.45 and C - 2.60/0.69. These are smaller than reported in reference [6] for PBT solutions at comparable concentration of the rodlike polymer.

The observation of a maximum in the stress $\sigma(t)$ under deformation at constant strain rate $\kappa > \tau_c^{-1}$, is another feature usually found with flexible chain polymers [19,22,24] and reported for solutions of PBT in reference [6]. Frequently, the strain $\gamma' = \kappa t_m$ at the time t_m for the maximum stress is nearly independent of κ, unless $\tau_c\kappa$ is very large. Of course, $\gamma' > \gamma$, and often γ' is about 2 [19,22,24]. Values of γ' were found to be in the range 1.5 to 2.0 for the broad maxima observed with samples of series A.

Additional nonlinear transient viscoelastic and rheo-optical behavior is shown in Fig. 17 for solutions of Series A. In this case, the stress and the birefringence determined following relaxation of steady flow were used to compute $\hat{\eta}(t)/\eta_\kappa = \sigma(t)/\sigma_{ss}$ and $\hat{M}(t)/M_\kappa = \Delta n_{13}(t)/(\Delta n_{13})_{ss}$, where σ_{ss} and $(\Delta n_{13})_{ss}$ are the stress and flow birefringence in steady-state flow at shear rate κ, respectively— M_κ and η_κ are discussed in the preceding. Data shown for a variety of κ and compositions are observed to superpose when plotted as a function of a reduced time t/β_κ where, β_κ is about equal to $\beta_\kappa = \tau_\kappa R_\kappa^{(S)}$, see the insert in Fig. 22. Since $\tau_\kappa \leq \tau_c$, the relaxation is faster in the nonlinear case than for linear behavior. The solid lines in Fig. 22 are discussed below. As may be seen in Fig. 22, the stress relaxes much more rapidly than the birefringence. Similar behavior has been reported for both rodlike (see reference [6]) and flexible chain polymers [31].

Steady-State Nonlinear Visocelasticity Solutions of nylon-66 exhibited nonlinear behavior over the range of shear rates studied ($\kappa < 10\ s^{-1}$) only for the highest concentration studied. As usual [19], reduced plots of η_κ/η_0 versus $\tau_c\kappa$ superposed for these data. Since τ_c should be about proportional to $c\eta_0$ for these solutions, and is only 3.3 s (at 298K) for the highest c studied, the suppression of nonlinear behavior at the lower c under the conditions studied is reasonable.

The nonlinear viscoelastic behavior of PBT solutions has been reported in referencse [6]. The data obtained here are in accord with those results. Namely, both η_κ/η_0 and $R_\kappa^{(S)}/R_0^{(S)}$ are functions of $\tau_c\kappa$, independent of T, and essentially independent of c. Reduced plots of η_κ/η_0,

$R_k^{(S)}/R_o^{(S)}$, $\Delta n_{13}R_o^{(S)}$ vs. $\tau_c\kappa$ for most of the blends (as well as the nylon-66 free solution) are given in Figs. 23, 24 and 28 for solutions of PBT and nylon, and in Figs 25–27 for PBO, PabBP and their mixtures. These reduced plots include data at various temperatures, but since they are all independent of T over the range studied, in the interest of clarity, the values of T are not indicated for the data on series C. The reduced data for the PBO/PabBO blends are seen to coincide for the compositions studied.

DISCUSSION

Phase Equilibria. The phase equilibria data are compared with calculations using relations due to Flory [3] in Fig. 13 and 14,. A ratio x of the molar volumes of polymer and solvent of 260 for PBT-53, 280 for PBT-28, and 800 for nylon-66; an axial ratio 0f 145 was used for PBO. The values of x for the rodlike chains were chosen to reproduce the phase transition for the nylon-free solutions. The value of x for the flexible chain is not too critical, having modest affect on the calculated coexistence curve. The calculated isotropic binodal is in reasonable accord with the experimental results for series C samples—too few data are available for an assessment with series A samples. Quantitative agreement would be unexpected since the calculated curves are for monodisperse solutes. There are, however, some notable exceptions in Fig. 13, for which compositions were found to be isotropic, even though a related composition with the same weight fraction of PBT, but lower weight fraction of nylon-66, or vice-versa, was found to be nematic. This unexpected behavior is attributed to inadvertent contamination by a small amount of moisture. It is known that nematic solutions of PBT may be transformed to isotropic solutions by the slow gain of moisture from the atmosphere [32]. It is believed that this effect is caused by association of the rodlike chains with their axes parallel, thereby reducing the number of rodlike entities per unit volume below the value required for a stable nematic phase. Since this same association can drastically alter rheological behavior (see reference [6]), rheological data obtained on the solutions so affected are not reported here.

Linear Viscoelasticity As anticipated in the Introduction, for the compositions of interest here, the nylon-66 solutions have much lower η than do the PBT solutions. Nevertheless, as may be seen in Tables 4 and 5 and Fig. 21, the solution of a blend may have larger viscosity η than a solution of PBT at the same weight fraction PBT as in the blend. At the same time, as shown in Fig. 17, for the most part, the dependence of $R(t)/R_o^{(S)}$ on t/τ_c is independent of the concentration of nylon-66. This implies that the underlying distribution of retardation times scales as λ_v/τ_c for the nylon-66 concentration range studied here, despite the sometimes large

effects on η. It may be noted that the enhancement in η is more pronounced for blends with the longer rodlike chain.

The effects described above are attributed to the disparity between the elementary relaxation times τ_R and τ_F for the rodlike and flexible chains, respectively. Here, and in the following, the subscripts R and F designate properties for the rodlike and flexible chains, respectively. An estimate of τ_R is given by the theory of rodlike chain dynamics as the time required for a chain to undergo translation diffusion along its own length by one chain length [8]:

$$\tau_R \propto f L^2/D_{\|,o} \tag{19}$$

where $D_{\|,o}$ is the diffusion coefficient at infinite dilution for translation parallel to the chain axis, and f is the crowding factor accounting for constraints in a concentrated system (see Eqns. (4) or (5)); $L^2/D_{\|,o}$ is equal to $48\eta_s M[\eta]/RT$ for a rodlike chain [12]. In fact, τ_R is used in the estimate of η for the rodlike chains, with $\eta \propto \nu(L/a)^2\tau_R$ in the model leading to Eqn. (3), where a is the mean separation of rodlike chains perpendicular to their axes [8,13]. If this same form is preserved in the blends, as seems reasonable if $\tau_R >> \tau_F$, then the effect of the flexible chain on η must be attributed to effects on the crowding factor f. In this approximation, it is assumed that the factor Ω in Eqn. (3) is not affected by the low concentration of nylon-66 added, as may be reasonable since Ω is expected to depend on local friction. Furthermore, this is consistent with the identical dependence of the viscosity on temperature observed for solutions of PBT and blends of PBT with nylon-66.

As presented in Eqns. (4) or (5), f scales as the thermodynamic–like parameter $cL/M_L\alpha_{NI}$, multiplied by a factor (i.e., B or B'). The parameter α_{NI} is a measure of the proximity of a given solution to the isotropic-nematic phase transition. The conjestion that drives the latter being reflected in enhanced f as $cL/M_L\alpha_{NI}$ approaches unity for isotropic solutions. In studies on isotropic solutions of PBT and other rodlike chains, Eqn. (4) has been found to represent f needed to fit Eqn. (3) to experiment [6]. It seems reasonable to assume that f may still be expressed with Eqn. (4) or (5) for the blends, with a revised definition for α_{NI} to account for the additional constraints imposed by the flexible chain polymers [33]. To estimate the latter, we consider solutions with fixed c_R/c_F (and fixed L_R and L_F), such that the solutions approach phase separation with decreasing solvent concentration, i.e., for compositions defining a straight line passing through the apex ($c_R = c_F = 0$) in Fig. 13. The concentration $(c_R)_{NI,B}$ of the rodlike chain along such a line at the condition for phase separation will be used to estimate α_{NI}—an example is given in the upper part of Fig. 13 for $(c_R)_{NI,B}$ for solution C -

1.27/0.90, using a theoretical result for the coexistence curve discussed in the preceding. Of course $(c_R)_{NI,B}$ is smaller than the concentration $(c_R)_{NI}$ obtained with $c_F = 0$, and therefore its use results in enhanced f and η.

Sufficient data are available on phase equilibria for series C to estimate $(c_R)_{NI,B}/(c_R)_{NI}$ and hence η/η_R using Eqn. (3), along with either Eqns. (4) or (5). Here, η_R is the viscosity for a solution containing no flexible chain, but with the same concentration of rodlike chains as that in a blend having viscosity η. Use of the coexistence curve given by the solid line shown in Fig. 13 results in the estimates for η/η_R given in Fig. 29 for the C series with $w_R \approx 0.0128$ ($\varphi_R \approx 0.013$). As shown in Fig. 29, this approximation is reasonably good for solutions with $\varphi_F \leq 0.015$ (somewhat better with Eqn. (5) than with Eqn. (4)), but overestimates η/η_R for larger φ_F. Apparently, in this case the constraints that induce the phase separation as φ_F approaches the critical value (ca. 0.025) for phase separation for the fixed $\varphi_R \approx 0.013$ do not result in a corresponding restriction on the chain dynamics. Effectively, in this case B or B' must decrease markedly as φ_F approaches its critical value if it is assumed that η is given by the approximation discussed above.

Since limited material made it impossible to carry out detailed phase equilibria studies on series A, we rely instead on the Flory model to estimate the coexistence curve. The result given for the latter in Fig. 13 using $x_2 = 280$ and $x_3 = 800$ is used for the latter. Since the series A solutions are not at either constant φ_F or φ_R/φ_F, it is not convenient to compare the predicted and experimental results as in Fig. 29. One can, however, compute $(c_R/B)_{NI,B}/(c_R/B)_{NI}$ from η/η_R using Eqn. 4, or $(c_R/B')_{NI,B'}/(c_RB')_{NI}$ using Eqn. 5 for comparison with the values or $(c_R)_{NI,B}/(c_R)_{NI}$ estimated from the phase diagram. The results show that $(c_R/B)_{NI,B}/(c_R/B)_{NI}$ is close to the predicted $(c_R)_{NI,B}/(c_R)_{NI}$, with no change in B for $c_F < 0.025$, but would require B to decrease by ca. five percent as c_F increases to 0.03. A larger decrease in B' at all c_F would be required to fit the observed η/η_R using Eqn. 5.

We remark that over a limited range of compositions, η/η_R is approximately proportional to η_R/η_s for some of the series A samples. This is considered to be a consequence of the approximate power-law behavior of f over a limited range on c. Thus, over a limited range of the argument, $(1 - x)^{-2} \propto x^{\gamma}$, where γ depends on the range of x covered. Thus, for the series A samples with $\varphi_F < 0.2$, use of the power-law approximation to Eqn. (4) gives $f \propto (Bc_RL_w/M_L\alpha_{NI})$. Moreover, for the corresponding range of φ_F, inspection of the phase diagrams gives $(c_R)_{NI,B}/(c_R)_{NI} \approx 26\ \varphi_F^{0.6}$. Consequently, for these limited conditions, $\eta/\eta_R \approx 1800\ \varphi_F^{1.4}$. By comparison, for the nylon solutions, $\eta_{sp} \approx 6800\ \varphi_F^{1.4}$. It follows that for the

stipulated concentrations, η/η_R is about proportional to η_F/η_s. Although the proportionality with η_F/η_s. is similar to that predicted for the dependence of the rotational diffusion constant of a long rod molecule in a polymer melt [34], the source is deemed different, and no fundamental significance is attributed to the approximate proportionality observed here. To the contrary, with decreasing c_R and increasing c_F, η/η_R is much smaller than η_F/η_s. The data on R(t) for the solutions of the blends are remarkable in that $R(t)/R_0^{(S)}$ appears to depend only on t/τ_c for data at constant c_R, over a range of c_F, e.g., see Fig. 21. Qualitatively, this is consistent with the models disucssed above, in which the principal contribution to the viscosity is attributed to the constrained rotational diffusion of the rodlike components in the blend. We are unaware of any detailed calculations on this behavior.

The breadth of the distribution of relaxation times may be characterized by the ratio of successive$\tau^{(k)}$, where

$$\tau^{(\kappa)} = \frac{\Sigma' g_\nu \tau_\nu^k}{\Sigma' g_\nu \tau_\nu^{k-1}} \tag{20}$$

Here, the prime stipulates that the summation is over only the terminal part of the relaxation. Thus, τ_c is given by $\tau^{(2)}$ in this terminology. The data on the PBT solutions studied here give $\tau^{(2)}/\tau^{(1)}$ equal to 30 and 5 for PBT-28 and PBT-53, respectively, about independent of c_R. These values are both larger than predicted for monodisperse rodlike chains [23], and probably indicate that the molecular weight distribution is more broad for PBT-28 than for PBT-53. Since the shape of the reduced $R(t)/R_0^{(S)}$ vs. t/τ_c are independent of c_F at fixed c_R, the addition of nylon-66 does not change $\tau^{(2)}/\tau^{(1)}$.

The disparity between the rheological properties of PBT and nylon simplified the preceding analysis in some respects. A slightly more complicated representation is needed for the PBO/PabBO blends as the two components have similar rheological properties. In particular, the shear modulus $G_B(t)$ for the blend could be expressed in terms of the shear moduli $G_R(t)$ and $G_F(t)$ for the rod and flexible chain components as

$$G_B(t) = w_R^{-r} G_R(t/\tau_R') + w_F^{-f} G_F(t/\tau_F') \tag{21}$$

Here, w_R and w_F are the weight fractions of the rod and flexible chain components, respectively, τ_R' and τ_F' are certain average time constants associated, respectively, with the dynamics of these chains as they exist in the blend, and r and f are empirical exponents,

expected to lie between zero and some small number. It is assumed that the moduli $G_R(t/\tau_R')$ and $G_F(t/\tau_F')$ are similar to the corresponding moduli for the individual solutions with τ_R' and τ_F' replaced by the time constants τ_R and τ_F for those materials, respectively. As the relaxation spectra for the blends and the component solutions all have similar shapes, albeit shifted on the time scale, this assumption seems to be reasonable. One consequence of this is that the nonlinear flow curves of the viscosity versus the shear rate may all be superposed.

The disparity between $G_R(t/\tau_R')$ and $G_F(t/\tau_F')$ simplified the analysis of the rheological behavior of PBT/nylon blends. Conversley, their similarity complicates the description of the rheological behavior of PB)/PabBO blends. Thus, f was set equal to zero for the PBT/nylon case, and the contribution due to $G_F(t/\tau_F')$ was neglected for the time range and properties of interest owing to the large separation between τ_R' and τ_F' in that system.

In any case, the viscosity is then given as usual by Eqn. 11 with m = 2, and $F(\gamma) = 1$. to give the result

$$\eta_B = w_R^{-r}(\tau_R'/\tau_R)\eta_R + w_F^{-f}(\tau_F'/\tau_F)\eta_F \qquad (22)$$

where η_R and η_F are the viscosities of the rod and flexible chain component solutions, respectively. Arguments on the scaling behavior of flexible chains discussed in the preceding give $\tau_F'/\tau_F = -3f/2$, with f = 5/4. The estimate for τ_R'/τ_R is made following the procedure discussed above (r is set equal to zero above)., as in that work. Thus

$$\tau_R'/\tau_R = f(c_R/c_R\dagger)/f(c_R/c_R\dagger\dagger) \qquad (23)$$

where c_R is the concentration of the rod component in the mixture, $c_R\dagger = (c_R)_{NI}$ is the concentration of the rod required to form a nematic phase in the absence of any flexible chain, $c_R\dagger\dagger = (c_R)_{NI,B}$ is the latter in the blend, and f is the "crowding function" discussed above. The procedure to determine $c_R\dagger\dagger$ from the phase diagram discussed is discussed above.

The above expression for η_B differs from that discussed for the PBT/nylon case only by inclusion of the second term, made necessary here as η_F is not much smaller that η_R, as was the case in the study on PBT/nylon mixtures. As shown in Fig. 30, the expression provides a reasonable, though imperfect, fit to the experimental results on the PBO/PbO blends.

Transient Nonlinear Viscoelasticity. As might have been anticipated, the strain criterion observed here for onset of nonlinear creep with solutions of the blends is like that found for solutions of both rodlike and flexible chains. Moreover, the relaxation behavior shown in Fig. 22 is like that reported in reference [6] for solutions of PBT. As discussed in reference [6], $\hat{\eta}_\kappa(t)/\eta_\kappa$ and $\hat{M}_\kappa(t)/M_\kappa$ may be approximated, respectively, as

$$\hat{\eta}_\kappa(t/\tau_c)/\eta_\kappa = \hat{\eta}_o(t/\beta_\kappa)/\eta_o \tag{24}$$

$$\hat{M}_\kappa(t)/M_\kappa = \hat{M}_o(t/\beta_\kappa)/M_o \tag{25}$$

where

$$\frac{\hat{\eta}_o(t/\tau_c)}{\eta_o} = \frac{\Sigma' g_\nu \tau_\nu \exp(-t/\tau_c)}{\Sigma' g_\nu \tau_\nu} \tag{26}$$

$$\frac{\hat{M}_o(t/\tau_c)}{M_o} = \frac{\Sigma' g_\nu \tau_\nu^2 \exp(-t/\tau_c)}{\Sigma' g_\nu \tau_\nu^2} \tag{27}$$

and β_κ is a parameter, see below. These expressions are reasonable approximations to results calculated with Eqn. (11), along with the use of Eqn. (12) for $\hat{M}_o(t)$ (see reference [6]). In the latter expression, $\hat{M}_o(t)$ is the limiting behavior of $\hat{M}_\kappa(t)$ for small κ, and M_o is equal to $2C'R_o^{(S)}$. As shown in the insert to Fig. 21, the same β_κ is determined for data on $\hat{\eta}_\kappa(t/\tau_c)$ and $\hat{M}_\kappa(t)$. Moreover, as shown in the same insert, β_κ is very close to the parameter $\tau_\kappa = \eta_k R_\kappa^{(S)}$ calculated from data on the steady-state viscosity η_κ and the recoverable compliance $R_\kappa^{(S)}$ following cessation of (nonlinear) flow at strain rate κ. In this context, τ_κ, which is smaller than τ_c, serves as a measure of the more rapid relaxation observed following steady-state flow in the nonlinear range, i.e., for $\tau_c\kappa > 1$ [6].

Steady-State Nonlinear Behavior. The scaling of $R(t)/R_o^{(S)}$ with t/τ_c as a function of c_F for fixed c_R means that the reduced steady-state properties η_κ/η_o, $R_\kappa^{(S)}/R_o^{(S)}$ and M_κ/M_o should scale with $\tau_c\kappa$ unless the function $F(\gamma)$ in Eqn. (11) depends on c_F. As shown in Figs. 23–27, the expected behavior is obtained with the systems studied here. The broader relaxation time distribution (larger $\tau^{(2)}/\tau^{(1)}$) for PBT-28 in comparison with PBT-53 is reflected in a slower decrease of η_κ/η_o with increasing $\tau_c\kappa$ for solutions with PBT-28. The reduced curves for $R_\kappa^{(S)}/R_o^{(S)}$ and M_κ/M_o versus $\tau_c\kappa$ could be fitted by the use of Eqn. (11) in the forms represented by Eqns. (13) and (14), respectively—the details of this calculation are discussed

in reference [6]. An example of the fit is given in Fig. 23 for data on A-1.54/0 and A-1.43/0.96—comparable fits were obtained in all cases. In these calculations β was treated as an empirical parameter, in the expectation that β^{-1} would be close to the value $\beta^{-1} = \gamma'[1 + (\gamma/\gamma') - (\gamma/\gamma')^2/2]^{1/2}$ appearing in Eqns. (11)-(15). In fact, β^{-1} was found to be 4.17 for a nylon-66 solution ($w_F = 0.24$), and about 2.5 for the solutions of the blends. The calculated curves are limited to relatively low $\tau_c\kappa$ (< ca. 10) since the data on $R_0(t)$ did not include results for $t/\tau_c <$ ca. 0.1.

The results on M_κ/M_0 are less well represented by the use of Eqn. (11), as represented by Eqn. (15). As may be seen in Fig. 28, the data on $\Delta n_{13}R_0^{(S)}$ versus $\tau_c\kappa$ do conform essentially to a single reduced curve, but the behavior at low κ is unexpected. Values of $2C' = M_0/R_0^{(S)}$ entered in Tables 4 and 5 were obtained by fitting Eqn. (15) to the experimental data for $\tau_c\kappa >$ ca. 0.3. The results are in good agreement with C' reported in reference [6]. Although, M_κ was not obtained for $\tau_c\kappa < 0.2$ for solutions in series A, data were obtained for $\tau_c\kappa$ as low as 0.02 for solutions in series C. In every case, the latter gave larger M_κ (or larger $\Delta n_{13}R_0^{(S)}$) than expected for $\tau_c\kappa <$ ca. 0.3. That is, instead of reaching the limiting value 2C' expected at small $\tau_c\kappa$, $M_\kappa/R_0^{(S)}$ continued to increase at the lowest $\tau_c\kappa$ studied, see Fig. 28. Similar behavior was reported for solutions of PBT in reference [6]. The reason for the discrepancy at small $\tau_c\kappa$ is unknown. One possibility might be the presence of a small fraction of aggregates of the rodlike chains. These could have a different polarizability than the single chain, and could dominate the flow birefringence at small $\tau_c\kappa$, but make a negligible contribution at larger $\tau_c\kappa$. This would be the pattern of behavior expected with Eqns. (11) and (15) with G(t) having a few components at very large τ_ν, but small g_ν. Nevertheless, we note that solutions with sufficient association to result in a noticeable decrease in η exhibit suppressed M_0, reflecting the general shift of the distribution of relaxation times to smaller values, as the rotational contraints are reduced with fewer species. A similar trend was noted for the effect of association on $c_{N\Gamma}$ in reference [6] .

CONCLUSION.

Rheological and rheo-optical data of miscible mixtures of rodlike PBT and flexible nylon-66 in solution and mixtures of PBO and PabBO have been analyzed to show that most of the observed behavior can be placed in a simple and consistent frame. The set of reduced retardation times and weights (λ_ν/τ_c and r_ν) for the solution of the rodlike chain is found to be unchanged by addition of the flexible chain. By contrast, the viscosity □ and the time constant $\tau_c = \eta R_0^{(S)}$ change considerably on addition of the flexible chain. This behavior is attributed

to the dominance of contributions due to the constrained rotational diffusion of the rodlike component on the rheological properties of the blend. The set of reduced relaxation times and weights (τ_v/τ_c and g_v) deduced from the set of reduced retardation times and weights may be used with a single-integral constitutive equation of the BKZ-type to predict nonlinear behavior, including relaxation of the stress and birefrigence following steady-state shear, and steady-state properties such as the viscosity, the recoverable compliance and the flow birefringence as functions of the shear rate. A discrepancy in the latter behavior at low shear rate may reflect a small fraction of associated chains. The dependence of the linear (Newtonian) viscosity of the solution on the concentration of the flexible chain is believed to reflect the proximity of the composition to that for phase separation at fixed c_R/c_F. similar to the behavior with binary isotropic solutions of rodlike chains. This simplified model is not expected to apply under all conditions, as discussed above.

REFERENCES

1. W. F. Hwang, D. R. Wiff, C. L. Benner and T. E. Helminiak, J. *Macromol Sci. Phys.*, **B22**, 231-257 (1983).
2. M. Takayanagi, T. Ogata, M. Morikawa and T. Kai, *J. Macromol. Sci. Phys.*, !**B17**, 591-615 (1980).
3. P. J. Flory, *Adv. Polym. Sci.*,, **59**, 1-36 (1984).
4. W. F. Hwang, D. R. Wiff and C. Verschoore, *Polym. Engr. Sci.*, **23**, 789-791 (1983).
5. S.-G. Chu, S. Venkatraman, G. C. Berry and Y. Einaga, *Macromolecules*, **14**, 939-946 (1981).
6. S. Venkatraman, G. C. Berry and Y. Einaga, *J. Polym. Sci., Polym. Phys. Ed.*, **23**, 1275-1295 (1985).
7. Y. Einaga, G. C. Berry and S.-G. Chu, *Polym. J.*, **17**, 239-251 (1985).
8. M. Doi and S. F. Edwards, *The Theory of Polymer Dynamics*, Clarendon Press, Oxford, 1986.
9. J. A. Odell, A. Keller and E. D. T. Atkins, *Macromolecules*, **18**, 1443-1453 (1985).
10. G. C. Berry, *Disc. Farada, 79*, 141-148 (1985).
11. G. C. Berry and T. G Fox, *Adv. Polym. Sci.*, **5**, 261-357 (1968).
12. H. Yamakawa, *Modern Theory of Polymer Solutions*, Harper and Row, NY, 1971.
13. M. Doi, *J. Phys.*, (Paris) **36**, 607-611 (1975).
14. P. J. Flory, *Proc. R. Soc. London Ser.*, **A234**, 73-89 (1956).
15. S. F. Edwards and K. E. Evans, *J. Chem. Soc.*, Faraday Trans. 2, **78**, 113-121 (1982).
16. J. O. Park and G. C. Berry, *Macromolecules*, !**22**, 3022-3029 (1989).
17. W. W. Graessley and S. F. Edwards, *Polymer*, **22**, 1329-1334 (1981).
18. G. C. Berry and D. J. Plazek, In *Glass: Science and Technology*, Ed. by D. R. Uhlmann and N. J. Kreidel, Academic Press, NY, **Vol. 3**, Chapter 6, p. 319-362 (1986).
19. K. Nakamura, C.-P. Wong and G. C. Berry, *J. Polym. Sci., Polym. Phys. Ed.*, **22**, 1119-1148 (1984).
20. H. Markovitz, In *American Institute of Physics 50th.. Aniversary Physics Vade Mecum* , H. L. Anderson Ed., American Institute of Physics, New York, Chapter 19, p. 274-286 (1981).
21. J. D. Ferry, *Viscoelastic Properties of Polymers*, Wiley, NY, **3rd. Ed.**, 1980.
22. B. Bernstein, E. A. Kearsley and L. J. Zapas, *Trans. Soc. Rheol.*, **17**, 391-410 (1963).
23. M. Doi and S. F. Edwards, *J. Chem. Soc.*, Faraday Trans. 2, **74** , 1789-1801, 1802-1817, 1818-1832 (1978).
24. H. M. Laun, *Rheol. Acta*, **17**, 1-15 (1978).
25. H. Janeschitz-Kriegl, *Adv. Polym. Sci.*, **6**, 170-318 (1969).
26. C. C. Lee, S.-G. Chu and G. C. Berry, *J. Polym. Sci., Polym. Phys. Ed.*, **21**, 1573-1597 (1983).
27. M. Kurata, Y. Tsunashima, M. Iwama and K. Kamada, In *Polymer Handbook*, J. Brandrup and E. H. Immergut, Eds., Wiley, New York, **2nd. Ed.**, pp. IV-1 to IV-60 (1975).
28. G. C. Berry and C.-P. Wong, *J. Polym. Sci., Polym. Phys. Ed.*, !**13**, 1761-1781 (1975).
29. P. G. de Gennes, *Scaling Concepts in Polymer Physics*, Cornell University Press, Ithaca 1979.

30. G. Marrucci and N. Grizzuti, *J. Polym. Sci., Polym. Lett. Ed.*, **21**, 83-86 (1983); *J. Non-Newtonian Fluid Mech.*, **14**, 103-119 (1984).
31. K. Osaki, N. Bessho, T. Kojimoto and M. Kurata, *J. Rheol.*, **23**, 457-475 (1979).
32. K. Se and G. C. Berry, In *Reversible Polymeric Gels and Related Systems*, P. S. Russo, Ed., Chapter 10, p. 129-151 ACS Symp. Series, 1987.
33. V. J. Sullivan, *Rheology Phase Behavior and Dilute Solution Properties of Blends of the Rodlike Poly(p-Phenylene Benzobisoxazole) and Flexible Chain Poly (2,5-Benzoxazole) in Sulfonic Acid Solvents*,. Dissertation, Carnegie Mellon University, 1990.
34. P. G. de Gennes, *J. Physique* , (Paris), **42**, 473-477 (1981).

TABLE 4. Linear viscoelastic parameters for solutions containing PBT-28.[a]

Sample[b]	η/kPa s	$R_0^{(S)}$ /kPa^{-1}	τ_c/s
A-1.75/0	8.26	50	413
A-1.54/0	2.8	38	105
A-0.54/2.16	0.20	82	17
A-0.83/1.93	2.8	130	359
A-1.11/1.66	17.6	(120)[d]	2,110
A-1.10/1.10	10.5	75	788
A-1.43/0.96[c]	16.5	45	742
A-1.74/0.75	111	(89)[d]	9,880
A-1.95/0.49	(251)[e]	(77)[d]	19,300

[a]Entries for h and τ_c interpolated to $T = 297$ K by multiplication of data obtained at T by exp $W(297^{-1} - T^{-1})$, where $W = 4065$ K.

[b]The first and second numbers give the weight precent PBT-28 and nylon-66 in the solution, respectively.

[c]$M_0R_0^{(S)-1}$ /MPa^{-1} equal to 4.0 for this solution.

TABLE 5. Linear viscoelastic parameters for solutions containing PBT-53.[a]

Sample[b]	η/Pa s	$R_0^{(S)}$ /kPa $^{-1}$	τ_c/s	$M_0R_0^{(S)-1}$ /MPa $^{-1}$
C-0.43/1.79	5.51	...	...	...
C-0.87/0	10.8	8.0	0.086	3.4
C-0.86/1.58	24.0	10.5	0.25	...
C-1.29/0	38.0	9.5	0.36	4.0
C-1.29/0.45	46.2	9.2	0.43	3.5
C-1.28/0.68	51.2	10.0	0.51	4.2
C-1.27/0.90	57.0	9.3	0.53	4.3
C-1.27/1.12	68.2	12.0	0.82	4.0
C-1.28/1.35	73.0	12.0	0.88	...
C-1.30/1.58	76.0	10.5	0.80	3.7
C-1.29/1.81	102	8.8	0.89	...
C-1.71/0	124	11.5	1.43	2.6
C-1.70/0.67	92	8.2	0.75	4.2
C-1.72/0.89	174	12.2	2.12	4.2
C-1.72/1.01	153	10.0	1.53	...
C-1.73/1.13	162	9.7	1.57	3.0
C-2.11/0	305	10.5	3.20	...
C-2.11/0.45	360	13.0	4.68	3.8
C-2.14/0.67	217	9.0	1.95	2.8
C-2.11/0.77	315	11.0	3.47	...
C-2.18/0.92	355	10.5	3.73	1.8
C-2.54/0	730	11.5	8.40	2.0
C-2.54/0.22	720	11.0	7.92	3.0
C-2.51/0.37	810	12.0	9.72	...
C-2.57/0.45	1050	12.5	13.13	1.1
C-2.55/0.52	(805) (11.5)	(9.26)	...	...

[a] T = 297 K except for entries in parentheses; in the latter case, the measured η/ and τ_c for T = 313 K were multipled by 2.013 to convert to the equivalent data at T = 297 K had the sample remained isotropic.

[b] The first and second numbers give the weight percent PBT-53 and nylon-66 in solution, respectively.

TABLE 6. Linear viscoelastic parameters for solutions of PBO, PabBO and their mixtures

Sample[b]	η/Pa s	$R_0^{(S)}$ /kPa^{-1}	τ_c/s
00/1.00	7.62	6.6	0.0503
00/3.01	46.4	2.2	0.102
00/4.14	620	1.6	0.992
00/4.91	1420	1.1	1.56
00/6.10	2910	0.99	2.88
00/6.96	4410	1.4	6.17
1.04/00	6.4	...	...
1.96/00	44.5	1.1	0.0410
2.96/00	179	2.6	1.17
4.16/00	1100	4.4	4.84
4.92/00	1410	3.3	4.65
2.00/0.99	290	3.3	0.957
2.12/2.08	1230	3.6	4.43
1.98/3.10	2050	2.6	5.33
3.07/1.02	565	5.3	2.99
3.10/2.06	1600	4.8	7.68
3.05/3.05	4210	15	63.2

[a] $T = 298$ K

[b] The first and second numbers give the volume percent PBO and PabBO in solution, respectively.

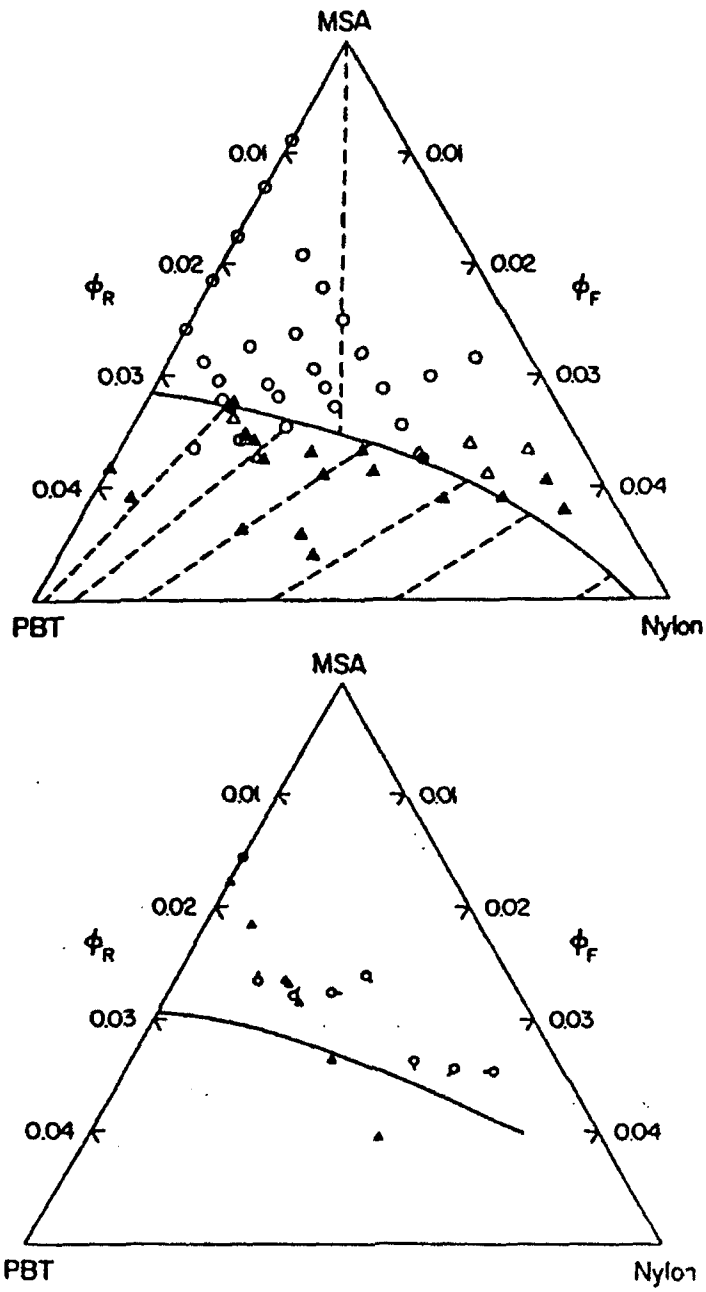

FIG. 13 Ternary diagrams for blends of PBT and nylon-66 in MSA. The unfilled and filled symbols represent isotropic and anisotropic compositions, respectively. The unfilled circles designate compositions used in rheological studies. The solid curve represents the binodal, and the heavy dashed line gives the tie lines, calculated as described in the text. The upper and lower figures are for series C and A, respectively. The light dashed line passing though the apex in the upper figure is discussed in the text.

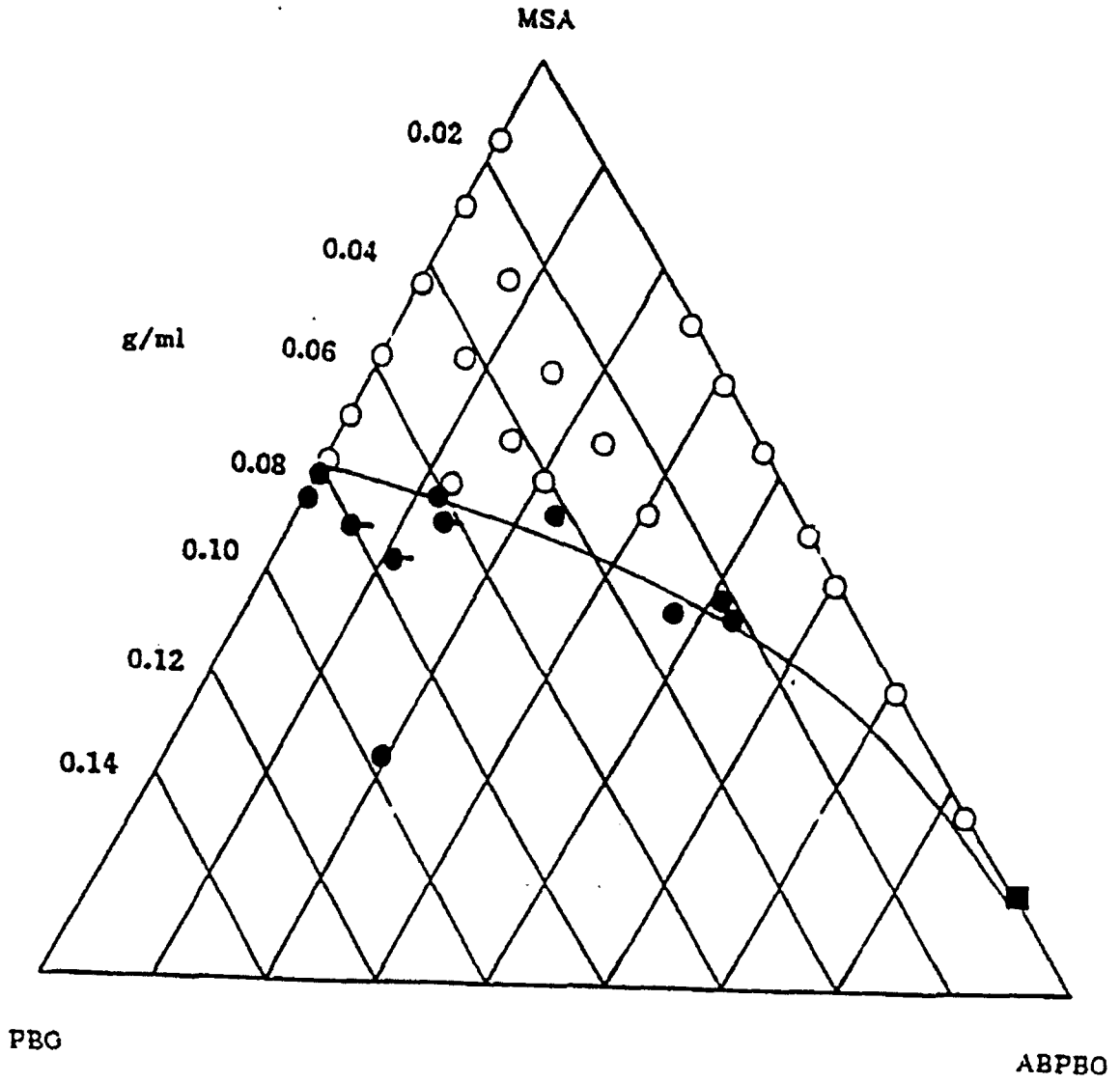

FIG. 14 Ternary diagrams for blends of PBO. The unfilled and filled symbols represent isotropic and anisotropic compositions, respectively. The unfilled circles designate compositions used in rheological studies. The solid curve represents the binodal.

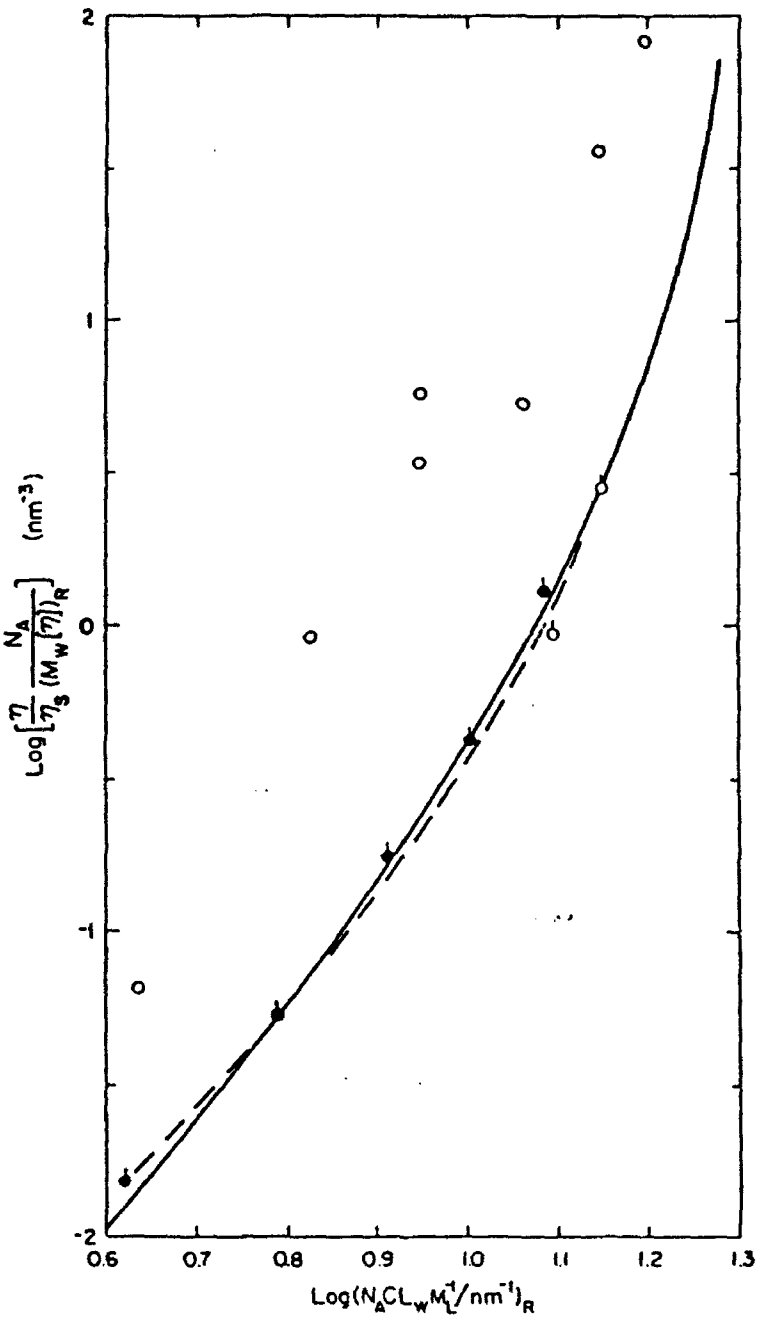

FIG. 15 The reduced viscosity $\eta/\eta_s(M_w[\eta])_R$ versus $(N_a c L_w/M_L)_R$ for solutions of PBT: series A (unfilled circles), and series C (filled circles), where η_s is the viscosity of the solvent. The symbols with a pip are for solutions with no nylon-66. The solid and dashed curves represent the use of Eqn. (1) with Eqns. (4) or (5), respectively; $\Omega = 1$ in both cases.

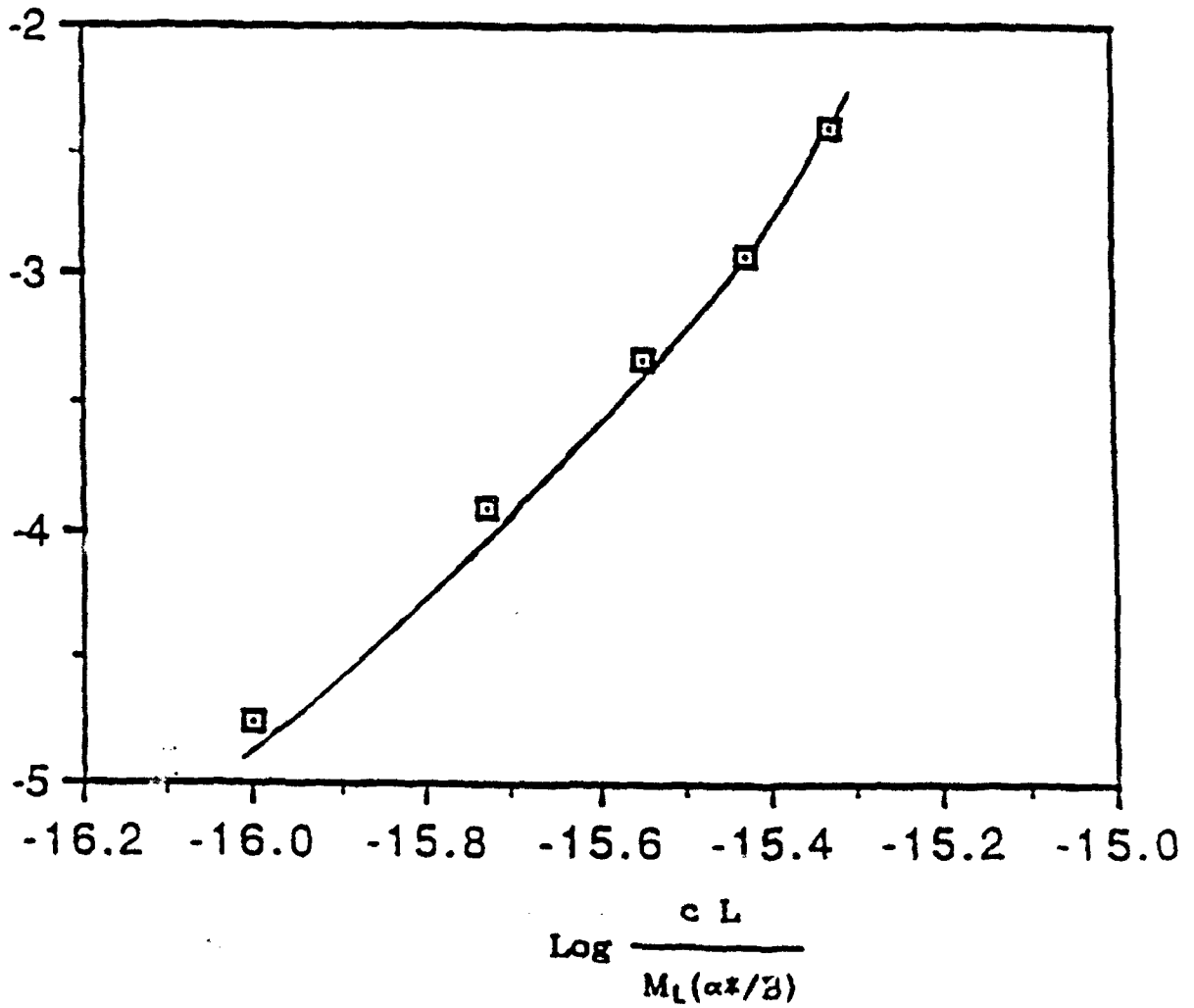

FIG. 16 The reduced viscosity $\eta/\eta_S(M_w[\eta](\alpha^*/B))_R$ versus $(N_a c L_w/M_L)_R$ for solutions of PBO, where η_S is the viscosity of the solvent. The solid and dashed curves represent the use of Eqn. (1) with Eqns. (4) or (5), respectively; $\Omega = 1$.

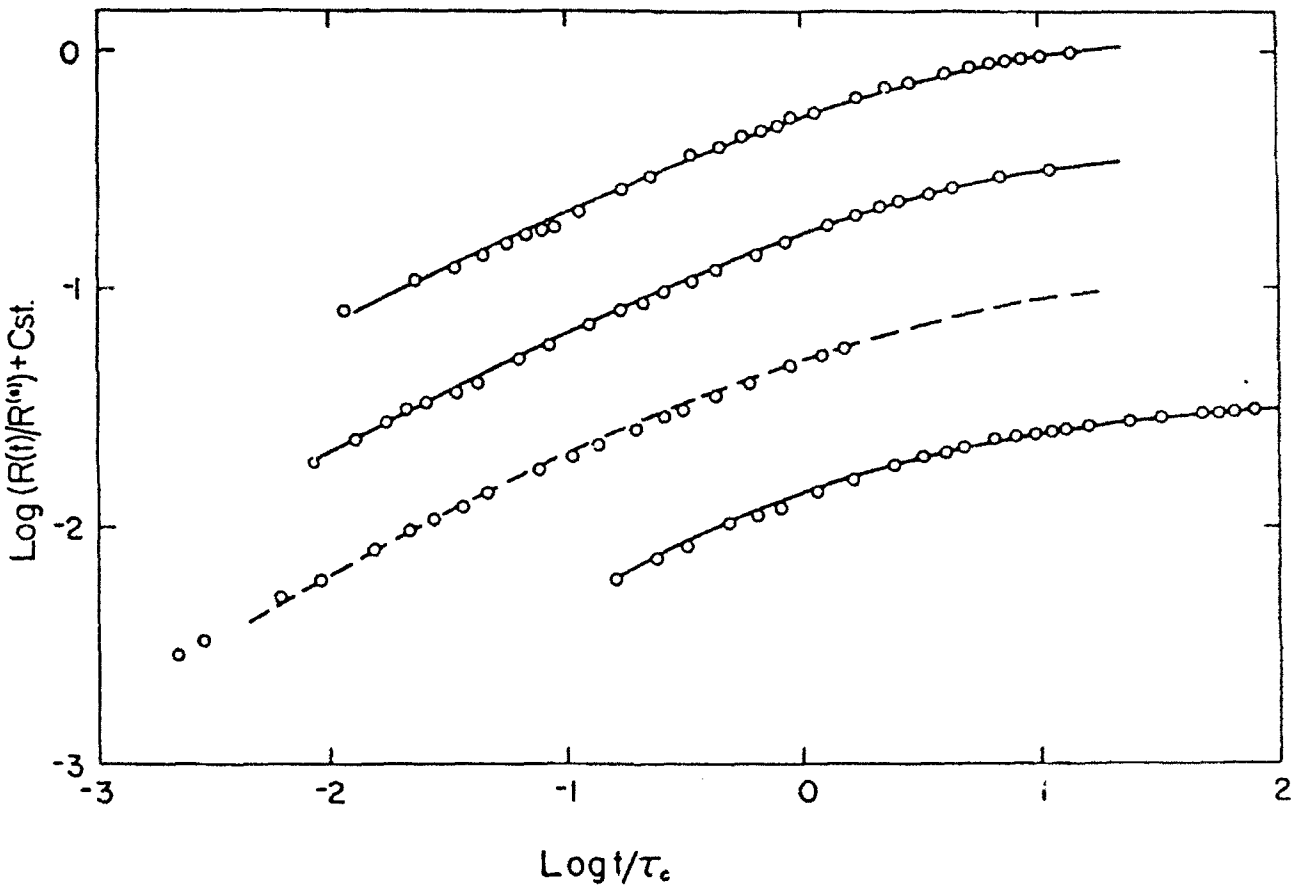

FIG. 17 The reduced linear recoverable compliance $R(t)/R_0^{(S)}$ versus reduced time t/t_c for solutions in series A and a solution of nylon-66. From top to bottom, A-1.54/0, A-1.11/1.66, A-1.43/0.96 and the nylon solution (w = 0.2381). The constant in the ordinate separates the curves by 0.5 units for clarity. Values of t_c and $R_0^{(S)}$ are given in Table 4, except for the nylon-66 solution, for which $R_0^{(S)} = 0.00056\ Pa^{-1}$ and $\tau_c = 3.3$ s.

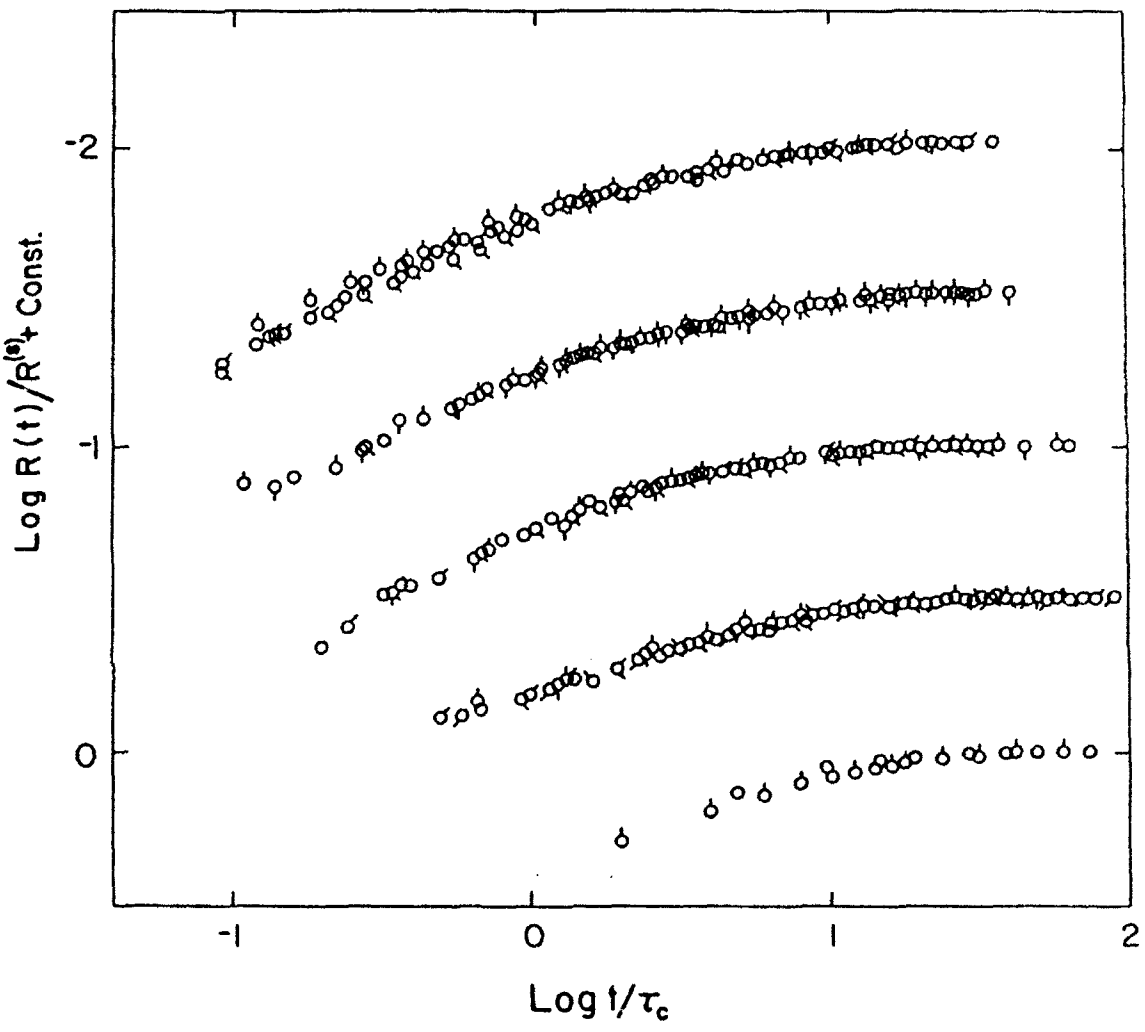

FIG. 18 The reduced linear compliance $R(t)/R_0^{(S)}$ versus reduced time for solutions in series C. The data are grouped in compositions with (essentially) common rodlike polymer concentration, with the samples having the highest concentration of rodlike polymer at the top (i.e., from top to bottom, C-2/54/F, C-2.11/F, C-1.72/F, C-1.29/F, and C-0.86/F). The data include samples with no nylon-66 (no pip) and indicate data with increasing nylon-66 as the pips rotate clockwise from straight up. The constant in the ordinate spearates the curves by 0.5 units for clarity. Values of τ_c and $R_0^{(S)}$ are given in Table 5.

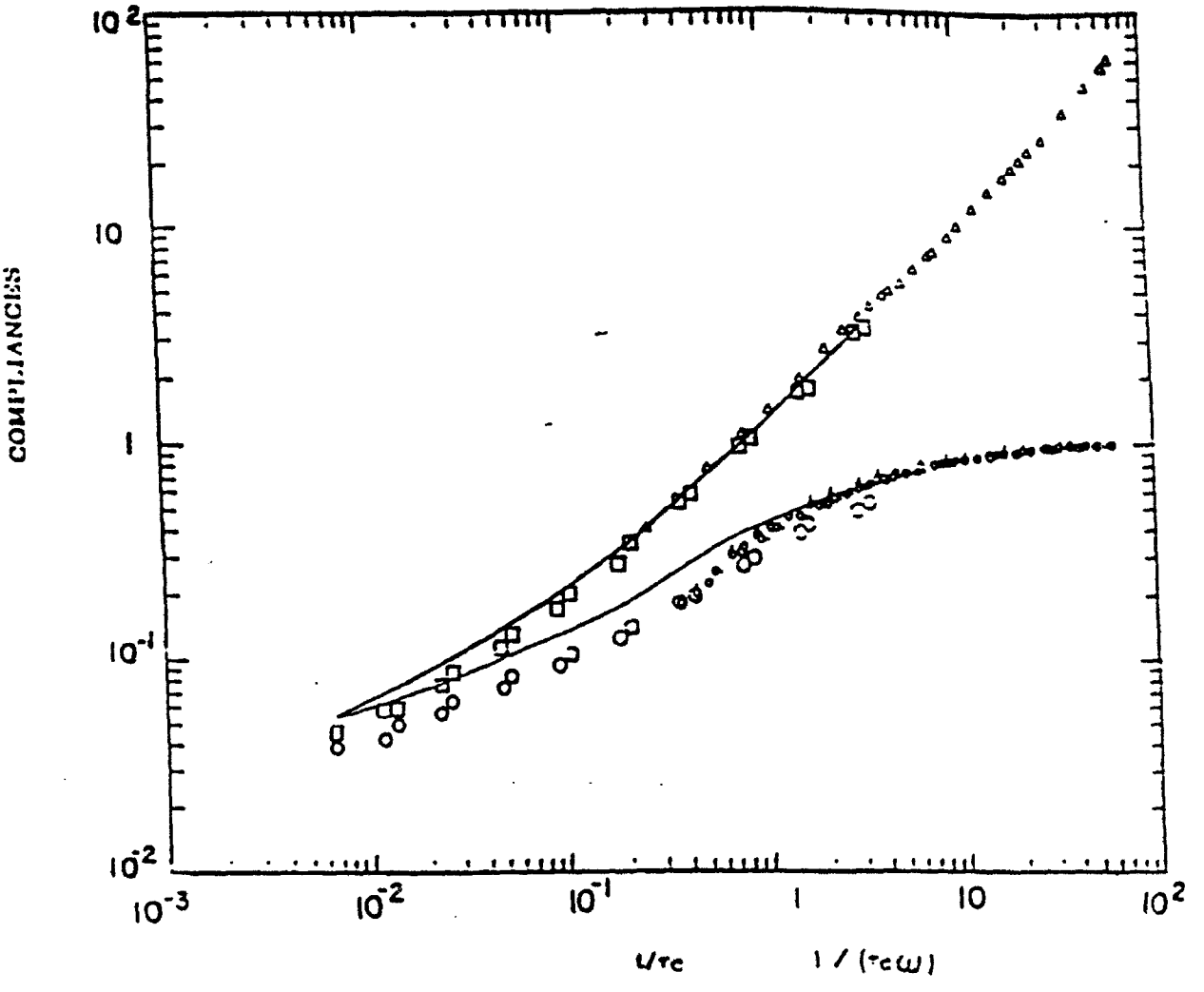

FIG. 19 Composite plot of reduced compliances versus t/τ_c for a solution of PBO ($\varphi = 0.0305$): $J'(\omega)/R_0^{(S)}$, large circle; $J''(\omega)/R_0^{(S)}$, squares; $J(t)/R_0^{(S)}$, triangles, and $R(t)/R_0^{(S)}$, small circles. The upper line gives $J_d(\omega)/R_0^{(S)}$, and the lowere line gives $J_{d,R}(\omega)/R_0^{(S)}$.

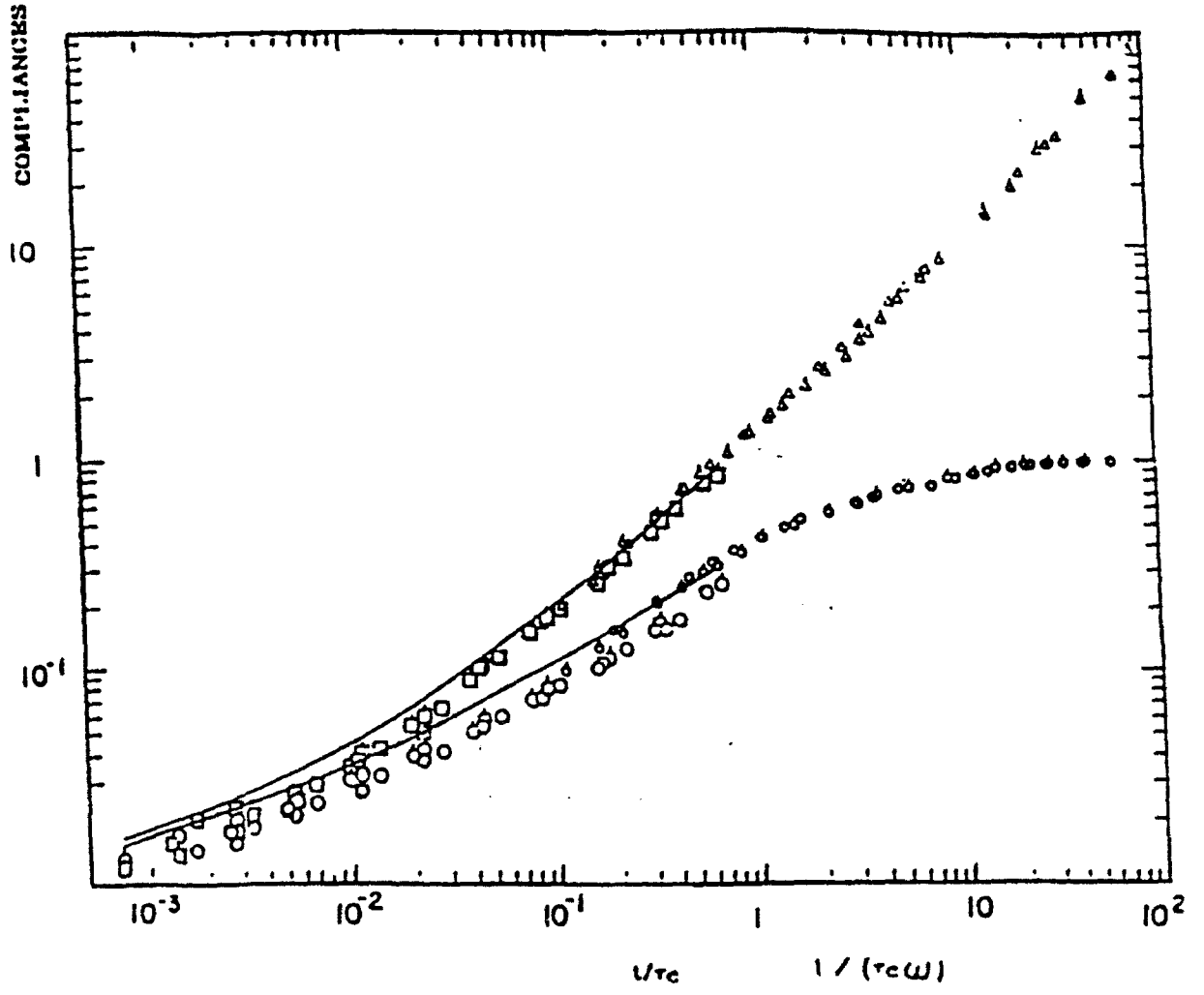

FIG. 20 Composite plot of reduced compliances versus t/τ_c for a solution of a blende of PBO and PabBO for compositions of 3.10/2.06 (no pips) and 3.07/1.02 (with pips): $J'(\omega)/R_o^{(S)}$, large circle; $J''(\omega)/R_o^{(S)}$, squares; $J(t)/R_o^{(S)}$, triangles, and $R(t)/R_o^{(S)}$, small circles. The upper line gives $J_d(\omega)/R_o^{(S)}$, and the lowere line gives $J_{d,R}(\omega)/R_o^{(S)}$.

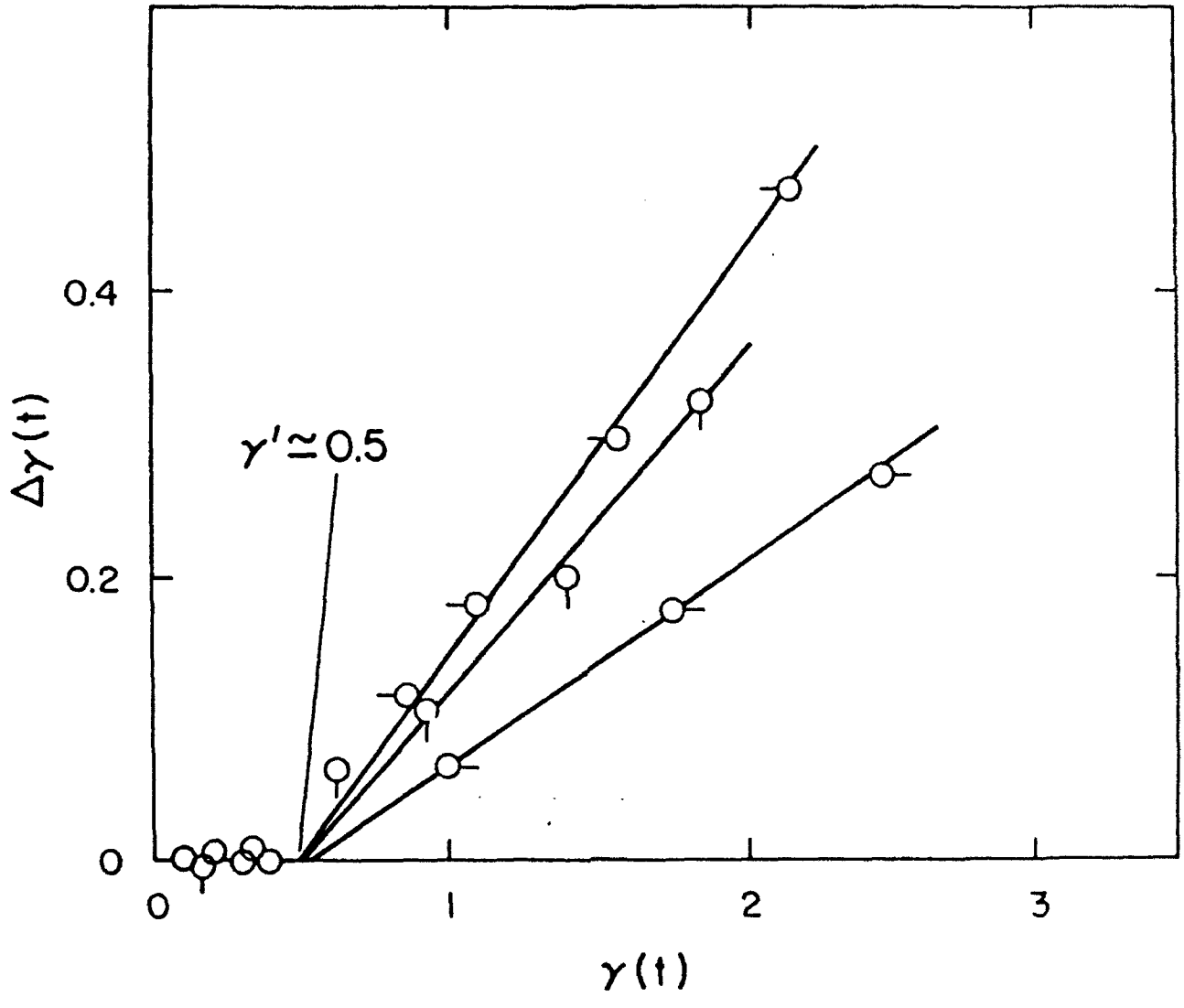

FIG. 21 The differential strain $\Delta\gamma(t) = \sigma[J_\sigma(t) - J_0(t)]$ versus $\gamma(t)$ for A-1.10/1.10. The data give a critical strain γ' equal to 0.5.

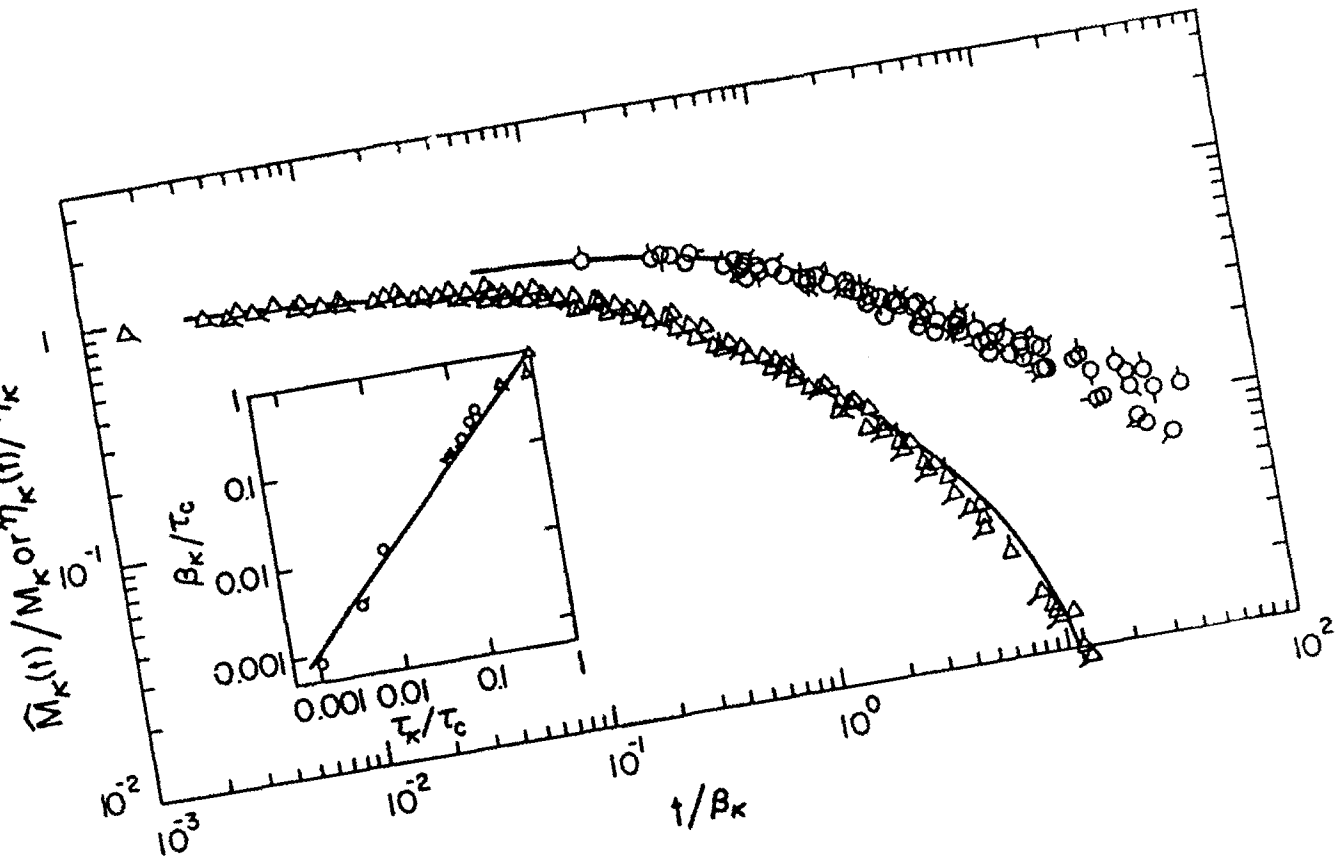

FIG. 22 Reduced flow birefringence relaxation function $\hat{M}_K(t)/M_K$ (circles) and stress relaxation function $\hat{\eta}_K(t)/\eta_K$ (triangles) for solutions in series A. The temperature was 301K except where noted by an asterisk, for which T = 288K. The symbols denote samples and strain rates (s^{-1}) as follows:

A-1.54/0	---	7.52×10^{-4}
A-1.95/0.49	0.422	---
A-1.74/0.75	---	2.51×10^{-5} and 5.02×10^{-5}
A-1.11/1.66	0.146	---
A-0.83/1.93	0.357	---
A-0.54/2.16	0.192	0.015
A-0.54/2.16	0.260	---
A-0.54/2.16	0.366	---
A-0.54/2.16	0.575	---

For the circles, the pips rotate clockwise from straight up from top to bottom of the column. For the triangles, the pips rotate clockwise from straight up with decreasing shear rate except for $k = 7.52\times10^{-4}$, for which no pip is used. The insert gives β_K/τ_c versus τ_K/τ_c for the solutions identified above.

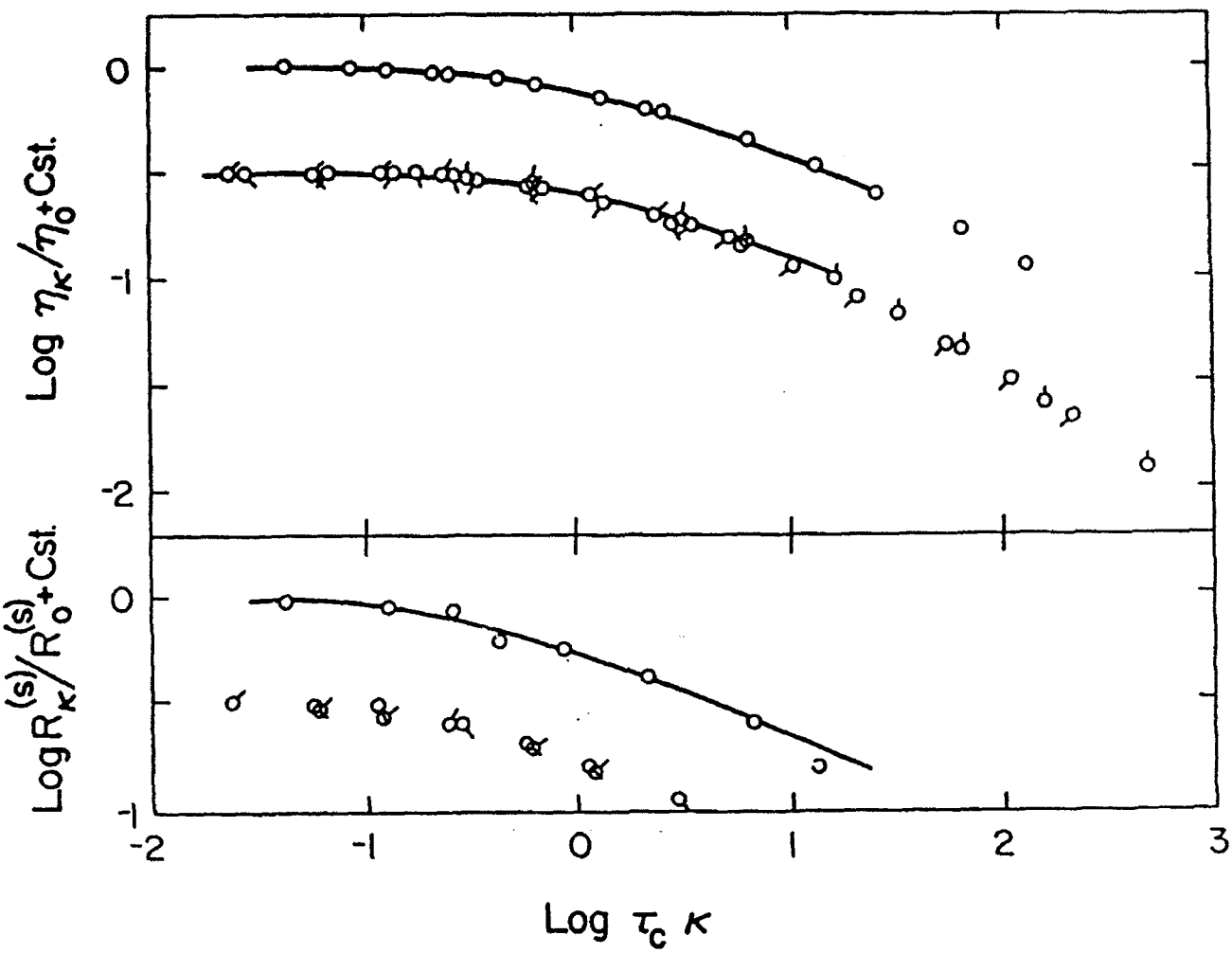

FIG. 23 The reduced steady-state viscosity η_κ/η_o and recoverable compliance $R_k^{(S)}/R_o^{(S)}$ versus the reduced shear rate $\tau_c\kappa$ for two of the solutions of mixtures of PBT and nylon. The upper and lower data sets in each panel are for A-1.54/0 and A-1.43/0.96, respectively. The former are at 301 K and the latter are at 301, 313, 328 or 335 K as the pips rotate clockwise from up. The curves are calculated as described in the text. Values of η_κ, $R_o^{(S)}$ and t_c are given in Table 5.

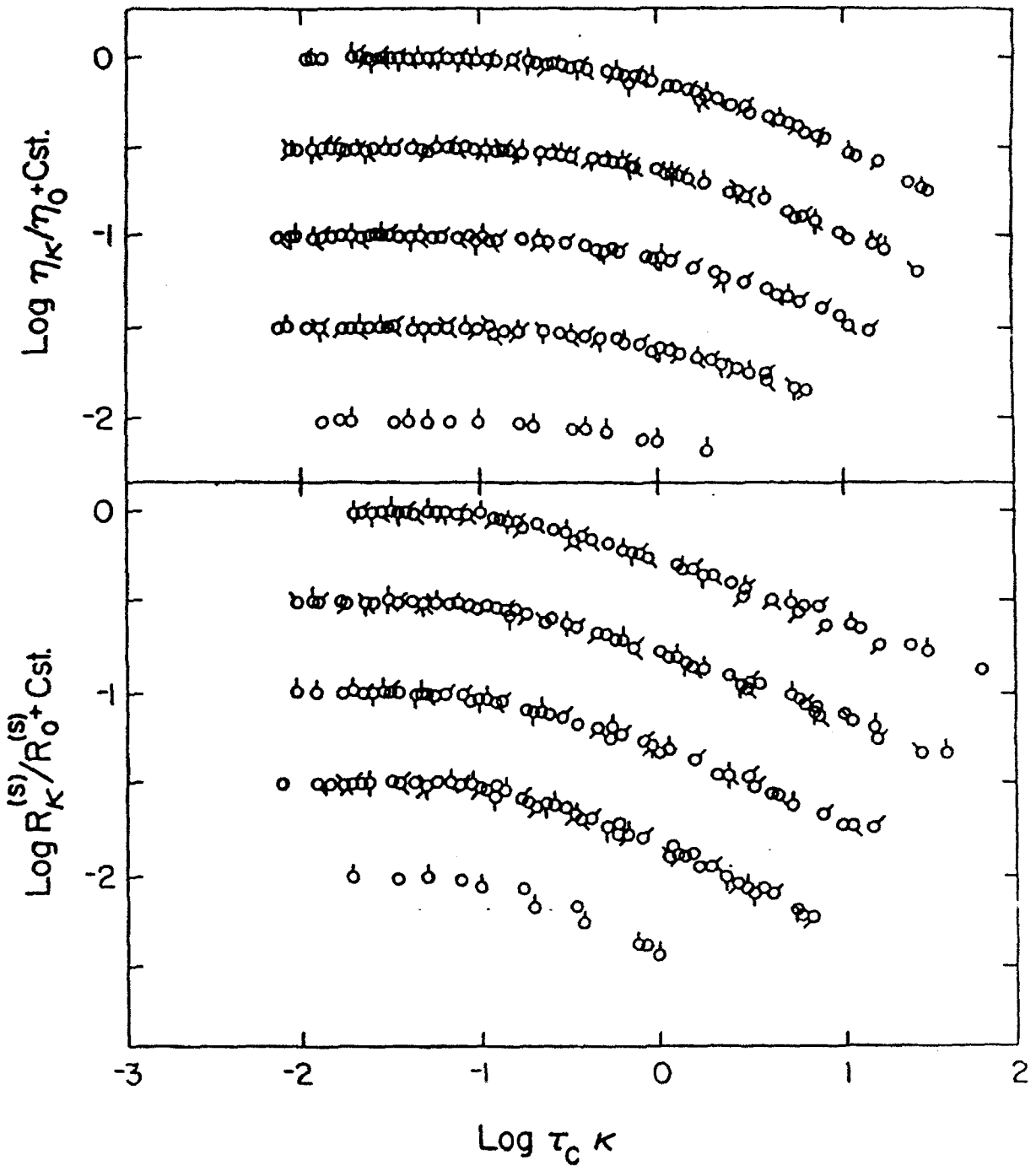

FIG. 24 The reduced steady-state viscosity η_κ/η_0 and recoverable compliance $R_k^{(S)}/R_o^{(S)}$ versus the reduced shear rate $\tau_c\kappa$ for solutions of mixtures of PBT and nylon listed in Table 5. The data are grouped in each panel as in Fig. 23 (e.g., C-2.54/F samples at the top). The data cover a span of temperature, as discussed in the text; temperature are not indicated in the interests of clarity. Values of η_κ, $R_o^{(S)}$ and τ_c are given in Table 5.

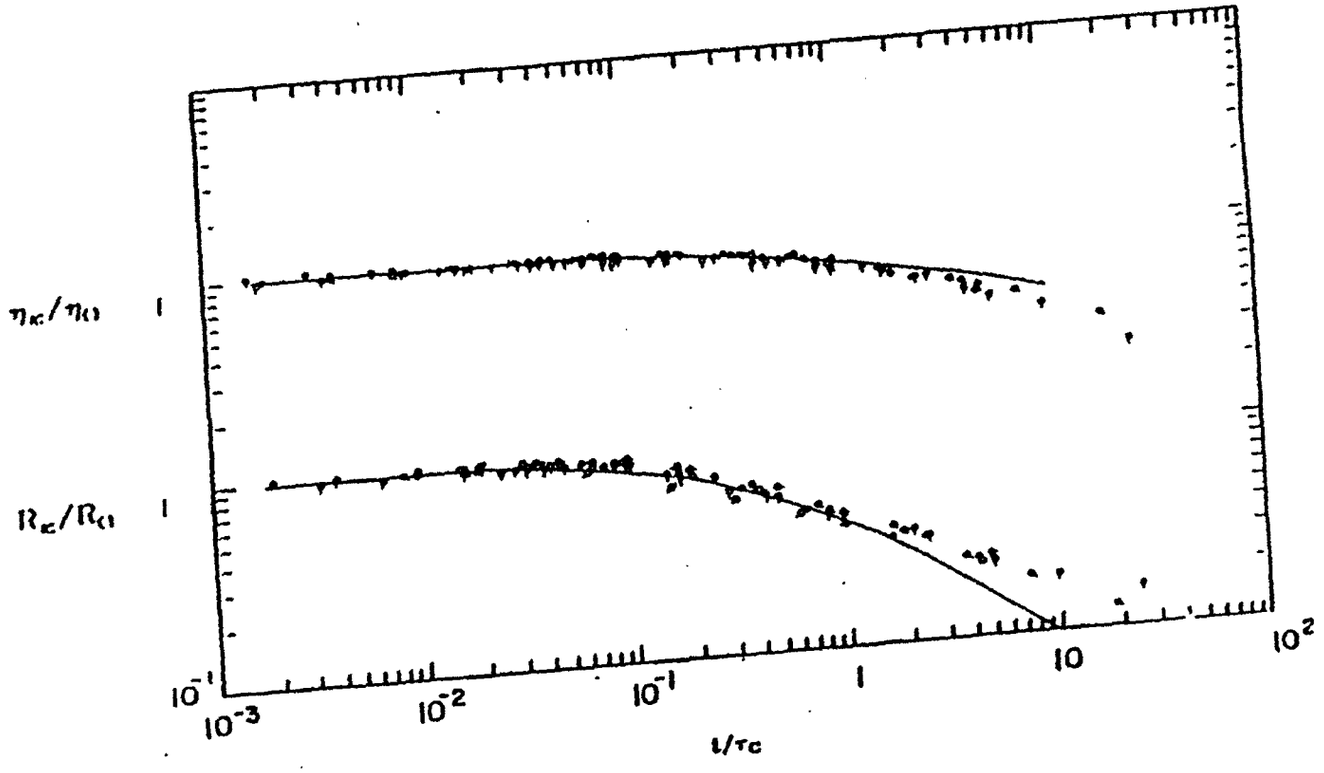

FIG. 25 The reduced steady-state viscosity η_κ/η_0 and recoverable compliance $R_k^{(S)}/R_0^{(S)}$ versus the reduced shear rate $\tau_c\kappa$ for solutions of PBO listed in Table 6, with pips rotating clockwise with increasing concentration. Values of η_κ, $R_0^{(S)}$ and τ_c are given in Table 5. The curves are calculated with Eqns 13 and 14, using the experimental data on the distribution of relaxation times.

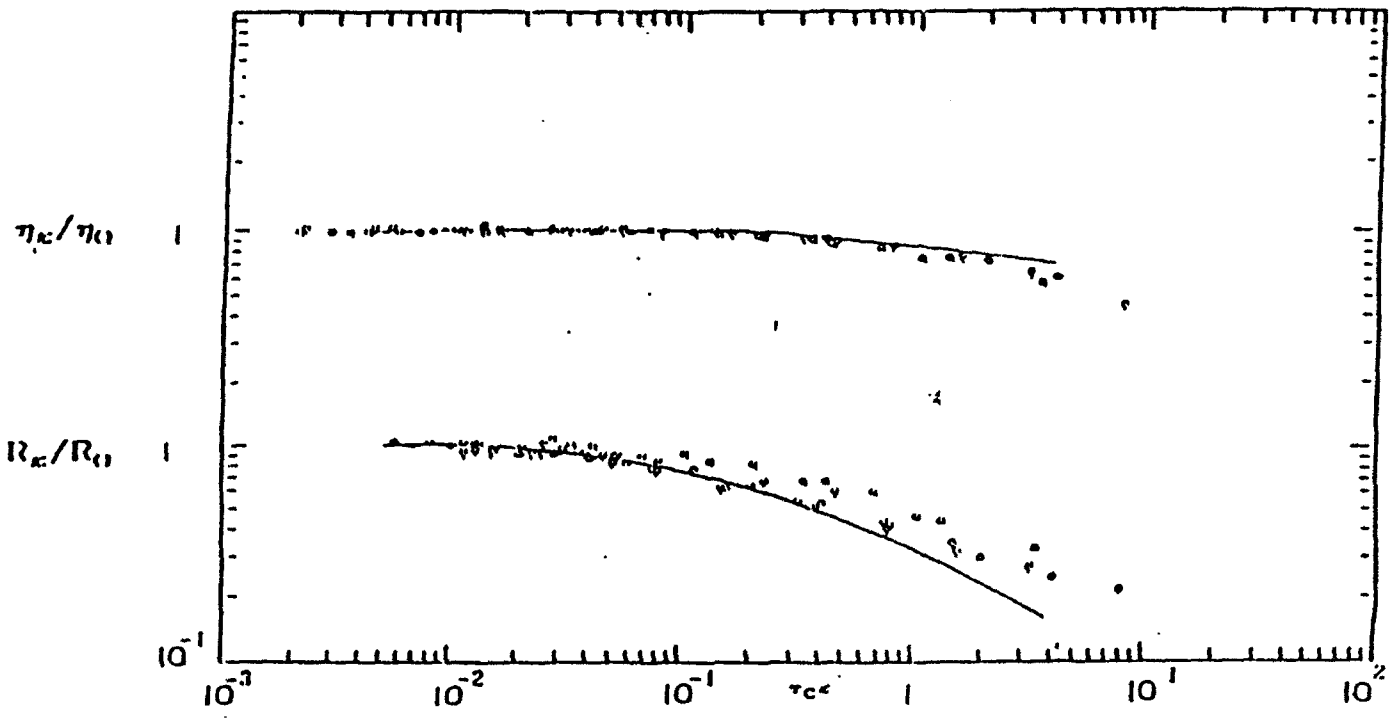

FIG. 26 The reduced steady-state viscosity η_κ/η_0 and recoverable compliance $R_k^{(S)}/R_0^{(S)}$ versus the reduced shear rate $\tau_c\kappa$ for solutions of PabBO listed in Table 6, with pips rotating clockwise with increasing concentration. Values of η_κ, $R_0^{(S)}$ and τ_c are given in Table 5. The curves are calculated with Eqns 13 and 14, using the experimental data on the distribution of relaxation times.

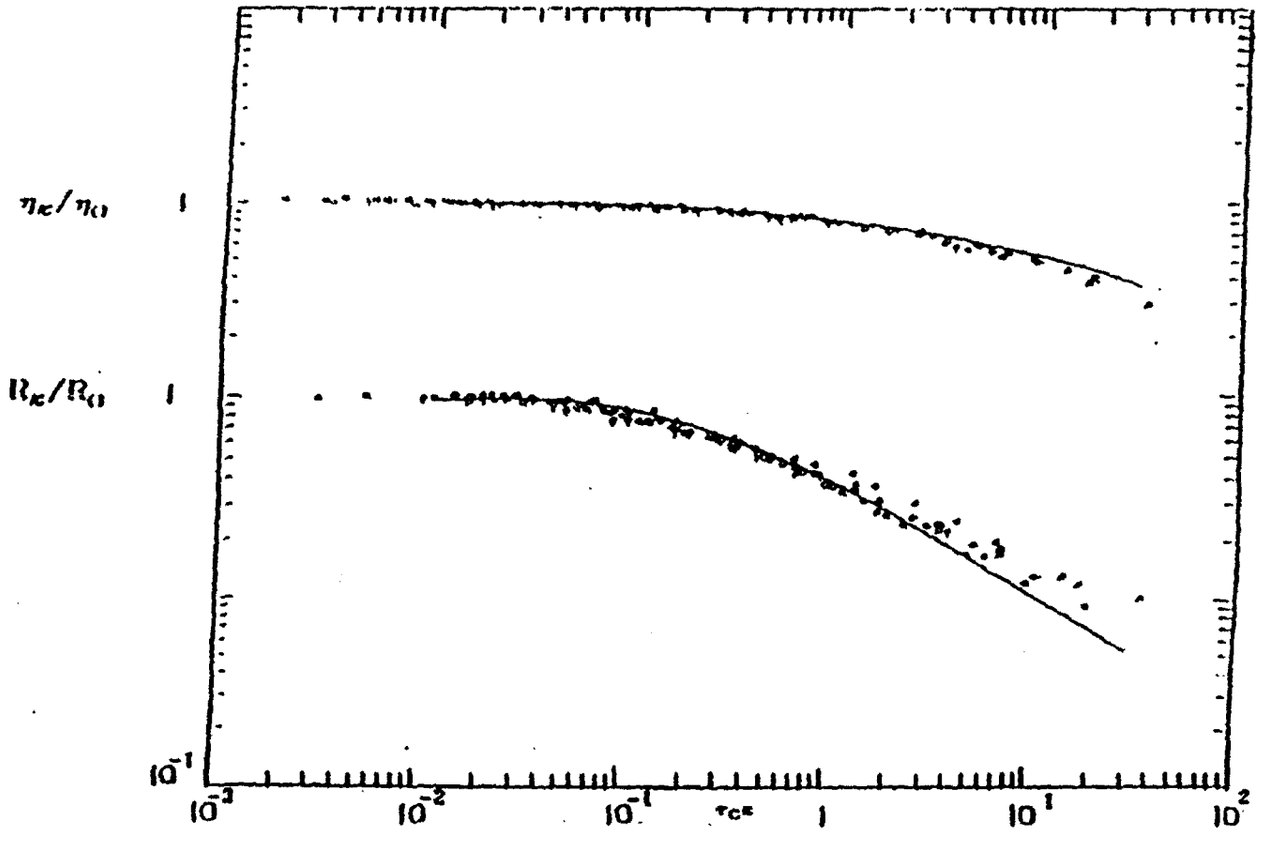

FIG. 27 The reduced steady-state viscosity η_κ/η_0 and recoverable compliance $R_k^{(S)}/R_0^{(S)}$ versus the reduced shear rate $\tau_c\kappa$ for solutions of mixtures of PBO and PabBO listed in Table 6, with pips rotating clockwise with increasing concentration. Values of η_κ, $R_0^{(S)}$ and τ_c are given in Table 5. The curves are calculated with Eqns 13 and 14, using the experimental data on the distribution of relaxation times.

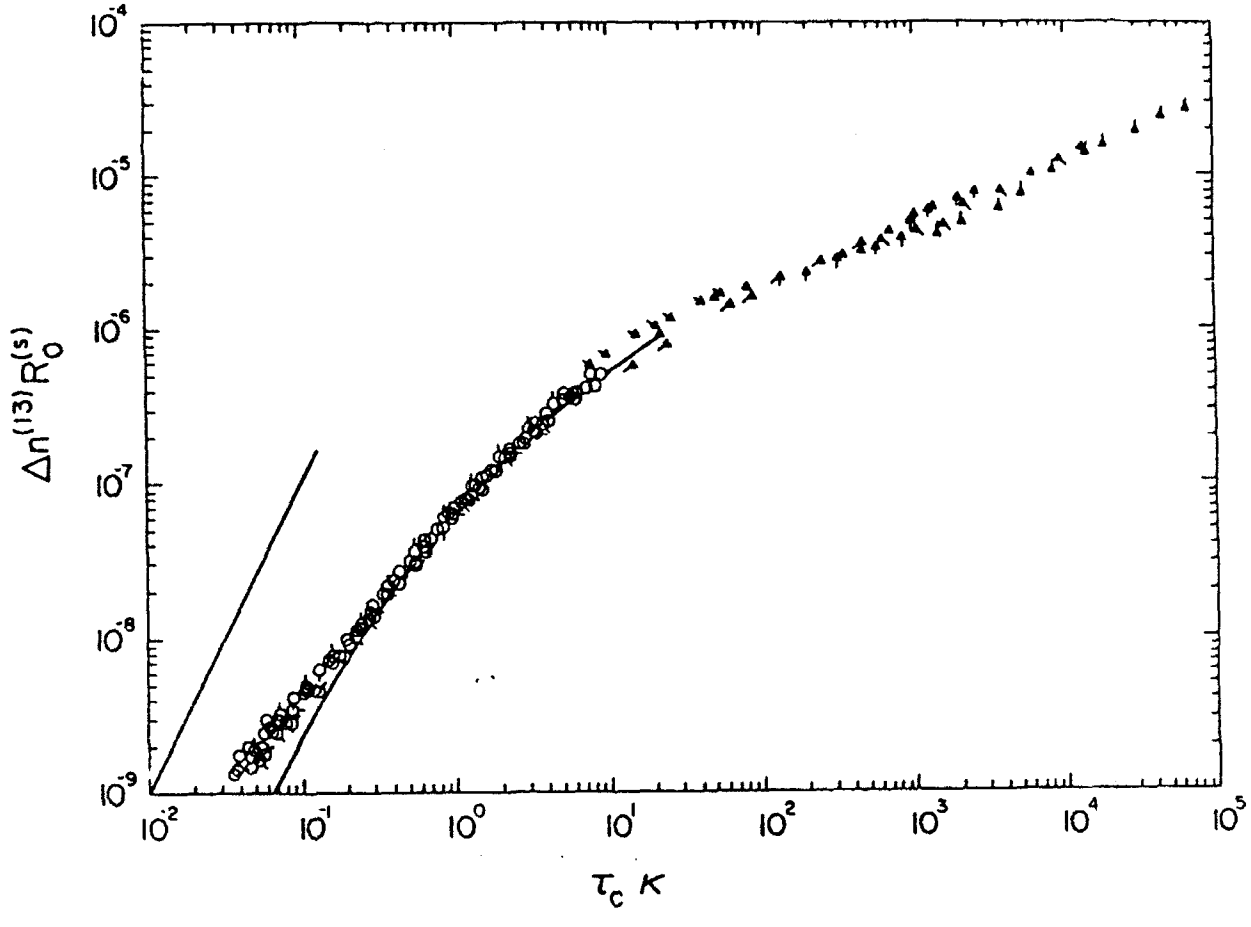

FIG. 28 The flow birefringence function $\Delta n_{13} R_0^{(S)}$ versus the reduced shear rate $\tau_c \kappa$ at 301K for blends PBT and nylon in series A (filled circles) and series C (unfilled circles). For the former, the pips rotate clockwise from up for A1.95/0.49, A-1.10/1.10, A-1.11/1.66, A-0.83/1.93, and A-0.54/2.16. For the latter the pips rotate clockwise from up for C-1.29/0, C-1.29/0.45, C-1.28/0.68, C-1.27/0.90, C-1.27/1.12 and C-1.30/1.58. The straight line has slope 2 expected for small $\tau_c \kappa$.

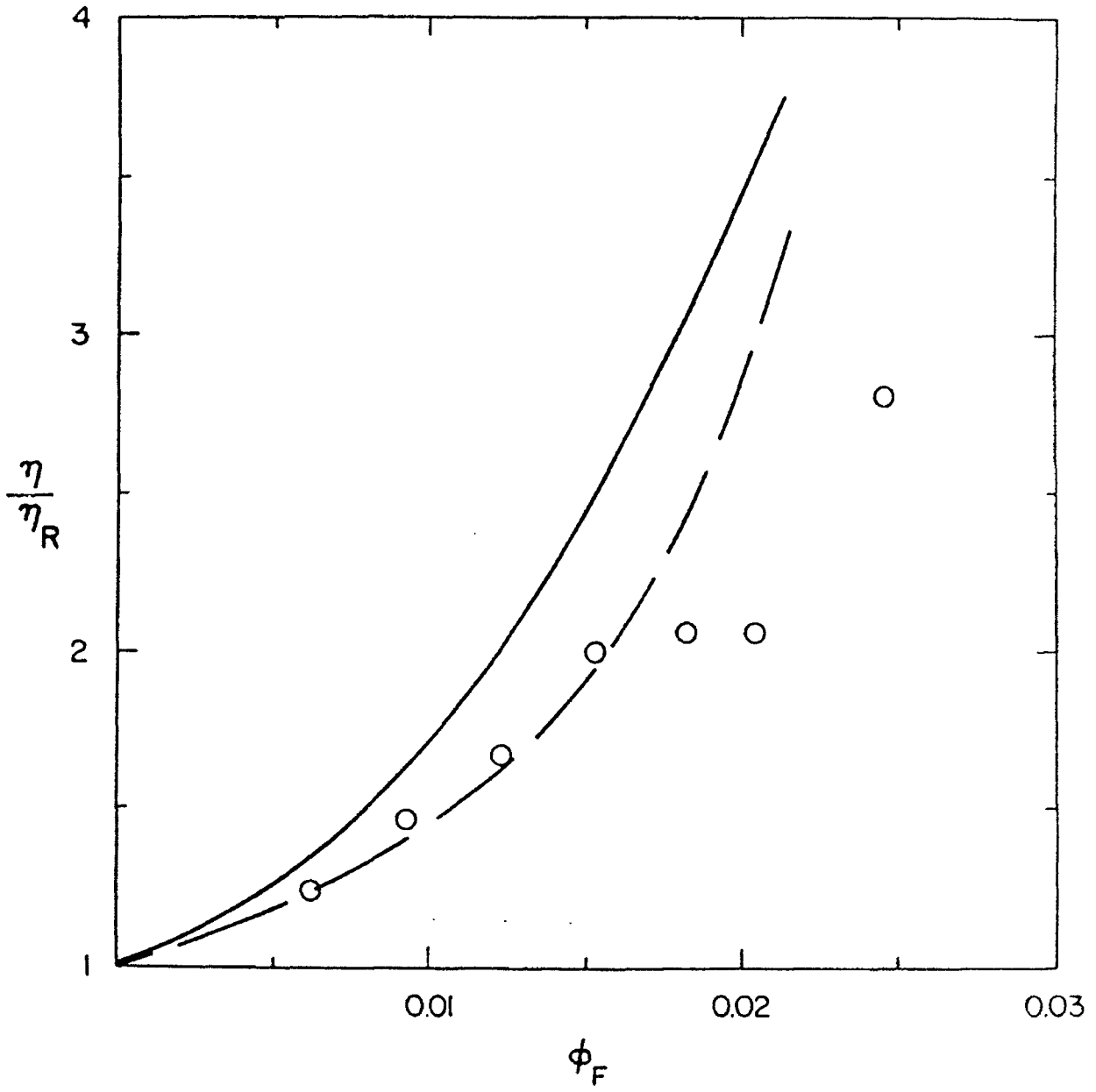

FIG. 29 The ratio η/η_R of the viscosities of a blend of PBT and nylon and a solution of PBT with the same concentration of rodlike chains, but no nylon-66, as a function of the nylon-66 volume fraction in the blend for a series C-1.28/F samples. The solid and dashed curves represent the use of Eqn. 3 along with Eqns. 4 or 5 respectively, as discussed in the text.

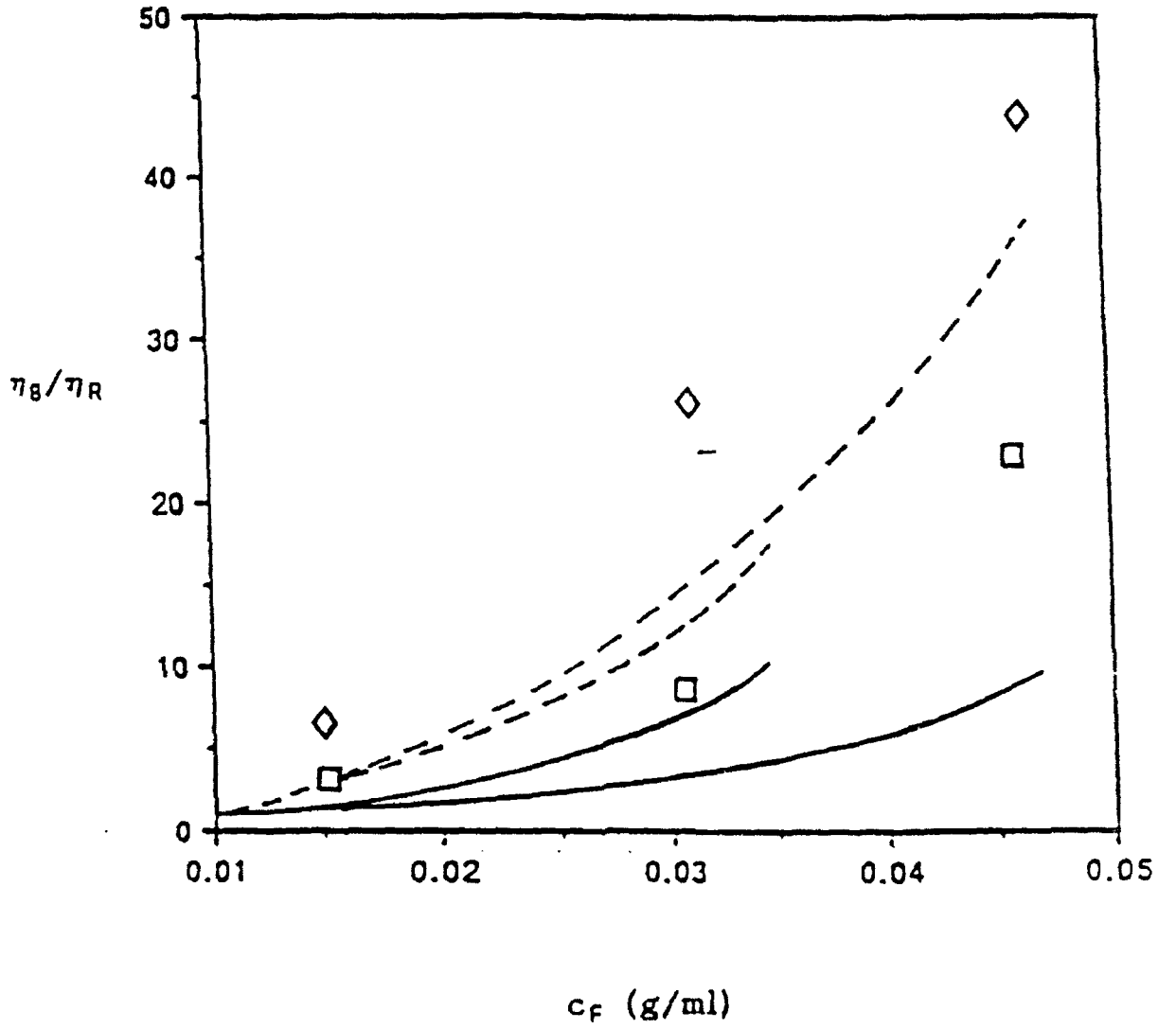

FIG. 30 The ratio η/η_R of the viscosities of a blend of PBO and PabBO and a solution of PBO with the same concentration of rodlike chains, but no PabBO, as a function of the PabBO concentration in the blend for solutions with φ_R of 0.0198 (triangles) and 0.0310 (squares) The solid and dashed curves represent calculations of the contribution due only to the PBO, and the dashed line includes contributions from both components, as discussed in the text.

APPENDIX

PERSONNEL

In addition to the P.I., personnel associated with AFOSR-89-0125 in the report period have been

Dr. Hedi Mattoussi	Post-doctoral Associate
Dr. K. Suresh	Post-doctoral Associate
Dr. Gary D. Patterson	Professor, Dept. Chem., CMU
Dr. Churl S. Kim	Ph.D. Graduate student (1988)
Dr. Mohan Srinivasarao	Ph.D. Graduate student (1990)
Dr. Vincent J Sullivan	Ph.D. Graduate student (1990)
Ms Shunqiong Yue	Ph.D. Graduate student
Ms N. Desvignes	Technical Assistant

"Rheological Behavior of Blends of Rodlike and Flexible Chain Polymers in Isotropic Solution", Churl S. Kim, Ph.D. Dissertation, Department of Chemistry, Carnegie Mellon University,1988.

"Rheo-Optical Studies on a Polymer Liquid Crystal Under the Influence of Flow or Magnetic Fields", Mohan Srinivasarao, Ph.D. Dissertation, Department of Chemistry, Carnegie Mellon University,1990.

"Rheology, Phase Behavior and Dilute Solution Properties of Blends of the Rodlike Poly[p-phenylene benxbisoxazole] and Flexible Chain poly[2,5-benzoxazole] in Sulfonic Acid Solvents", Vincent J Sullivan, Ph.D. Dissertation, Department of Chemistry, Carnegie Mellon University,1990.

PUBLICATIONS 1988-1991

Publications with support from AFOSR-89-0125 denoted by "AFOSR'

1988

AFOSR112. Rheological, Rheo-optical and Light Scattering Studies on Nematic Solutions of Poly[1,4-phenylene-2,6-benzobisthiazole], G. C. Berry, Kazunori Se, and Mohan Srinivasarao, in *High Modulus Polymers*, Ed. by A. E. Zachariades and R. S. Porter, Marcel Dekker, New York (1988), p. 195 .

113. Remarks on a Relation Among the Intrinsic Viscosity, The Radius of Gyration and the Translation Friction Coefficient, G. C. Berry, *J. Polym. Sci., Part B: Polym. Phys.*, 26, 1137 (1988).

AFOSR114. Rheological Studies on Blends of Rodlike and Flexible Chain Polymers, C. S. Kim, V. S. Sullivan, and G. C. Berry, Confr. Proceed, 46th. Tech. Confr., Soc. Plastics Engineers 34, 990 (1988).

115. Rheological Studies of Dispersions of Spherical Particles in a Polymer Solution, D. W. Meitz, L. Yen, G. C. Berry and H. Markovitz, *J. Rheology* 32, 309 (1988).

116. Electrophoretic, Dynamic and Static Light Scattering On Charged Polymer Emulsions, F.-M. Lin, G. C. Berry, R. L. Frye, and L. C. Scala, *J. Appl. Polym. Sci.* 35, 1377 (1988).

117. Dynamic Light Scattering From Polymer Solutions, G. D. Patterson and G. C. Berry, in *Molecular Conformation and Dynamics of Macromolecules in Condensed Systems*, Ed. by M. Nagasawa, Elsevier, New York p. 73 (1988).

AFOSR118. Rheological Properties of Nematic Solutions of Rodlike Polymers, G. C. Berry *Mol. Cryst. Liq. Cryst.*, 165, 333 (1988).

119. Solution Properties of Xanthan, Light Scattering and Viscometry on Dilute and Moderately Concentrated Solutions, T. Kojima and G. C . Berry, *Polymer*, 29, 2249 (1988).

120 . Polymer Solutions, E . F. Casassa and G . C . Berry, in *Comprehensive Polymer Science*, Vol. 2, Ed. by G. Allen, Pergamon Press, New York Chapter 3, (1988).

121. Studies on Aligned Nematic Solutions of a Rodlike Polymer,G. C. Berry and M. Srinivasarao, in Dynamic Behavior of Macromolecules, Colloids, Liquid Crystals and Biological Systems, Ed. by H. Watanabe, Hirokowa Publ. Co., Tokyo, 1988, p. 389.

AFOSR122. Properties of Solutions of Rodlike Chains From Dilute Solutions to the Nematic State, G. C. Berry, in *The Materials Science and Engineering of Rigid Rod Polymers*, Mat. Res. Soc. Symp. Proceed. Vol. 134, Ed. R. K. Eby and D. E. Lemore (MRS, Pittsburgh, 1989), p.181.

1989

123. A Rotational Rheometer for Rheological Studies With Prescribed Strain or Stress History, G. C. Berry, M. H. Birnboim, J. 0. Park, D. W. Meitz, and D. J. Plazek, *J. Polym. Sci., Part B: Polym.Phys.*, 27, 273 (1989).

124. Molecular Composites from Rod and Flexible Polyquinolines, J. K. Stille, A. Parker, J. Tsang, G. C. Berry, M. Featherstone,D. R. Uhlmann, S. Subramoney and W-L. Wu, in Contemporary Topics in Polymer Science, Ed. by E. J. Vandenberg, Plenum Press, New York(1989), Vol. 5.

AFOSR125. Molecular Composites Formed by Solutions of a Rodlike Polymer (PBT) in Polyphosphoric Acid, A. F. Charlet and G. C. Berry, *Polymer*, 30,1462 (1989).

126. Moderately Concentrated Solutions of Polystyrene. 3. Viscoelastic Measurements at the Flory Theta Temperature, J. 0. Park and G. C. Berry, *Macromolecules*, 22, 3022 (1989).

AFOSR127. Rheology of Blends of a Rodlike Polymer (PBO) and Its Flexible Chain Analog, V. J. Sullivan and G. C. Berry, Proceedings, Materials Research Society, Boston, November 1989.

1990

128. Moderately Concentrated Solutions of Polystyrene. IV. Elastic and Quasi-Elastic Light Scattering at the Flory Theta Temperature, S-J. Chen and G. C. Berry, *Polymer*, 31, 793 (1990).

129. Studies on Dilute Solution of Phenyl Ether Ketone Copolymers, C. Wei-Berk and G. C. Berry, *J. Polym. Sci., Part. B: Polym. Phys.*, 28, 1873 (1990).

AFOSR130. Studies on Dilute Solutions of Rodlike Macroions. 5. Electro-static Effect on Intermolecular Association, C Wei-Berk and G. C. Berry, *J. Appl. Polym. Sci.*, 45, 261 (1990).

131. Condensation and Summary of "Tracer Diffusion of Linear Polystyrene in Entanglement Networks" by Nemoto, *et al*, G. C. Berry, *Chemtracts -Macromolecular Chem.*, 1, 126 (1990).

132. Characterization of Association in Polymer Solutions by Light Scattering Methods, G. C. Berry, Proceedings 3rd. Light Scattering Research Seminar, Tokyo, 6 June 1990, p. 1.

AFOSR133. Rheological Properties of Rodlike Polymers in Solution. 4.Rheology of Blends of Nylon and a Rodlike Chain, C. S. Kim and G. C. Berry, *J. Rheology*, 34,1011 (1990)

134. Condensation and Commentary of "Carbon-13 Nuclear Magnetic Resonance Measurements of Local Segmental Dynamics of Polyisoprene in Dilute Solutions: Nonlinear Viscosity Dependence" by S. Glowinkowski, *et al*, G. C. Berry, *Chemtracts-Macromolecular Chem.*, 1,295 (1990)

1991

135. Rheology of Nematic Solutions of Rodlike Chains: Comparison of Theory and Experiment, G. C. Berry and M. Srinivasarao, *J. Statistical Phys.* 62, 1041 (1991).

136. Rheo-optical Studies on Aligned Nematic Solutions of a Rodlike Polymer, M. Srinivasarao and G. C. Berry, *J. Rheology* 35, 379 (1991).

137. Dynamic Light Scattering from Polymer Solutions Under Nonhydrodynamic Conditions, G. D. Patterson and G. C. Berry, *J. Noncrystalline Solids* 131-133, 799(1991).

AFOSR138. The Third Order Susceptibility of Nematic Solutions of PBT, H. Mattoussi and G. C. Berry, *Polym. Preprints Am. Chem. Soc.* 32(3) 690 (1991).

139. Rheological and Rheo-Optical Studies on Nematic Solutions of a Rodlike Polymer: Bingham Award Lecture, G. C. Berry, *J. Rheology* 35, 943 (1991).

AFOSR140. Nonlinear Optical Properties of PBT in Nematic Solutions, H. Mattoussi, P. G. Kaatz, G. D. Patterson and G. C. Berry, in *Optical and Electronic Properties of Polymers*, Ed. J. M. Torkelson and J. A. Emerson, *Matl. Res.Soc. Symp. Proceed.* 214, 11 (1991).

AFOSR141. Birefringence and Order of Liquid Crystal Polymer Solutions, H. Mattoussi, M. Srinivasarao, P. G. Kaatz and G. C. Berry, in *Optical and Electronic Properties of Polymers*, Ed. J. M. Torkelson and J. A. Emerson, *Matl. Res.Soc. Symp. Proceed.* **214**, 157 (1991).

1992

AFOSR142. Refractive Indices Dispersion and Order of Lyotropic Liquid Crystal Polymers, H. Mattoussi, M. Srinivassarao, P. G. Kaatz and G. C. Berry, *Macromolecules*, 25, 2806 (1992).

AFOSR143. Polymerization Kinetics of Rigid Rodlike Molecules. 2. Polymerization of Poly(1,4-phenylene-2,6-benzobisthiazole), PBT in the Nematic State, C. P. Spencer and G. C. Berry, *Polymer*, 33, 1909 (1992)

AFOSR144. Anisotropic Third-Order Susceptibility of a Nematic Solution of a Rodlike Polymer (PBT), H. Mattoussi and G. C. Berry, *Mol. Cryst. Liq. Cryst.*, **223**, 41, (1992).

AFOSR145. Birefringence and Dispersion of Uniaxial Media, H. Mattoussi, M. Srinivassarao, P. G. Kaatz and C C. Berry, *Mol. Cryst. Liq. Cryst.*, **223**, 69, (1992).

146. Magnetic Field Induced Instability In An Aligned Nematic Solution of a Rodlike Polymer, M. Srinivassarao and G. C. Berry, *Mol. Cryst. Liq. Cryst.*, **223**, 99, (1992).

AFOSR147. Third-Order Susceptibilities of Nematic and Isotropic Solutions of a Rodlike Polymer (PBT), H. Mattoussi and G. C. Berry, in *Proceed Second Pacific Polymer Conference*, Ed. Y.Imanishi, Springer-Valig, in press.